Acoustic Cavity Technology For High Performance Injectors

CR 151331

NAS 9-14232

FINAL REPORT

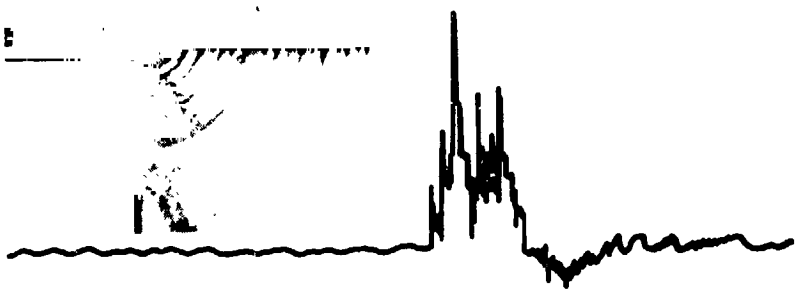

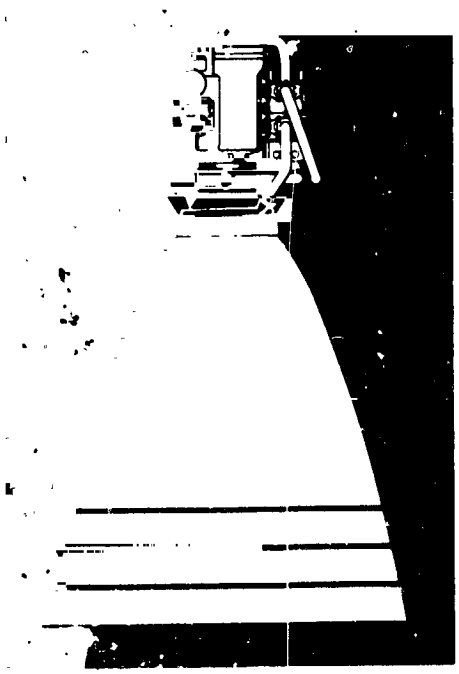

Report No 14232-3-1
1 October 1976

Aerojet Liquid Rocket Company
SACRAMENTO, CALIFORNIA 95813

Acoustic Cavity Technology for High Performance Injectors

Final Report

NAS 9-14232-3-1

Prepared by

Aerojet Liquid Rocket Company
A Division of Aerojet-General Corporation
Sacramento, California, 95813

Contract NAS 9-14232

Prepared for

National Aeronautics and Space Administration
Lyndon B. Johnson Space Center
Primary Propulsion Branch
Houston, Texas, 72058

Foreword

Aerojet Liquid Rocket Company submits this Final Report as part of the program, Acoustic Cavity Technology for High Performance Injector, NAS 9-14232.

The work was conducted under the cognizance of Mr. R. C. Kahl of NASA/JSC who was contract monitor. Aerojet management includes Larry Bassham, Program Manager, Dave Kors, Operations Project Manager, and Roy Michel, Project Engineer.

Many individuals contributed their skills and efforts to the attainment of program goals. Gene Hron was responsible for fabrication of the test hardware. Testing was conducted with efficiency and thoroughness by test engineers, Arnold Keller and Pete Stretch, along with instrumentation engineer, Duane Robertson. The perplexities of test data correlation and numerous acoustic and stability analyses were fronted by Jim Fang, Ross Hewitt, John Hidahl, Bill Lawver, and Jim McBride.

Abstract

This contract, Acoustic Cavity Technology for High Performance Injector, NAS 9-14232, was undertaken to show the feasibility of damping more than one mode of rocket engine combustion instability by means of differently tuned acoustic cavities sharing a common entrance. A secondary program objective was to develop analytical procedures and acoustic modeling techniques for predicting the stability behavior of acoustic cavity designs in hot firings.

The program had two major aspects: full scale testing of various common entrance, dual cavity configurations, and subscale testing for the purpose of obtaining motion pictures of the cavity entrance region, to aid in determining the mechanism of cavity damping. As a part of the full scale testing, extensive acoustic modeling was undertaken to screen candidate configurations. Speakers driven by signal generators were used to simulate acoustic modes, and both single and multiple leg cavities were evaluated. Damping effectiveness of selected cavity configurations was tested in full scale hot firings using a 6000 lbF thruster and an injector known to be unstable in three acoustic modes. In the subscale testing, high speed motion pictures were taken through quartz windows in the side plate of the narrow rectangular chamber. Various cavity tune and entrance configurations were examined.

TABLE OF CONTENTS

LIST OF FIGURES

LIST OF FIGURES (cont.)

LIST OF FIGURES (cont.)

LIST OF TABLES

I. INTRODUCTION

The primary objective of this program was to establish the feasibility of damping more than one mode of rocket engine combustion unstability by means of differently tuned acoustic cavities sharing a common entrance. The major advantage of such "dual cavity" configurations over conventional bitune devices -- in which two types of cavities are arranged in some symmetrical pattern around the circumference -- is that standing acoustic modes cannot set up at points of poor damping around the periphery and that cavity entrance area is reduced for a given cavity volume. Figure 1 illustrates bitune and dual cavity concepts and shows how standing modes can set up with the former but not the latter. The secondary program objective was to develop analytical techniques along with simple bench test procedures for predicting the stability behavior of acoustic cavity designs in hot firings.

The program consisted of five tasks which relate to three major areas of investigation: (1) acoustic bench tests to screen candidate cavity configurations, using a "two-dimensional" lucite model of the chamber and one or two speakers driven by signal generators to simulate the acoustic modes; (2) subscale hot firings with a "two-dimensional" chamber designed to permit high speed motion picture photography of the injector/cavity region; (3) full scale hot firings with a 6000 lbF thrustor and an injector known to be unstable in three acoustic modes, to evaluate the damping effectiveness of various multimode, common entrance configurations.

Two such dual cavity devices indicated multimode damping capability. The cavity legs in one were positioned axially and radially; in the other, both legs were oriented in the radial direction.

The high speed movies obtained with the subscale unit are apparently the first ever taken of stable and unstable combustion in the cavity entrance region. The most remarkable features observed in the movies were the coupling between the acoustic mode and the propellant flow field during unstable combustion, and the shortening of the distance travelled by the propellant prior

Dual Cavity Versus Bitune Cavity

BITUNE CAVITY

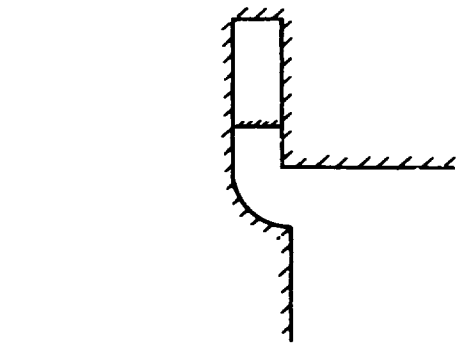

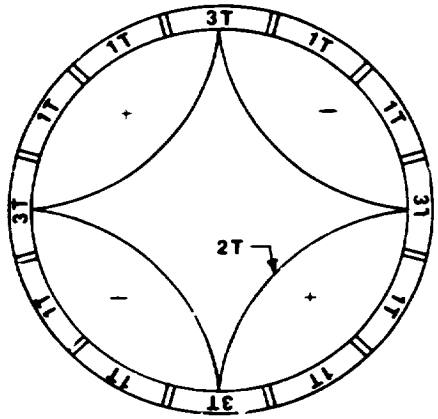

LIMITATION -

STANDING MODE CAN SET UP
AT POINTS OF POOR DAMPING

DUAL CAVITY

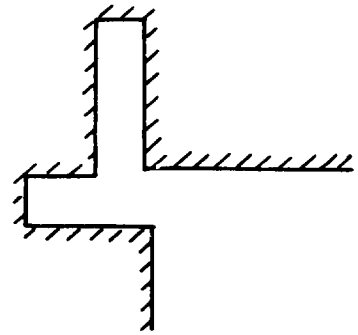

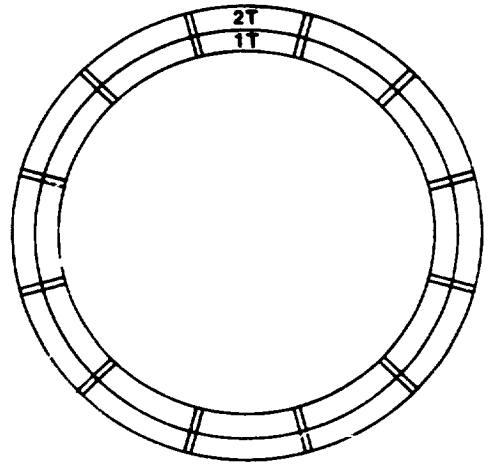

BENEFIT -

100% CAVITY EFFECTIVENESS

Figure 1

to complete combustion as a result of unstable operation. In general, the movies showed minimal interaction between the cavity and the chamber region.

The analytical results testify to the progress being made in understanding combustion stability and developing analytical techniques for predicting stability characteristics. Correlation of cavity pressure amplitudes measured in subscale testing with the basic cavity model quantified values for the damping and inlet resistance parameters and the cavity gas sound speed. Correlation of pertinent stability results in full scale testing demonstrated the capability of the overall analytical methodology encompassed by the Injector Face Acoustic Resonator (IFAR) computer program developed by Aerojet; application of the program to dual cavity configurations represented an extension of previous analytical capabilities. In a sense this has been an "ideal" program, because it involved analysis, acoustic modeling, subscale testing, and full scale testing, and because the analysis could relate these other three areas to each other.

The primary program objectives regarding multimode damping was achieved in full scale testing. Secondary objectives to develop analytical and bench test techniques were fulfilled by the modeling, subscale and full scale test efforts.

II. SUMMARY

The program consisted of five tasks as follows:

Task I - Design and Analysis
Task II - Hardware Fabrication
Task III - Demonstration Test
Task IV - Design Update
Task V - Reporting

It is more convenient to divide the program into the three areas of concentration, however: acoustic modeling, subscale/photographic (2D chamber) testing, full scale (dual cavity) testing.

Acoustic modeling was performed with a "two-dimensional" chamber/cavity model instrumented with high frequency pressure transducers; single and dual frequencies were driven by acoustic speakers. Single cavities up to 4.0-in. long were evaluated in both axial and radial orientations; dual cavities in series and parallel configurations, the latter in three geometrical arrangements, were also tested.

Subscale/photographic testing was also conducted in a "two-dimensional" chamber to allow high speed motion picture photography through quartz windows in the cavity entrance region. The injector utilized an X-doublet element pattern; six cavity configurations were evaluated, and 45 tests were conducted, using monomethylhydrazine and nitrogen tetroxide as propellant. Most firings were bombed with 2.0 grain RDX bombs; first width (1W) mode instabilities were experienced with three of the cavity configurations.

The full-scale test program used hardware sized for a 6000 lbF thrust application and a mixed element--splash plate and X-doublet--injector

II, Summary (cont.)

known to produce at least three modes of instability. Forty-one tests were conducted, again with monomethylhydrazine and nitrogen tetroxide. Eleven different cavity configurations formed by varying the arrangement of insertable blocks in the cavity housing were evaluated, using fifty-eight 6.5 grain RDX bombs. Two of these configurations showed excellent multimode damping.

III. RESULTS AND CONCLUSIONS

A. ACOUSTIC MODELING

The acoustic modeling experiments indicated that a dual resonance condition can be achieved with a dual leg, single entrance cavity, as was later confirmed in the full scale testing, and that each leg appears to use the entire entrance area. The experiments also showed that maximum damping of the primary mode of interest (depressed first width) was obtained when the two were legs physically parallel and the longer leg was adjacent to the face. In single cavity tests, an L-shaped cavity was found to have an acoustic length 20% longer than the mean centerline distance, and in dual cavity tests the damping of the lower frequency leg was attenuated by interaction with the high frequency leg.

Acoustic modeling was instrumental in defining the wave paths for the analytical representation of the full scale dual cavity configurations. The low signal-to-noise ratio obtained at some frequencies limits the usefulness of modeling techniques and necessitates a great degree of care by the investigator and a high level of sophistication in the instrumentation and data processing equipment. The use of piston-like sliders to adjust cavity length proved to be a constant source of irritation because of the leakage, and corresponding acoustic misrepresentation, introduced. Finally, simulation of mean flow through the chamber and recirculating flow in the cavity appears to be an aspect that should not be overlooked in future modeling efforts, because of the potential effects of such flow on cavity damping.

B. SUBSCALE (2-D) TESTING

Three of the six cavity configurations tested were bomb-stable at all operating conditions: the 1.0 in. length,* the 1.5 in. length, and the 0.5 in. length with 0.25 in. overlap. Two were unstable at all operating points: the 0 in. length and the rounded inlet 0.5 in. length. The sixth, the 0.5 in.

---

* as measured from the injector face

III, B, Subscale (2-D) Testing (cont.)

length unit, was unstable at low and nominal chamber pressures -- less than 140 psia -- but stable at higher values. The first width mode frequency experienced was comparable to the first tangential mode of the full scale hardware.

High speed movies of the cavity entrance region showed the propellants to be poorly mixed during stable operation, extending more than 2.0 in. -- the field of view -- down the chamber without being fully combusted. Flow of raw propellant into the cavity was minimal but did occur with most configurations, often in a cyclic manner. Hot gas did flow into the cavity at a 45° angle, however, as evidenced by a zone of blue coloration indicative of the OH, NH, and CH radicals.* Gas recirculation in the cavity was apparent. Unstable operation, and postbomb recovery of some configurations, was marked by a shortening of the propellant streams prior to full combustion, to a distance that varied cyclically but was as low as 0.4 in. Wavering back and forth of the propellant streams was also observed, at a frequency corresponding to the unstable mode. During unstable operation some uncombusted propellant entered the cavity in a cyclic manner.

The analytical model of the cavity closely correlated the ratio of pressure amplitudes measured at the back and entrance of the cavity, and thus provided values for the damping and inlet resistance parameters and the cavity gas sound speed. These values, and the cavity model itself, were used to correlate the stability of the full scale test configurations.

The 2-D thruster was developed primarily to allow visualization of the cavity entrance region; it served this purpose admirably. Photographic results were of excellent quality. The high speed camera is a useful tool for such studies, and with sufficient external illumination very high frame

* Harrje, D. T., ed., Liquid Propellant Rocket Combustion Instability, NASA SP-194, p. 487.

rates may be achieved; the present testing utilized frame rates as high as 11,000 pictures per second although most of the movies were taken at 6,000 pictures per second. A stroboscopic light source, synchronized with the camera, was used in several tests to provide a very short period of illumination; although the strobe did not perform satisfactorily, it did show some aspects of combustion field behavior not evident in the color movies, particularly when used as a back light.

The 2-D hardware was not intended to be a predictive tool per se for full scale combustion stability; nonetheless, it is of interest to note that the rounded inlet and larger overlap cavity configurations behaved in subscale tests as they did in earlier full scale testing conducted in NAS 9-13133, i.e., unstable and stable respectively.

C. FULL SCALE TESTING

Five basic cavity configurations, including six additional variations of one configuration, were tested. Two of these -- a dual radial leg arrangement and an axial-radial leg arrangement -- provided excellent bomb stability, although the limited number of tests compromises the statistical significance of the results. Some first longitudinal (1L) mode was experienced during the start transient with almost all configurations; this was beyond the range of cavity tune and thus not germane to the interpretation of results. At high chamber pressure, all configurations were stable.

The Injector Face Acoustic Resonator (IFAR) model correlated the full scale stability trends quite closely, even to the extent that the mode of instability experienced was generally correctly correlated. Extension of the cavity model to dual cavity configurations was a direct "fallout" of the acoustic modeling work: the quiescent nature of the one cavity leg while the other is in

resonance was brought to light by cork dust pattern observations. The subscale work also contributed to the full scale analysis with the quantification by the cavity model of various input parameters.

The mechanism of acoustic cavity damping is the combination of mode shape alteration and energy dissipation within and at the entrance of the cavity. Cavity tune is important as damping effectiveness does not appear to extend over a broad band of frequency. Tune appears to be most sensitive to cavity gas sound speed. The 1L and 2T modes experienced prior to the establishment of steady-state conditions in the cavity is predictable with the IFAR program, assuming reduced sound speeds in the cavity.

Acoustic bench tests and subscale hot firings, in conjunction with appropriate analysis, are potentially useful techniques for gaining an understanding of full scale stability behavior. The need for carefully conceiving such tests is quite apparent, however.

Dual cavity concepts can provide multimode damping capability and appear suited to flight engine systems, notwithstanding mechanical design complexities introduced primarily by cooling considerations.

IV. RECOMMENDATIONS

The following recommendations are grouped according to the areas of endeavor:

Acoustic Modeling

1. The effect of gas recirculation in the cavity ought to be modeled.

2. Mean flow through the chamber should be modeled.

3. The cavity entrance and exit loss should be determined by imposing a mean flow in and out of the cavity.

4. The use of sliding pistons to vary cavity length should be avoided.

Subscale/Photographic Testing

1. The effect of injection velocity, chamber pressure, and Mach number, which are parameters in the ALRC stability model, should be confirmed by varying the throat area in the 2-D chamber.

2. Other injector patterns should be evaluated.

3. Different experimental methods, such as high speed shadowgraph motion pictures -- intended but not accomplished because of technical difficulties -- or laser anemometry, should be utilized.

4. The use of laser anemometry in conjunction with standard high frequency pressure measurement techniques should be considered as a means of directly evaluating cavity admittance.

IV, Recommendations (cont.)

5. Narrow, rectangular chambers such as were used here should have ample provision to prevent warpage of the side plates -- a continually worsening problem throughout the testing. The capability of altering the chamber width to change the acoustic mode frequencies would be a worthwhile feature in such hardware.

Full Scale Testing

1. Further development of the dual radial and axial-radial cavity geometries should be pursued.

2. The use of dual cavities in conjunction with other high performance injector elements should be considered.

3. Statistical significance should be emphasized in stability testing, and operating point should be recognized as a variable in the statistics.

4. The role of cavity entrance and exit losses on damping bandwidth should be investigated further.

5. The effect on damping characteristics of fuel film cooling injected across the cavity entrance should be evaluated.

6. Instrumentation to determine cavity gas sound speed should be routinely installed; this means, at the very least, high frequency pressure transducers located at the back and entrance to the cavity. In the case of dual cavities both circuits should be instrumented and an additional transducer at the branch point would be useful.

IV, Recommendations (cont.)

7. Instrumentation to better characterize the cavity gas temperature should be developed. Thermocouples, or thermocouple rakes, must have high temperature capability and quick response. The effect of lead losses, radiation to the cavity walls and from the combustion products, and the local convective environment must all be considered when interpreting the indicated responses.

Analytical Methods

The IFAR model developed by ALRC can be improved in several ways:

1. Better definition of the stability parameters n and τ in terms of injector pattern and various injector parameters is necessary.

2. Velocity coupling -- i.e., coupling of the acoustic wave and propellant velocity -- should be considered; the IFAR analysis treats only pressure coupling.

3. Feed system coupling should be included.

4. Injector admittance is not currently considered in the model and should be.

V. APPLICATION OF RESULTS

The primary result of this program was to demonstrate the damping effectiveness of differently tuned acoustic cavities sharing a common entrance. Such dual tuned cavities improve several aspects of bitune arrangements, in which two types of cavities are arranged symmetrically about the injector circumference. The improvements of dual tuning include: (1) prevention of standing modes oriented between symmetrically arranged cavities, (2) reduction in entrance area for a given cavity volume, (3) potential reductions in weight and cavity heat load. Accordingly, the application of dual tuned cavities to present or future engine systems is obvious.

The acoustic bench tests, hot firings, and analytical modeling have all furthered the understanding of combustion stability and cavity damping. While continued progress in this area has been evident for some time at Aerojet, the subscale correlation for the first time gave a good measure of cavity gas sound speed and various damping parameters, and the full scale correlations showed that the analytical procedures could be readily extended to complicated cavity geometries. What comes out of this then is considerable refinement and an increased confidence in the analytical methodology under development.

VI. ACOUSTIC MODELING

A. INTRODUCTION

Acoustic modeling was done as a part of Task I to guide the design of cavity configurations for full scale testing and, in conjunction with analytical methods, to improve the understanding of cavity damping mechanisms. Candidate cavity configurations were selected on the basis of providing multimode damping corresponding to the 1T, 2T, and 1R modes anticipated in hot firing, having a common inlet for multiple cavities, and maintaining dimensions within realistic geometrical limits.

The basic cavity configurations involved legs in parallel, legs in series, or combined parallel-series arrangements. The "two-dimensional" (rectangular) chamber model was constructed of lucite and fitted with high frequency pressure instrumentation, primarily in the cavity region. Two acoustic drivers -- speakers -- provided different signals as desired. Cork dust in the chamber, which accumulates in patterns corresponding to the resonant modes, allowed visual observation of the model patterns established.

The model tests showed that dual resonance is possible with a single cavity entrance, that damping effectiveness varies with orientation of the legs in the parallel leg configurations and that the series arrangement is inferior to the parallel leg system. In addition, the cork dust patterns observed in the cavities were instrumental in correctly defining the acoustic lengths used for analyzing the full scale dual cavity hot fire results.

B. TEST SETUP

Equipment used in testing is shown in Figure 2. It comprised the lucite model and acoustic driver, an analyzer which tracks on the driver frequency and gives on vumeters the amplitude and phase angle relationships of two input frequencies, a computer which after digitizing of the input stores and operates on the data, and finally a printer for printout of results.

Acoustic Bench Test Setup

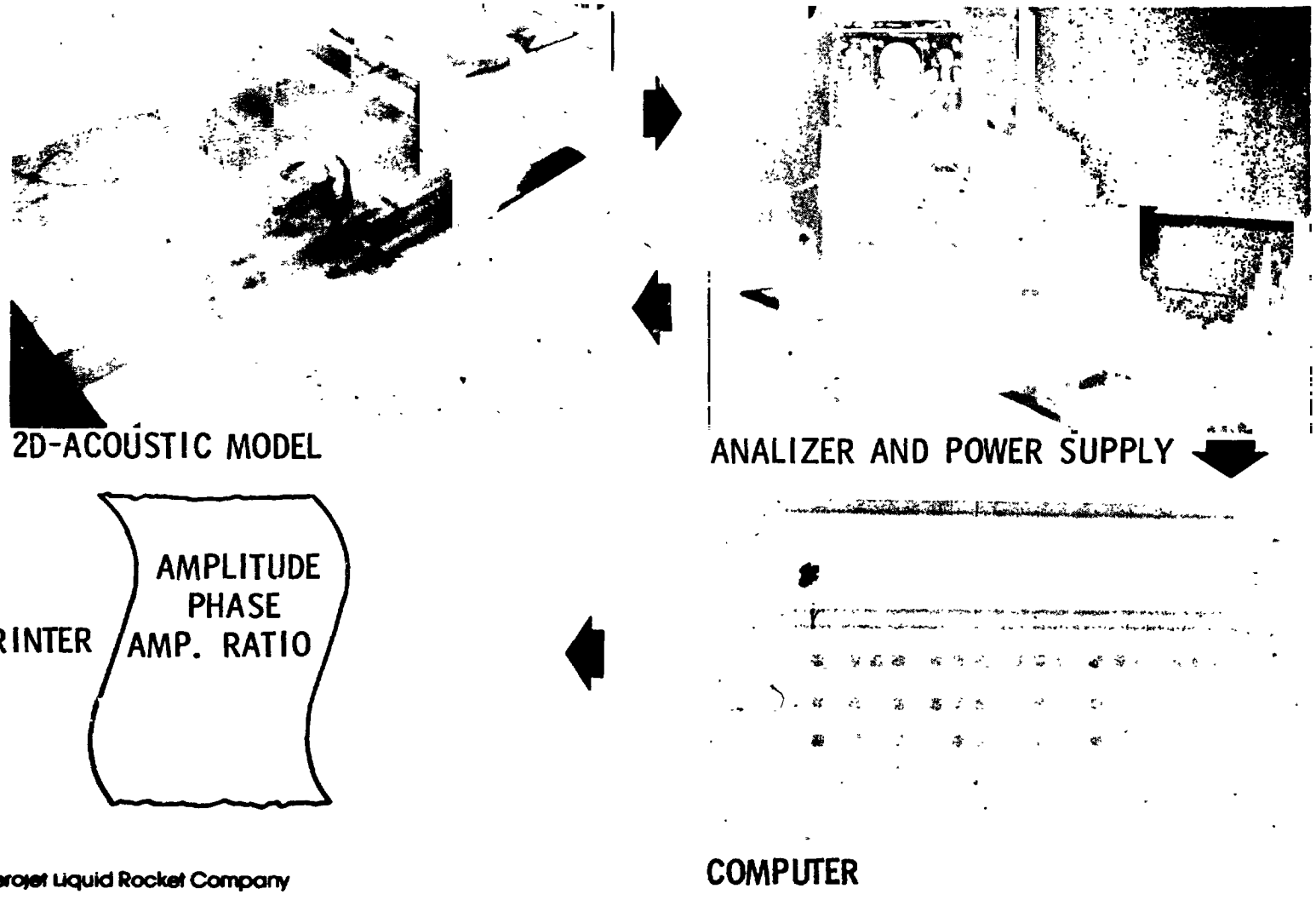

Aerojet Liquid Rocket Company

Figure 2

VI, B, Test Setup (cont.)

The chamber model had internal dimensions of 8.00 in. width, 14.00 in. length, and 1.50 in. height. The calculated resonant frequencies, for a sonic velocity of 1130 ft/sec were as follows:

Mode	Frequency,(Hz)
Width Modes:	
First width (1W)	847
Second width (2W)	1695
Length Modes:	
First length (1L)	484
Second length (2L)	969
Third length (3L)	1453
Combined Modes:	
1L + 1W	976
2L + 1W	1287
3L + 1W	1682
1L + 2W	1763

That these frequencies were not exactly obtained is an indication of minor leakage or driver/wall interactions.

Cavities were located on both sides of the chamber; the end-closures of the cavities were adjustable so that cavity tune could be varied. Five high frequency pressure transducers were used. Three were located in the cavities, two in the chamber. The cavity transducers were located in the end closures and at the intersection of cavities for the parallel leg designs, and at the entrance and base of each cavity in the series arrangement. The chamber instruments were located near the injector and in the end closure plate of the injector.

Two driver locations were utilized: one near the injector face/chamber wall intersection, the other at the far end of the chamber.

VI, Acoustic Modeling (cont.)

C. PROCEDURE

The test procedure involved sweeping the frequency range of interest (400 to 1400 Hz) to identify all of the modes of the chamber/cavity combination, using the pressure transducer reading as well as visual observation of the cork dust. The signal generator was then set at the various resonant frequencies and power input to the driver adjusted to a constant 25 watts; the amplitude meter gain was adjusted to yield full scale deflection for this condition. The frequency was then varied above and below the resonant value until the amplitude was reduced by 3db or to 0.707 of its full scale value. The bandwidth across the reduced amplitude points, Δf, and the resonant frequency, f_o, were thereupon recorded.

Cavity resistance was inferred from the ratio of pressures measured at the entrance and back of the cavity. The analyzer could be operated to give the phase and amplitude ratio of any of the five input frequencies. As a check on noise and electrical interference the same signal could be input to both channels of the analyzer; the phase and amplitude ratio should be 0° and 1.0 in that case. Generally, a reading within 2° (phase) and 0.1 (amplitude ratio) was considered acceptable for measurement purposes.

D. MODAL PATTERNS

Various modal patterns delineated by the cork dust in the chamber are shown on Figures 3 through 6. Figure 3 shows the first width (1W) mode with and without cavities; the scale of the test fixture is also shown. With zero length cavities the 1W resonant frequency is 823 Hz. Addition of 4.5 in. cavities depresses the 1W mode to 585 Hz.

Width Mode Shapes

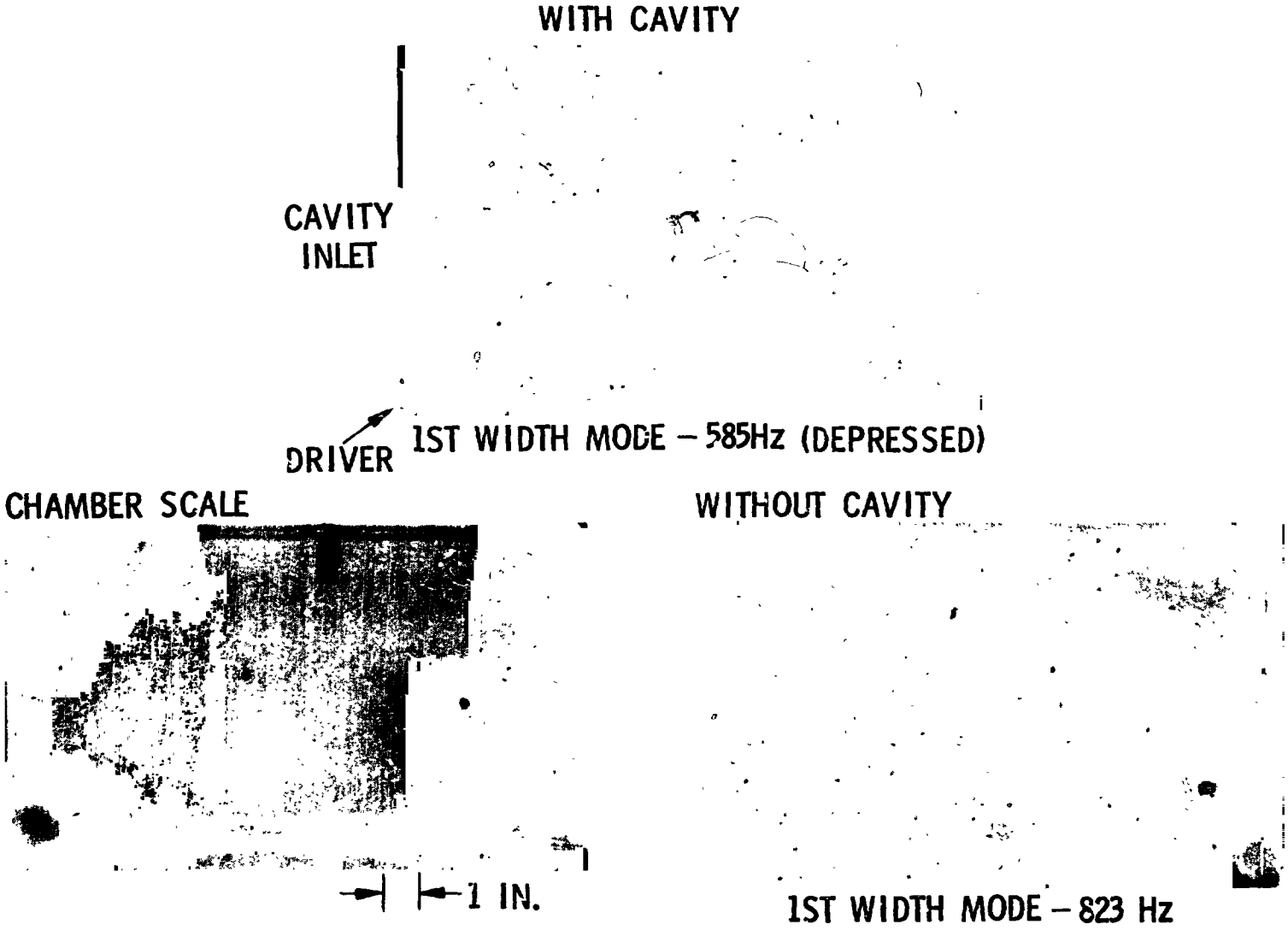

Figure 3

VI, D, Modal Patterns (cont.)

Figure 4 shows the first and second longitudinal modes, 1L and 2L, with and without cavities. The third longitudinal mode, 3L, is pictured on Figure 5. Finally, the combined modes, 1W + 1L and 1W + 2L, are given on Figure 6.

E. SINGLE CAVITY TESTING

Initial testing was done with single (one leg) cavities to establish a baseline for dual (two leg) cavity performance and to validate the test setup and experimental procedure.

Bandwidth measurements maximized with a cavity length equal to the calculated 1/4 wave length of the 1W mode in the chamber without cavities. The effective length of the "axial" cavity proved to be about 20% longer than that of the "radial" cavity, as shown on Figure 7; length here is defined as centerline distance from the cavity backwall to the cavity entrance at the chamber wall, and "radial" is in reference to the centerline of the simulated chamber. The explanation for the increased effective length of axial cavities is not apparent.

The 1W mode frequency was depressed by the single cavities, as expected. Figure 8 shows the depressed frequency and corresponding bandwidth as a function of cavity length. Damping ratio, $\delta/\delta c$, as defined by bandwidth and resonant frequency

$$\delta/\delta_c = \Delta f/2f_o$$

increased with cavity length to the maximum length tested, 5 in., as shown in Figure 9. It is notable that cavity lengths less than 1/8 wave length based on the undepressed 1W mode had limited damping effect.

Longitudinal Mode Shapes

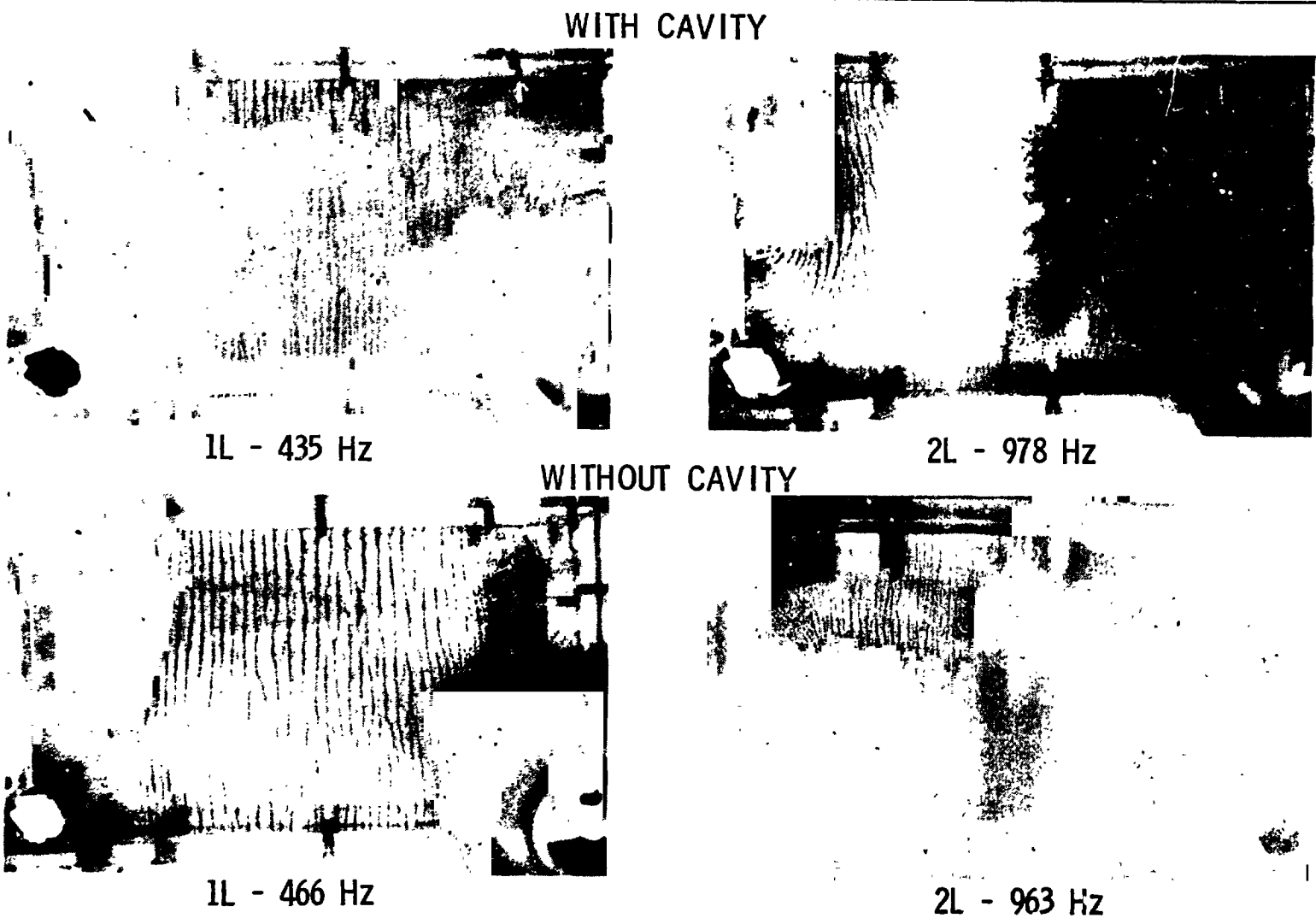

Figure 4

Longitudinal Mode Shapes

WITH CAVITY

3L 1428 Hz

CAVITY END

DRIVER

WITHOUT CAVITY

3L 1425 Hz

Aerojet Liquid Rocket Company

Figure 5

Combined Modes

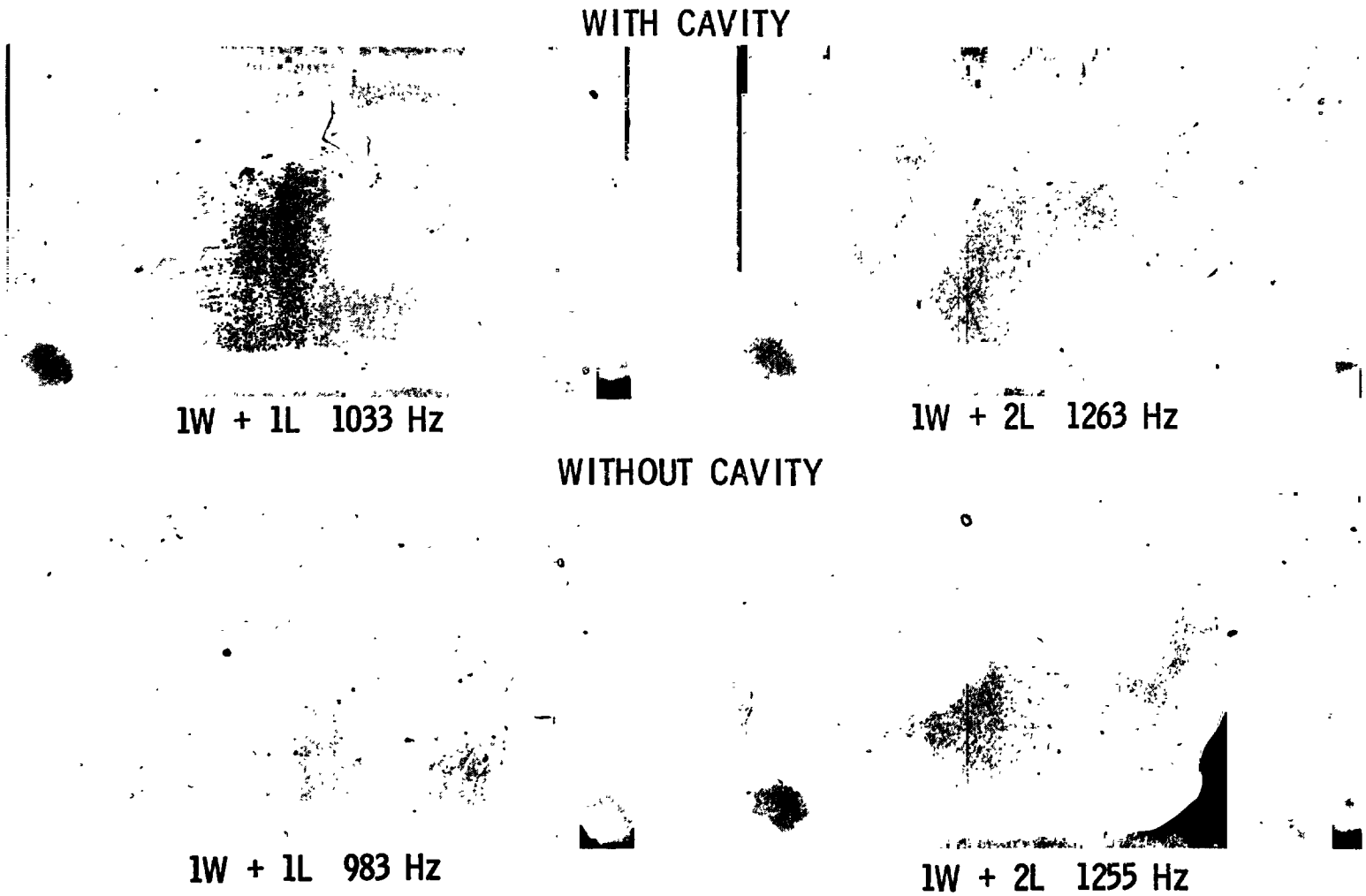

Figure 6

Single Cavity Survey

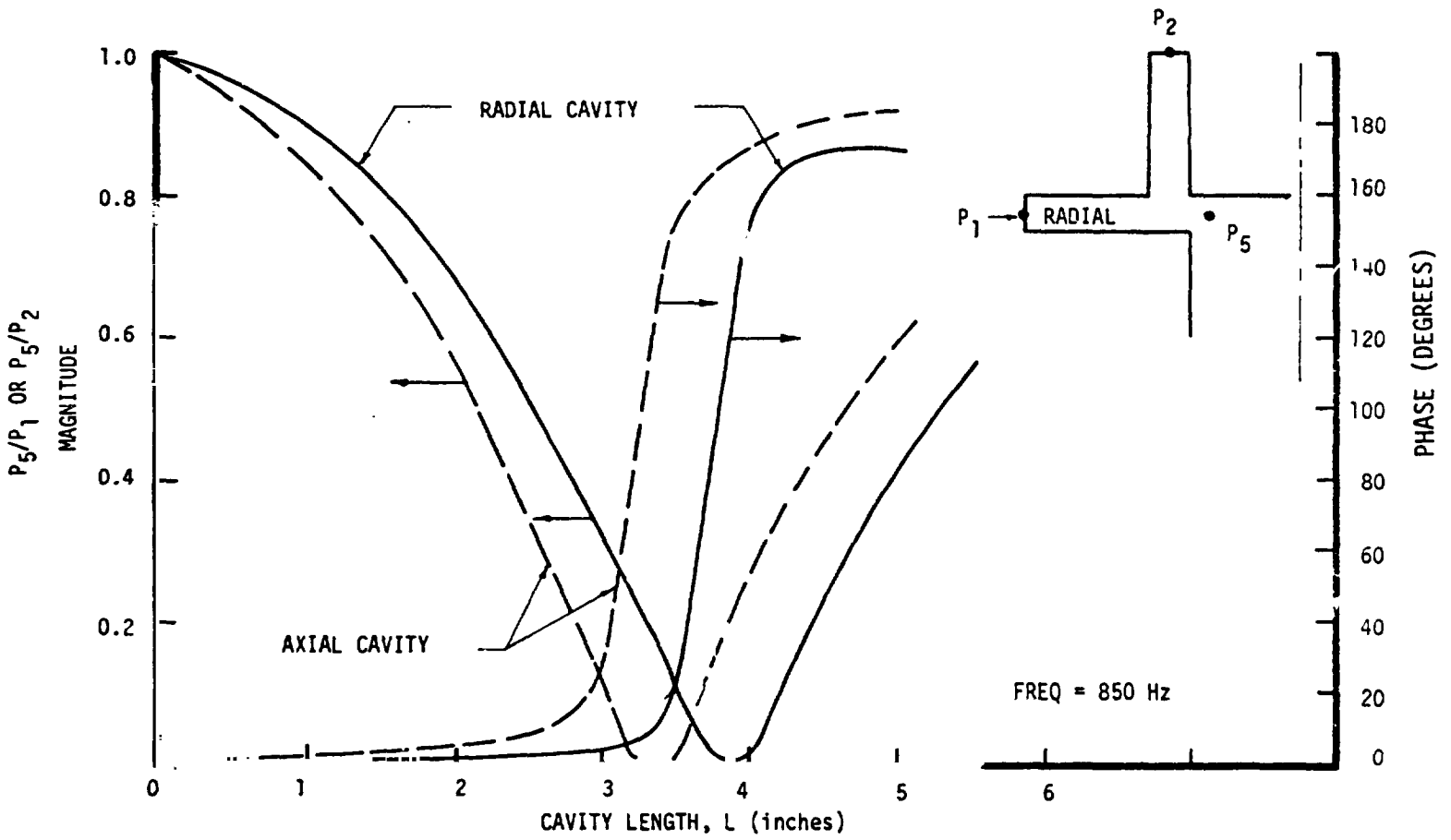

Aerojet Liquid Rocket Company

Figure 7

Bandwidth And Frequency Depression For A Single Cavity vs Length

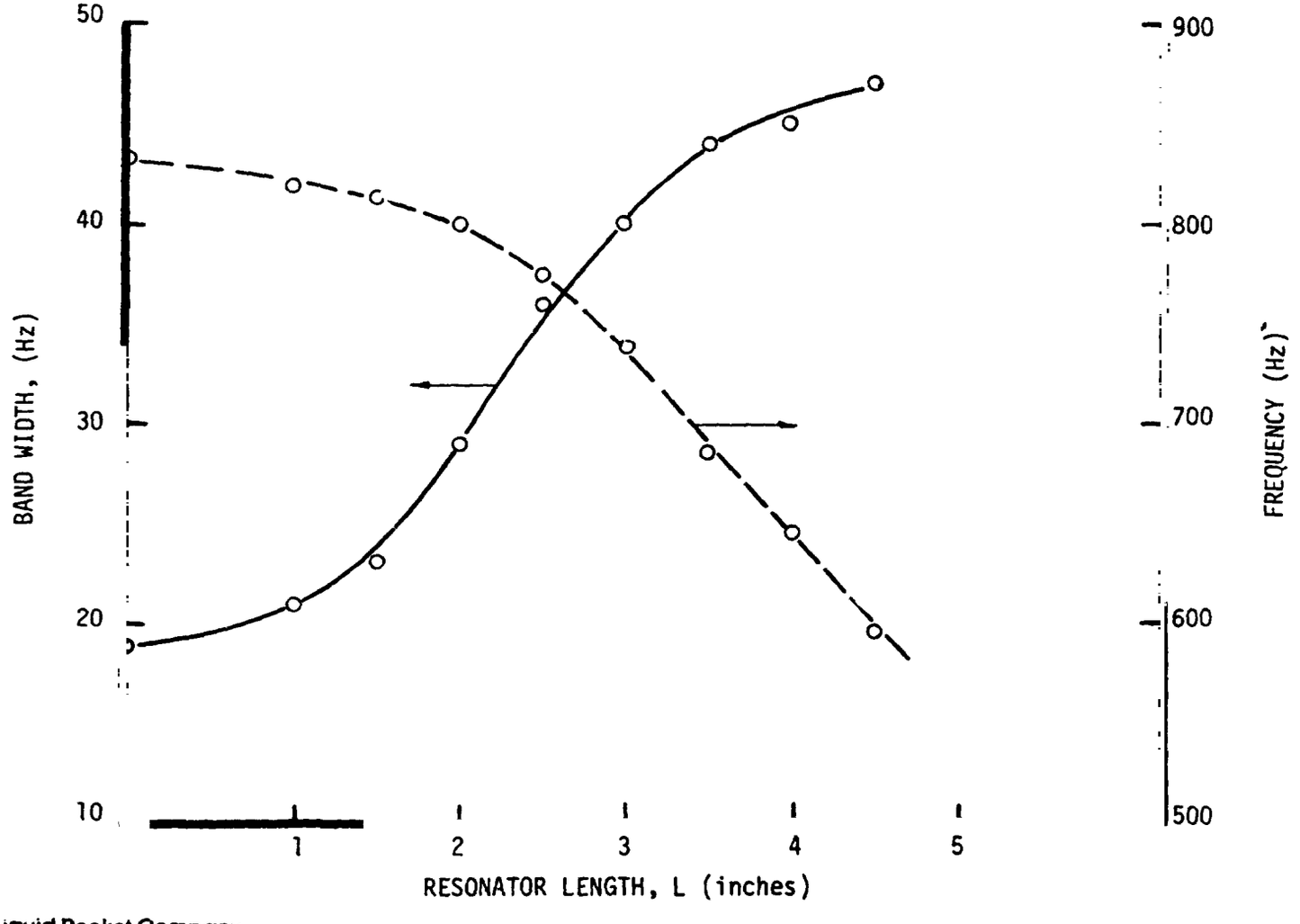

Aerojet Liquid Rocket Company

Figure 8

Damping Ratio vs Resonator Length For a Single Cavity

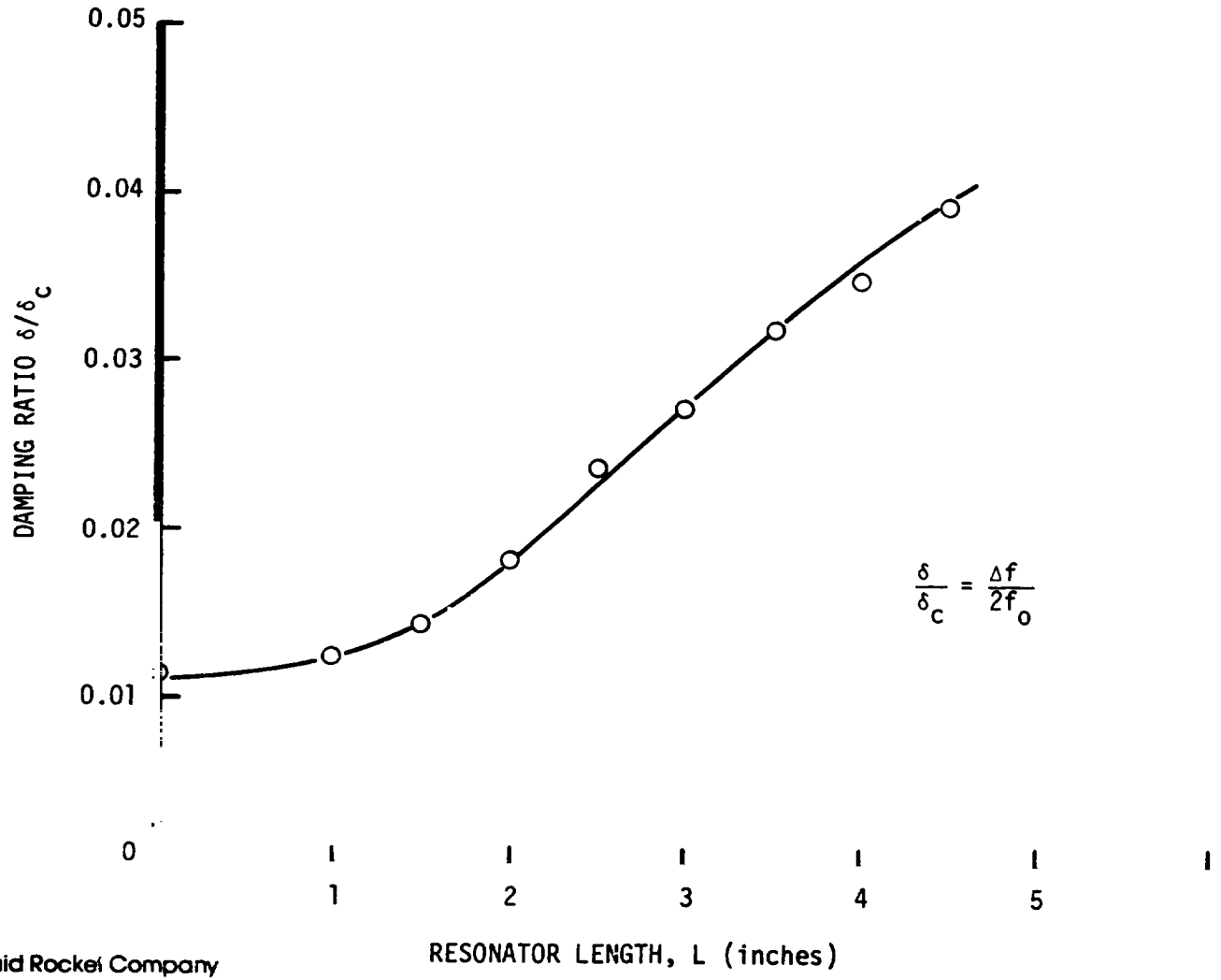

Aerojet Liquid Rocket Company

Figure 9

VI, E, Single Cavity Testing (cont.)

An investigation was made to determine if radial or axial cavities provide more damping. Results are shown on Figure 10 for the combined 1W + 1L mode, which was selected on the basis of being representative of the undamped chamber frequency. With shorter cavities, the radial configuration is superior; with longer cavities the axial configuration is superior.

Damping characteristics for various axial cavity lengths and all chamber modes between 400 and 1400 Hz are summarized in Figure 11 which plots bandwidth versus the ratio of depressed chamber frequency to theoretical resonant frequency of the cavity based on actual length. Damping is maximized at a frequency ratio of 0.8 approximately, i.e., at a point where the chamber frequency is depressed about 20% from cavity resonance. Thus the cavity gives the appearance of having an effective length about 20% greater than the actual length.

F. DUAL CAVITY TESTING

Most of the testing of dual cavity configurations involved cavity lengths of 4.0 and 2.0 in., which correspond respectively to maximum suppression of the 1T mode and midrange suppression of the 2T and 1R modes in the hot fire hardware.

To identify the interaction between the two cavity legs, one series of tests was conducted with both legs the same length, however, This condition would result in both cavities being equally active and produce maximum interaction in terms of velocities at the cavity intersection. The test procedure was identical to that of the single cavity tests wherein the frequency of the driver and the power input were held constant while cavity length was varied. Results are summarized in Figure 12. Both cavities were found to have equal effective lengths, which is contrary to the single cavity test results in which the axial cavity appeared to have a longer effective length, and the effective lengths appeared to be 25% greater than the actual centerline distances. For cavity lengths greater than the 3 in. resonant length, the

Axial vs Radial Cavity Bandwidth (1W 1L Mode)

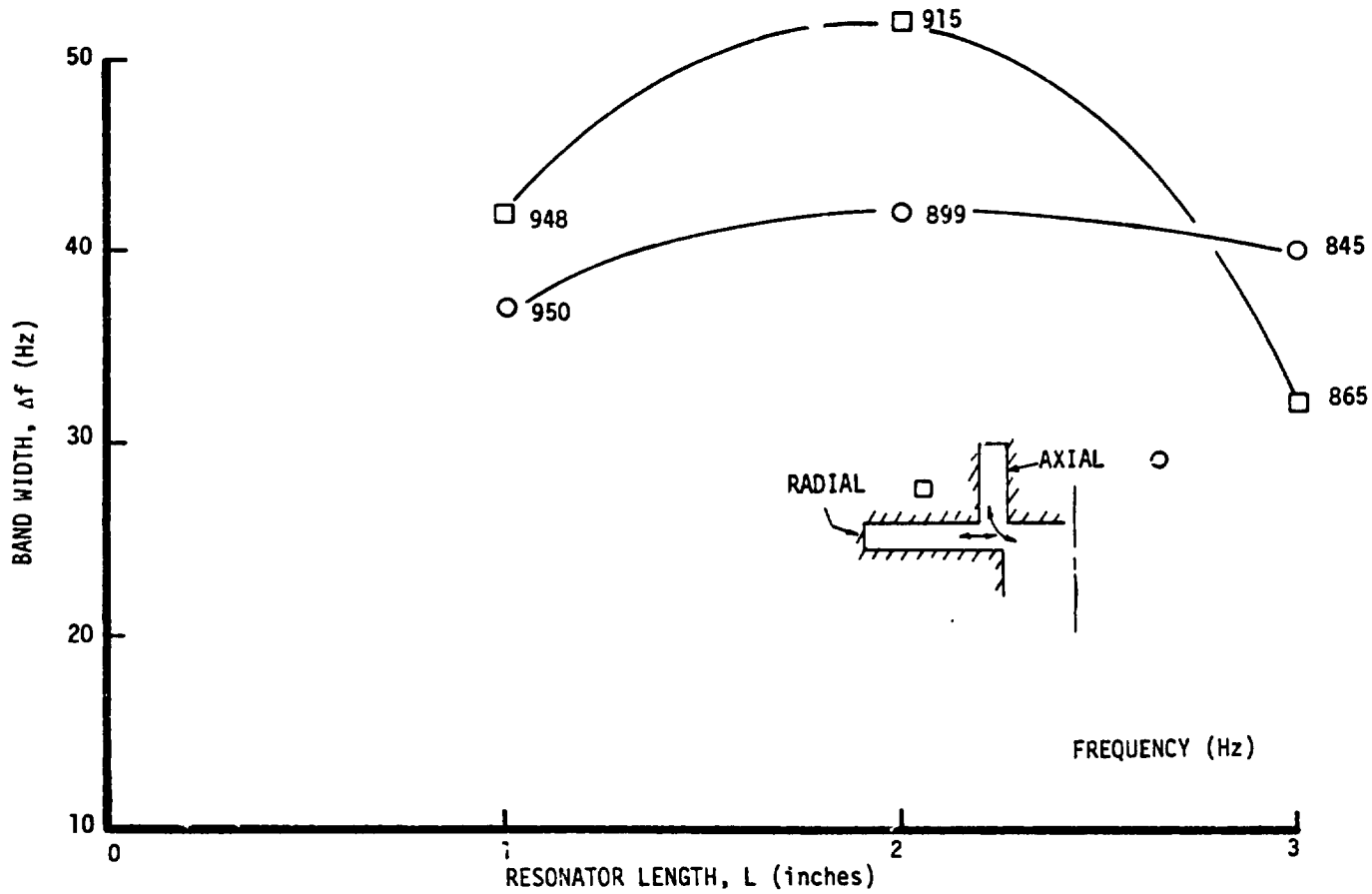

Figure 10.

Effective Cavity Tune

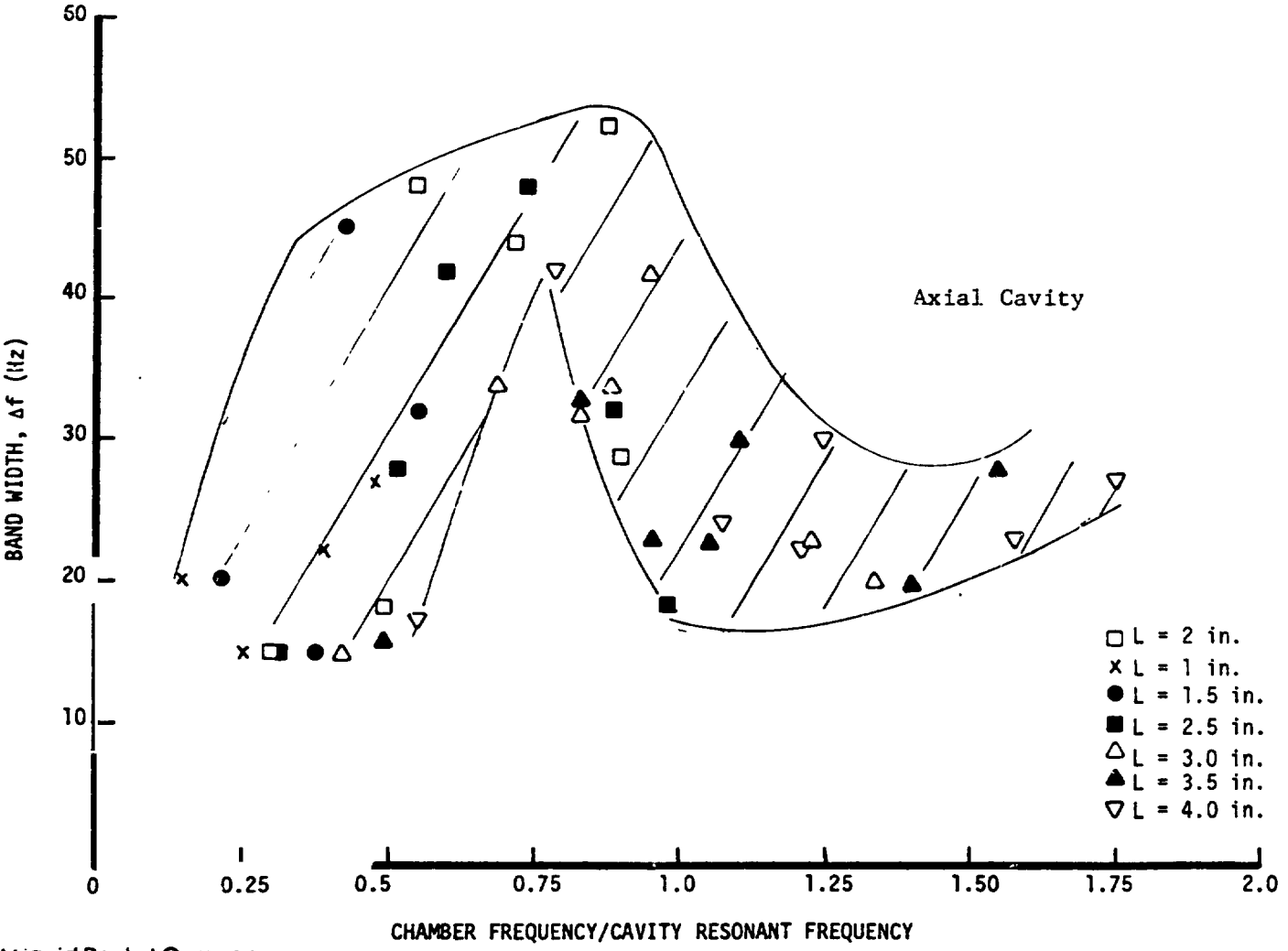

Aerojet Liquid Rocket Company

Figure 11
Page 28

Dual Cavity Survey

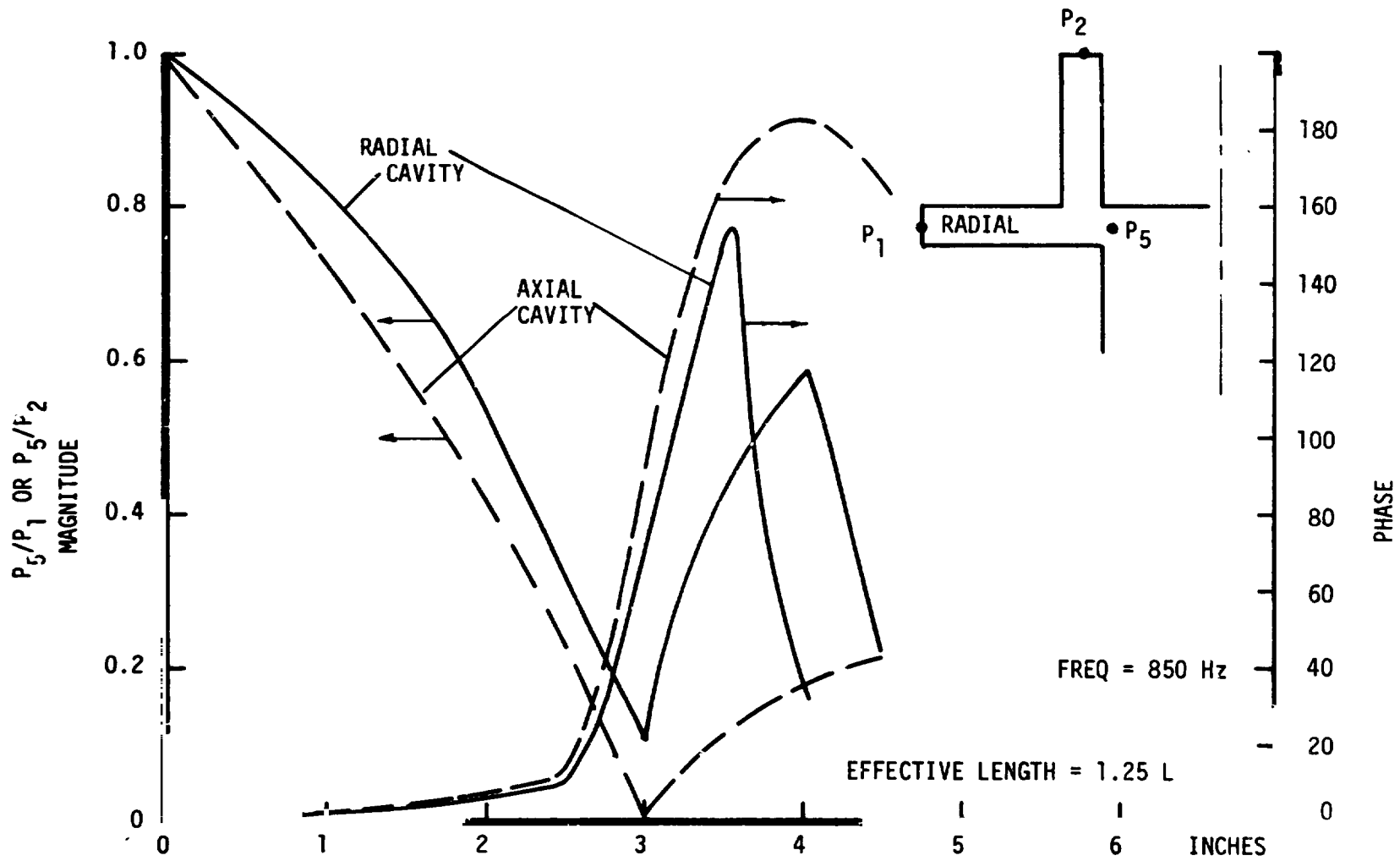

Aerojet Liquid Rocket Company

Figure 12

pressure amplification does not continue as it did with single cavities, indicating a possible interaction between cavities.

Cork dust patterns within the cavities gave further evidence of cavity interaction. With cavity lengths of 2.0 and 4.0 in., and a frequency of 840 Hz, only the 4.0 in. leg showed any activity, since it was approximately 1/4 wave length. At a frequency of 1670 Hz activity in the 2.0 in. leg was maximum since it corresponded to 1/4 wave length; activity in the 4.0 in. cavity was nil since it approximated a 1/2 wave length.

Interaction between the two cavities was further explored with the resonator at 2 and 4 in. by exciting the system with two frequencies simultaneously. Attention was focused on frequencies of approximately 600 and 1450 Hz as they approximate the ratio of the modes expected in the hot test engine. The results of these tests are tabulated below; the bandwidth, f_o, is measured about the frequency, and damping ratio, δ/δ_c, is also calculated on that basis.

DUAL FREQUENCY SUMMARY, $L_1 = 4.0$, $L_2 = 2.0$ IN.

Test	f_o	Δf_o	f_1	Damping Ratio at f_o $\frac{\delta}{\delta_c} = \frac{\Delta f_o}{2f_o}$
1	586	52	0	.045
2	586	52	870	.045
3	591	43	1430	.035
4	1473	38	0	.015
5	1473	38	613	.015

The higher frequency, if sufficiently high, can influence damping of the lower frequency, as can be seen by comparing tests 1 and 3; intermediate

frequencies have no such effect, however, to wit tests 1 and 2. A possible explanation for this behavior is found in the single cavity tests -- Figures 8 and 9 -- which showed that as long as the cavity length was less than 1/8 wave length the cavity had little effect.

The lower frequency did not, however, affect damping of the higher frequency, i.e., tests 4 and 5 wherein the damping ratio is calculated for the higher frequency.

Damping characteristics for all dual cavity configurations tested are presented in Figure 13. These configurations include a series arrangement as well as three parallel leg arrangements, with the legs at 0, 45, and 90°, and a no cavity configuration. Leg lengths of 2 and 4 in. were utilized in the parallel arrangements. Various modal patterns are noted; these include the 1L, 2L, 3L, 1W and depressed 1W, and the combined modes 1W + 1L, 1W + 2L, and 1W + 3L.

For the depressed first width mode, the 0° parallel leg configuration provided the greatest amount of damping, followed by the 45 and 90° parallel arrangements, and better damping was obtained with the 4 in. leg adjacent to the injector. The closeness of the bandwidth data does temper the validity of these assessments however.

G. RESISTANCE MEASUREMENTS

One test series was devoted to determining the resistance across the cavity entrance; a single 4 in. radial cavity was used for this purpose. The procedure involved measuring the pressure -- amplitude and phase angle -- at three locations as shown on the accompanying sketch and solving the equations

Bandwidth vs Frequency for Dual Cavity Configurations

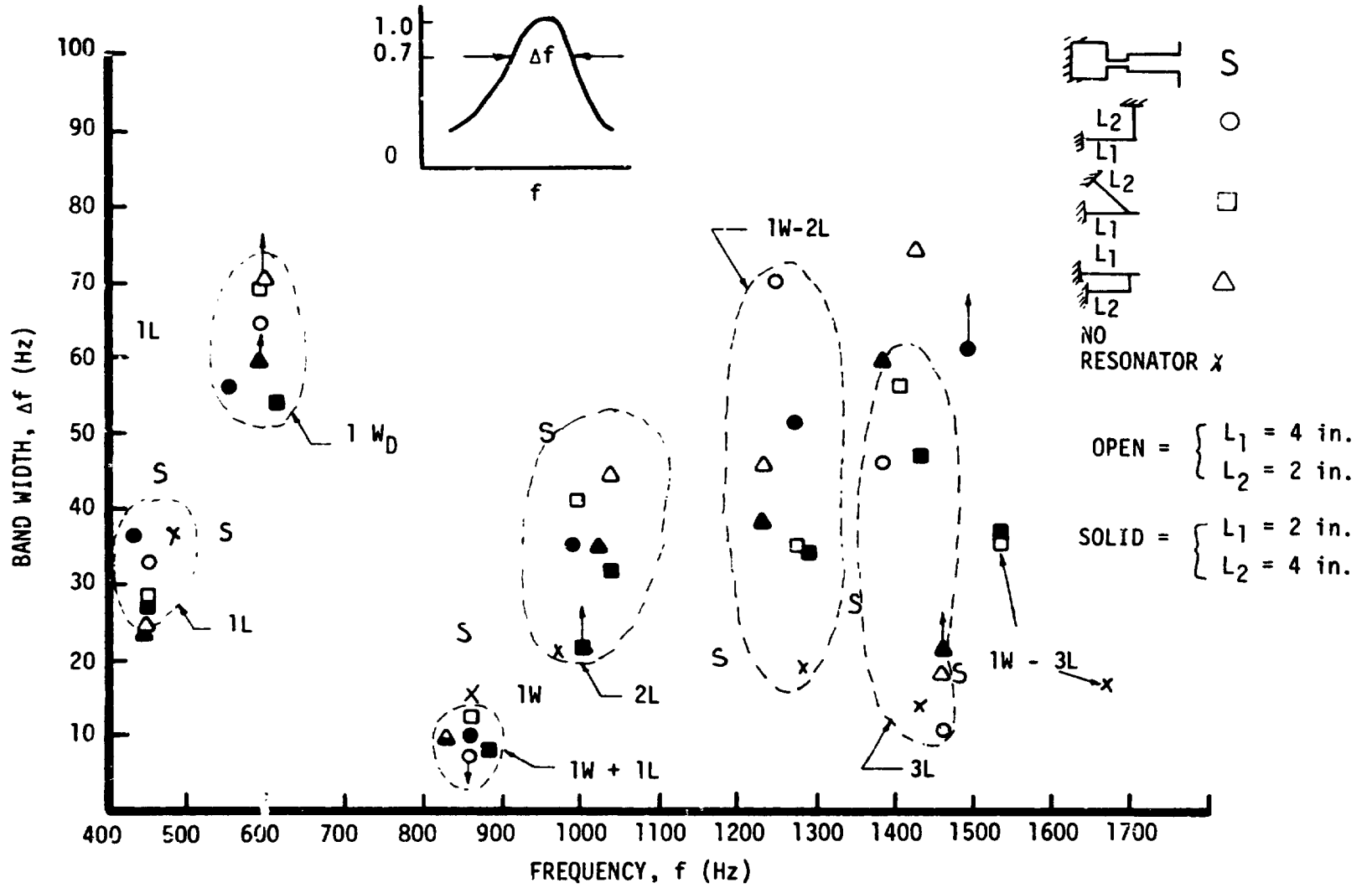

Figure 13

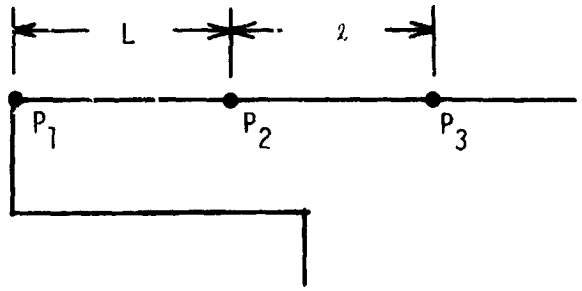

developed below. Although the method is straightforward, measurement accuracy is limited at anti-resonant points because of the low signal-to-noise ratio.

Considering a short section of the cavity which includes the entrance, a force balance will be given by

$$\left(P_3' - P_2'\right) A - Ru' = \frac{\rho \ell A}{g} \frac{\partial u'}{\partial t}$$

where P' is the fluctuating component of pressure, u' is the velocity, A the cross-sectional area, ρ the density, g the gravitational constant, and t time. Assuming u' to be sinusoidal

$$u' = u_o e^{i\omega t}$$

$$\frac{\partial u'}{\partial t} = i\omega u_o e^{i\omega t} = i\omega u'$$

and the first equation can be rewritten

$$\left(\frac{P_3'}{P_2'} - 1\right) = \frac{R}{A} \frac{u'}{P_2'} + \frac{i\omega\rho\ell}{g} \frac{u'}{P_2'}$$

From the simple wave equation

$$\frac{\partial^2 P}{\partial x^2} = \frac{1}{C^2} \frac{\partial^2 P}{\partial t^2}$$

VI, G, Resistance Measurements (cont.)

and the momentum equation for acoustics

$$\frac{\partial P}{\partial x} = -\frac{\rho}{g}\frac{\partial u}{\partial t}$$

It can be shown that

$$\frac{u'}{P_2'} = -\frac{ig}{\rho c}\tan\frac{\omega L}{c}$$

and substitution into the rewritten first equation gives

$$\left(\frac{P_3'}{P_2'} - 1\right) = -\frac{iRg}{A\rho c}\tan\frac{\omega L}{c} + \frac{\omega \ell}{c}\tan\frac{\omega L}{c}$$

Equating real and imaginary parts yields

$$\text{Real: } \left(\frac{P_3'}{P_2'}\right)_R = \frac{\omega \ell}{c}\tan\frac{\omega L}{c} + 1$$

$$\text{Imaginary: } \left(\frac{P_3'}{P_2}\right)_I = \frac{-Rg}{A\rho c}\tan\frac{\omega L}{c}$$

or, if ϕ is the phase angle between P_3' and P_2'

$$\frac{P_3'}{P_2'}\cos\phi = \frac{\omega \ell}{c}\tan\frac{\omega L}{c} + 1$$

$$\frac{P_3'}{P_2'}\sin\phi = \frac{Rg}{A\rho c}\tan\frac{\omega L}{c}$$

VI, G, Resistance Measurements (cont.)

The phase angle ϕ is determined directly by the co-quad analyzer, as is the pressure ratio P_3'/P_2', and $\frac{\omega L}{c}$ is determined from $\cos^{-1}\left(\frac{P_2'}{P_1'}\right) = \frac{\omega L}{c}$. Hence, both ℓ and R can be found.

Results are shown on Figures 14 and 15. Figure 14 presents the calculated length, ℓ; since the actual length is 0.5 in. the correspondence of calculated and actual values serves as a check on the validity of the procedure. For the case of most interest, the pressure node and velocity antinode were located between P_2 and P_3 -- i.e., the cavity was resonant -- and reasonable correspondence was obtained. At lower frequencies, this was not the case and in two regions the signal-to-noise ratio was insufficient to yoeld meaningful results. The calculated nondimensional resistance is shown in Figure 15; in the frequency range of interest a value of about 0.1 is indicated. This corresponds to a typical figure used in design evaluations.

H. CONCLUSIONS

The acoustic modeling perhaps raised more questions than were answered. In hindsight it is clear that certain tests might better have been done differently and that other tests might have yielded more useful information. This was somewhat of a pioneering effort, however, and little previous work was available for guidance. The bench tests did lead to the following conclusions:

(1) A dual resonance condition can be achieved with a dual leg, single entrance cavity.

(2) The damping of the lower frequency leg may be decreased by interaction with the higher frequency leg.

(3) The 0° parallel leg configuration appears to offer the maximum damping of the primary mode of interest, the depressed first width mode.

CALCULATED LENGTH

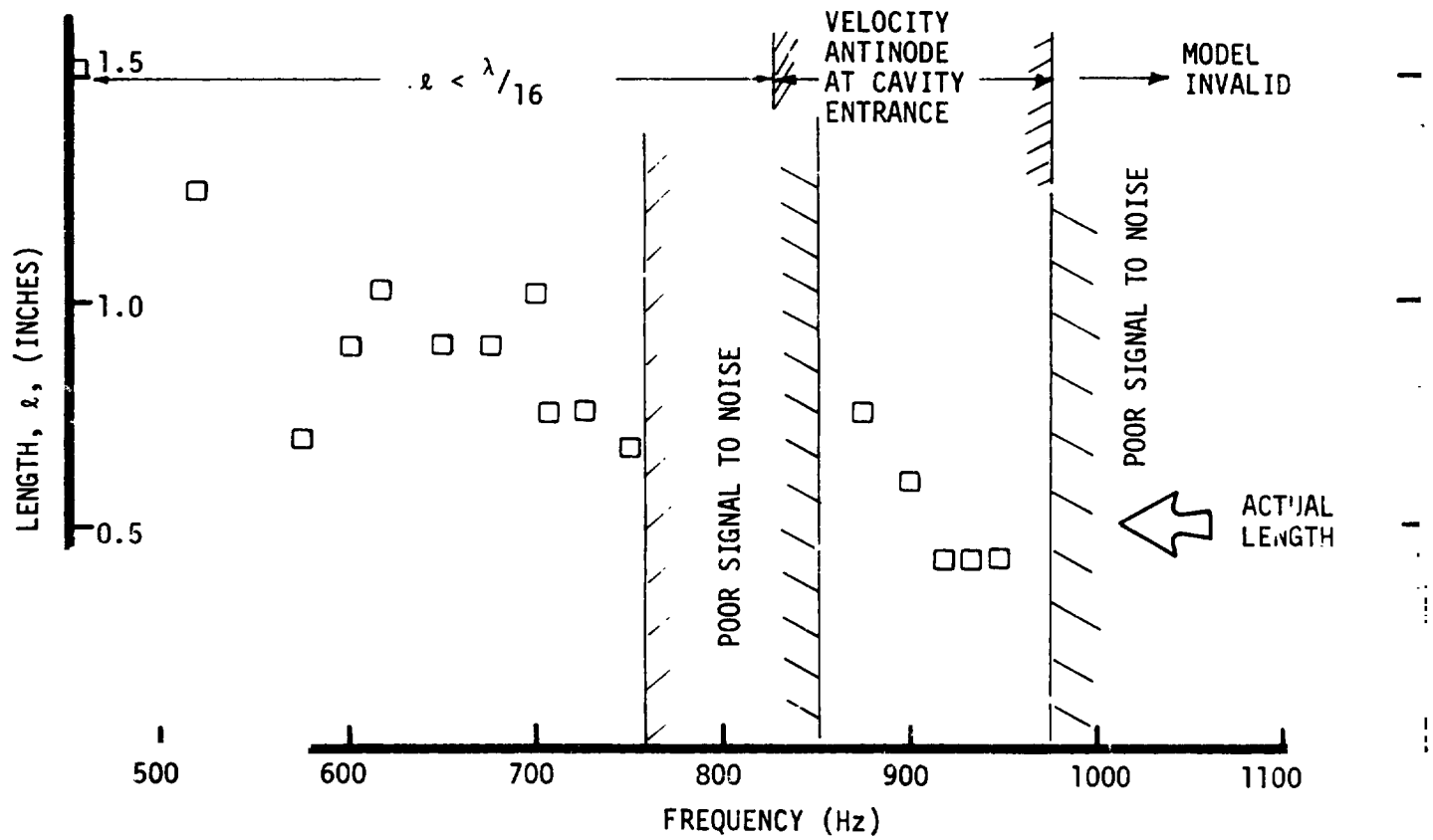

Aerojet Liquid Rocket Company

Figure 14

CALCULATED RESISTANCE

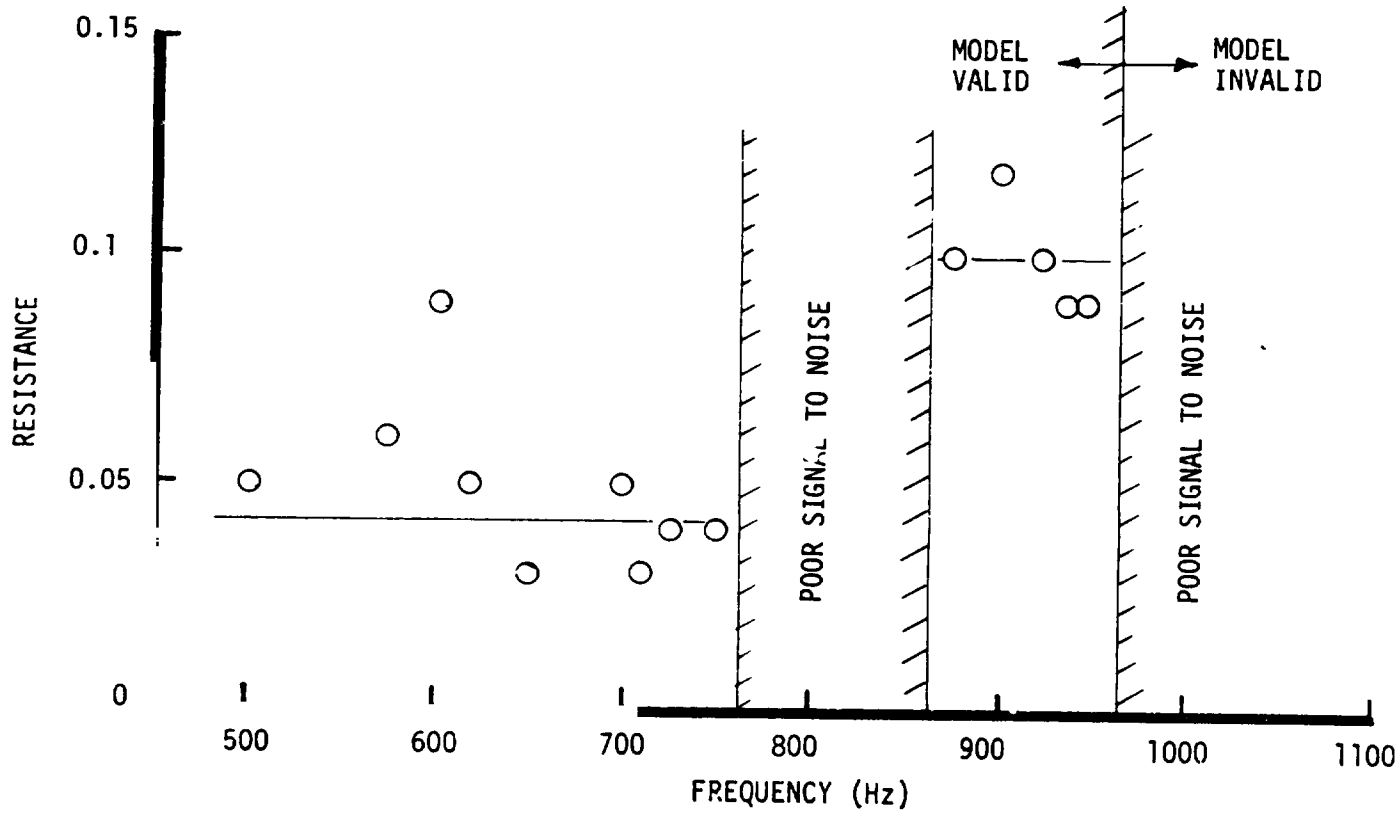

Figure 15

VI, H, Conclusions (cont.)

(4) Each cavity leg appears to use the entire entrance area for damping.

(5) The preferred location of the longer cavity is adjacent to the injector face, for the depressed first width mode.

(6) In single cavity tests, the L-shaped cavity appears to have an acoustic length 20% longer than the mean centerline length.

(7) Linear analysis of the cavity entrance resistance appears feasible over a limited frequency range near the cavity resonant point. Elsewhere, large errors are indicated or the signal-to-noise ratio is poor.

(8) Cork dust patterns observed in the cavities were useful in defining acoustic lengths in the analysis of hot fire configurations.

VII. ANALYTICAL METHODS

Stability prediction at ALRC enjoys a moderate degree of success using a computer program called IFAR--Injector Face Acoustic Resonator--which is based on the Crocco-Reardon sensitive time lag combustion model[1]. The significant advantage of IFAR over other analytical techniques is that it directly evaluates the effect of damping devices on combustion stability.

The component parts of the IFAR program are illustrated in Figure 16. Basically, IFAR solves the wave equation for the chamber geometry; the boundary condition at the injector end is defined by the combustion gas generation rate and the resonator or baffle admittance; at the other end the boundary condition is specified by the nozzle admittance. The combustion gas generation rate is derived from the Crocco-Reardon model which assumes a dead time exists between propellant injection and propellant combustion. The model further assumes that the combustion process becomes "sensitive" to the pressure field during a sensitive time period just prior to vaporization, which is considered instantaneous. The result is a pressure interaction index parameter, n, which describes the level of combustion sensitivity, and a sensitive time lag parameter, τ, which describes the combustion frequency sensitivity. The gas generator rate can therefore be described as a function of the n-τ parameters.

Resonator admittance is calculated by means of a wave equation representation which includes the affect of geometry and cavity gas temperature. Nozzle admittance is based on the modified Crocco-Reardon formulation developed by Zinn and Bell.[2] Nozzle admittance is a function of nozzle geometry and combustion gas properties.

---

[1] Crocco, L., and Cheng, S.'., Theory of Combustion Instability in Liquid Propellant Rocket Motors, AGARDograph #8, Butterworth's Sci. Pub. Ltd., London, 1956.

[2] Zinn, B. T., and Bell, W. A., The Prediction of Three-Dimensional Liquid Propellant Rocket Nozzle Admittances, NASA CR-121129, Feb. 1973.

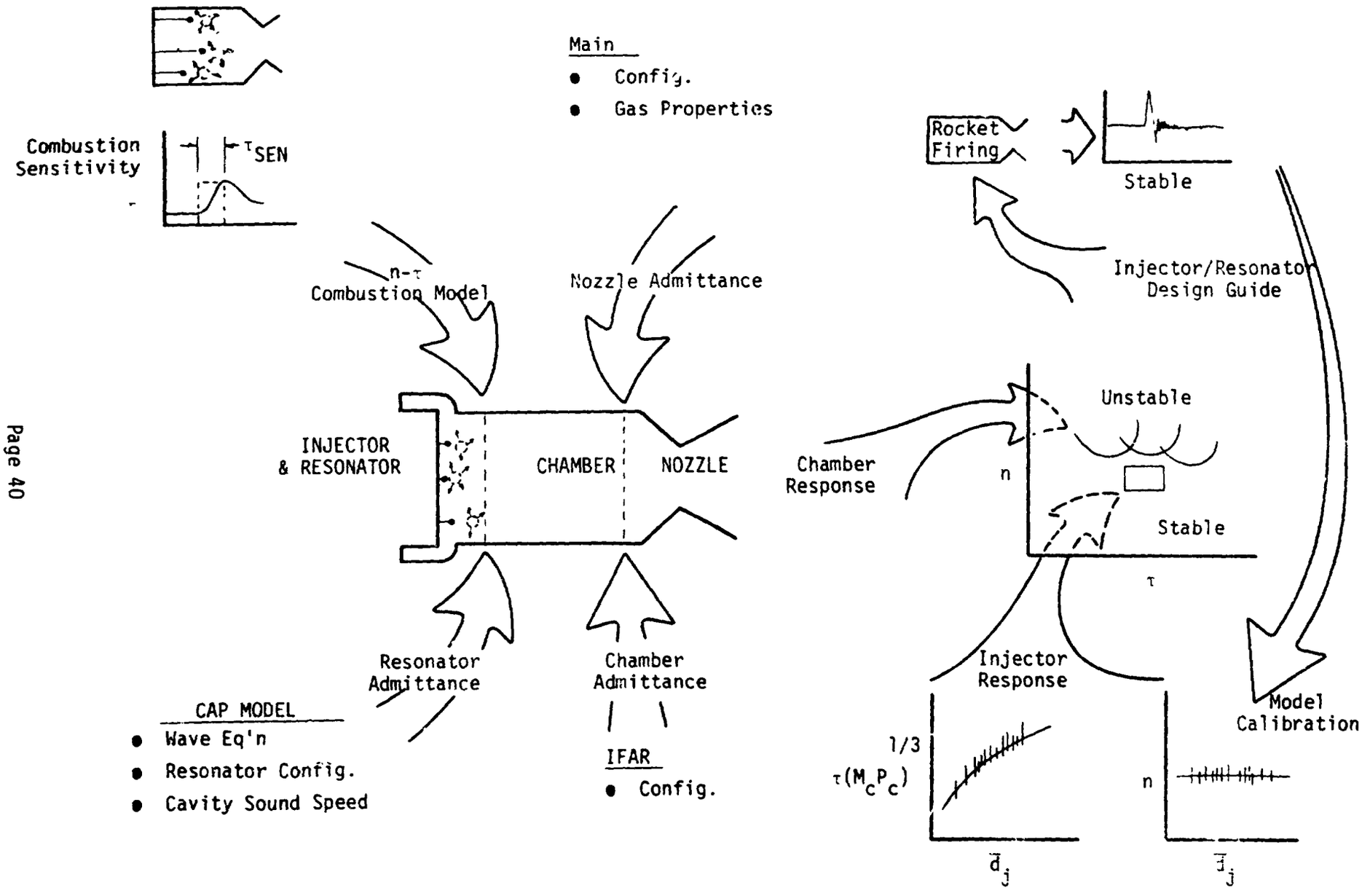

Figure 16. Injector Face Acoustic Resonator Stability Prediction Model

VII, Analytical Methods (cont.)

The IFAR output is a plot of the neutral stability boundary on the n-τ plane as presented in Figure 17. Curves are shown for a typical chamber configuration with and without resonators. Stability is indicated by the position of the injector response (n-τ) box relative to the neutral stability curve. The n-τ box is based on empirical data collected by Reardon,[3] as reproduced in Figure 18.

Upgrading the IFAR program is an ongoing effort at ALRC with the refinement of the cavity admittance calculation, generation of additional injector response data, and accumulation of more-and-more test experience.

[3] Reardon, F. H., et al, The Sensitive Time Lag Theory and its Application to Liquid Rocket Combustion Instability Problems, AFRPL-TR-67-314, March 1968

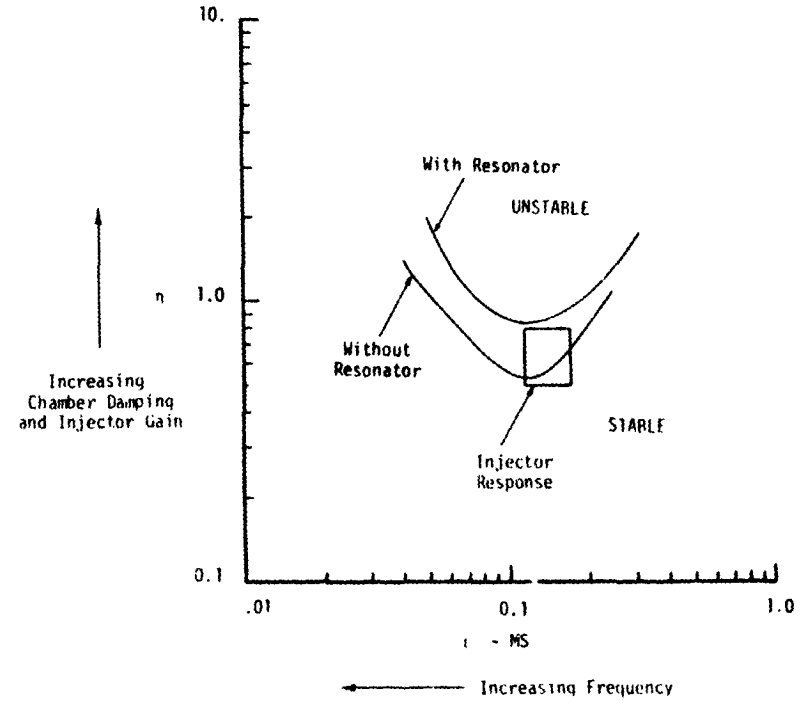

Figure 17. IFAR Stability Predictions

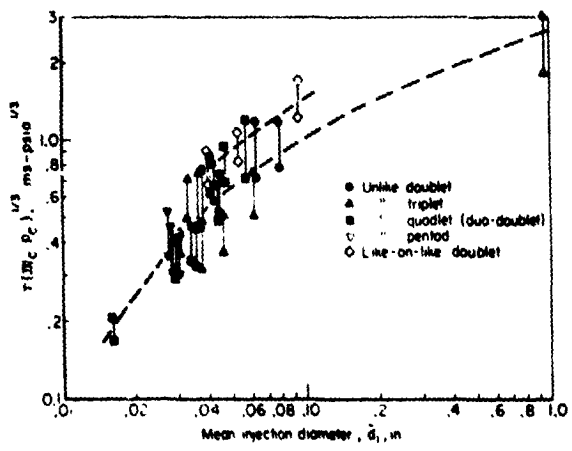

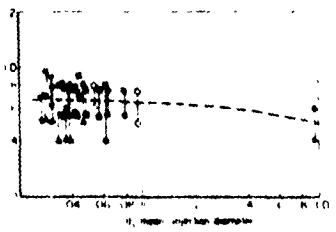

Figure 18. n-τ Injector Response Correlations

VIII. SUBSCALE (PHOTOGRAPHIC) TESTING

A. INTRODUCTION

The subscale or photographic test program was the second phase of the original (dual cavity) test program. Its purpose was to observe the combustion field and propellant flow behavior in the cavity entrance region, using high speed motion picture photography. These visual records, in addition to considerable temperature and pressure data, were intended to advance the understanding of physical events in the cavity and further clarify the mechanism of cavity damping.

The test hardware was a "two-dimensional" (rectangular) configuration, with a width of 1.0-in. in the plane of view, to isolate a limited number of interacting propellant streams and to allow adequate external illumination. Circular quartz windows on either side permitted photographic viewing and external illumination. The injector pattern consisted entirely of X-doublet (XDT) elements in the same orientation, relative to the acoustic cavities, as the identical elements of the full scale hardware. Six cavity designs were evaluated; these encompassed variations in cavity length and inlet configuration.

Forty-five tests were conducted. Most were bombed. Instabilities in the first width (1W) mode were induced with certain cavity configurations and the high speed movies of these are apparently the first ever taken of unstable conditions in the cavity region. Photographic quality was excellent.

The movies showed the propellant streams to be poorly mixed during stable operation, with alternate layers of the two propellants extending--mostly uncombusted--beyond the field of view, approximately 2.0-in. from the injector face. Interaction between the cavity and the main flow field was minimal except that the latter introduced a recirculation pattern in the cavity. The most notable changes arising from unstable operation were that the propellant streams

were completely combusted very near the injector face, the distance varying with the unstable mode frequency, and that the injected streams wavered back-and-forth, also at the unstable mode frequency.

Thermocouple data showed the cavity gas temperature profile to vary with cavity length and to be strongly influenced by inlet geometry. High frequency pressure transducer measurements taken at the entrance and back wall of the cavity allowed the energy loss at the entrance to be inferred and hence contribute to the ongoing effort to analytically model cavity/chamber interactions.

B. HARDWARE, INSTRUMENTATION, TEST FACILITY

The combustion chamber assembly consisted of a U-shaped chamber into which the injector and throat inserts are fitted and to which the side plates are bolted. The side plates each had two quartz windows for photographic purposes; these could be replaced with steel windows having additional temperature and high frequency pressure instrumentation. The injector had 78 elements, each consisting of one fuel and one oxidizer orifice, arranged in an X-doublet pattern which creates parallel and adjacent fans of the two propellants. The 78 elements were grouped in three rows of 26 elements each.

A photograph of the major components of the assembly is presented in Figure 19. Figures 20 through 29 are the design drawings of the individual components and assemblies of the fixture. The major parts are as follows:

Disassembled Hardware, 2-D Testing

Figure 19. Disassembled Hardware, 2D Testing

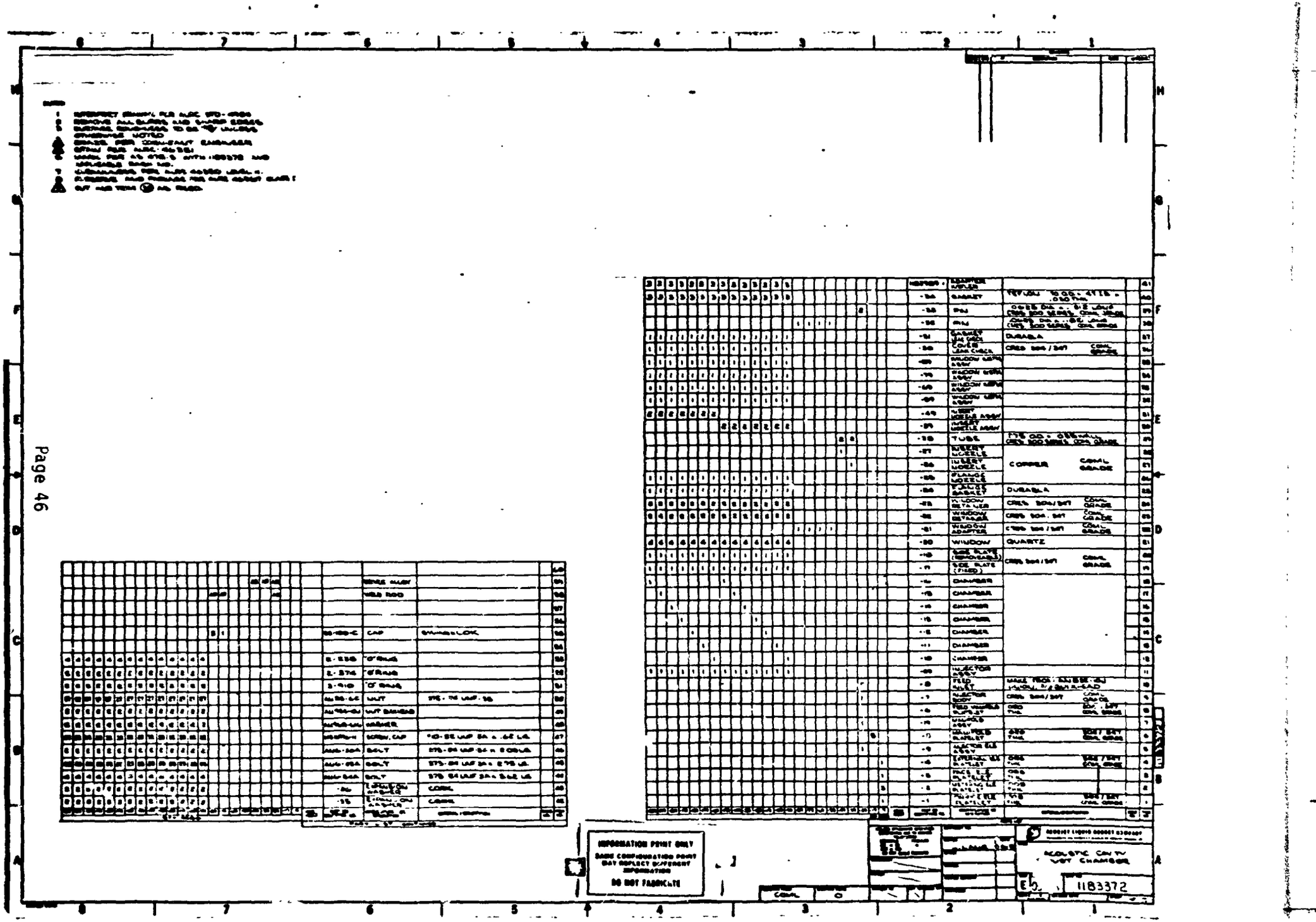

Figure 20. 2D Combustor Assembly Components

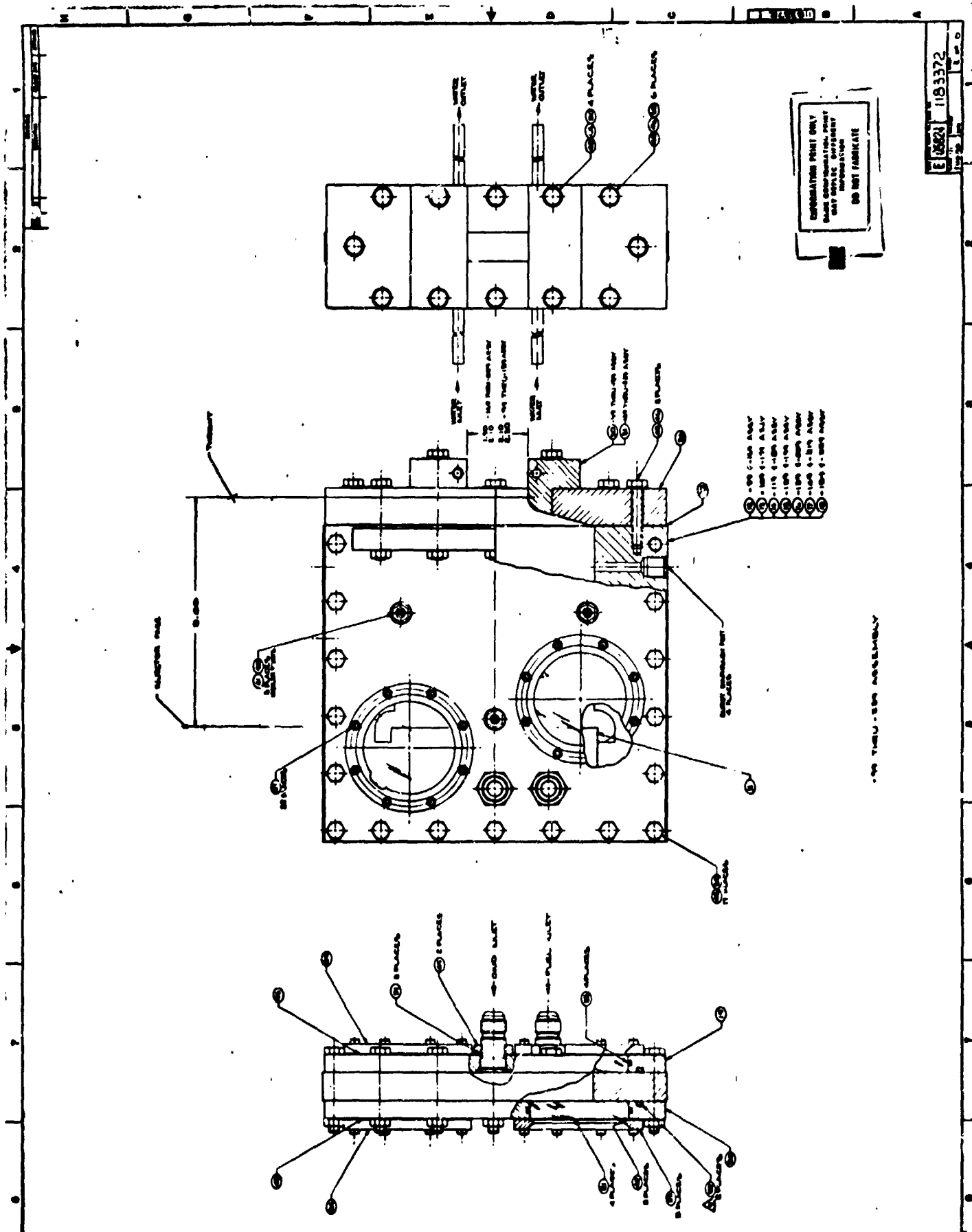

Figure 21. 2D Combustor Top Assembly

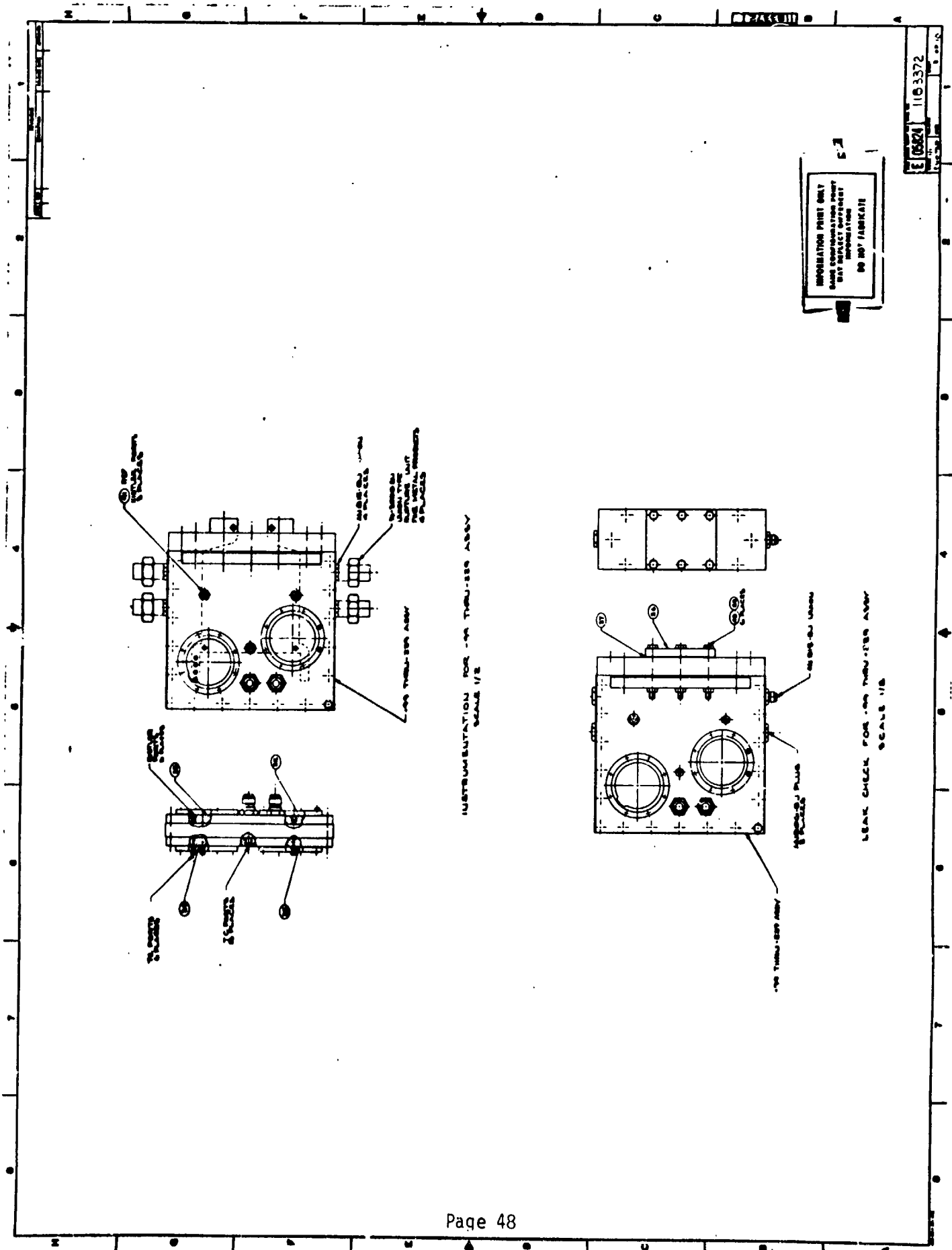

Figure 22. Instrumentation and Leak Check Fixture

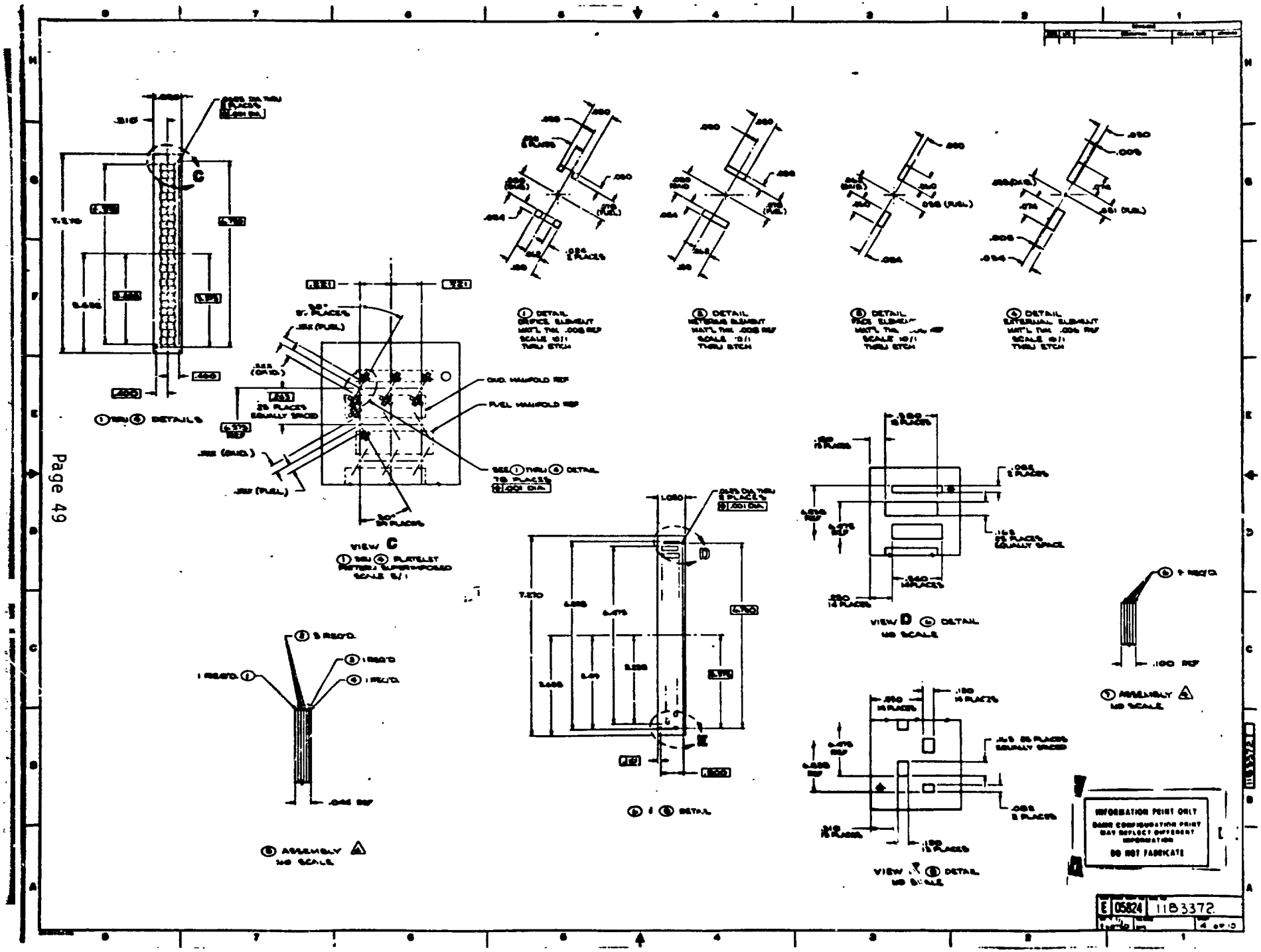

Figure 23. Injector Face Details

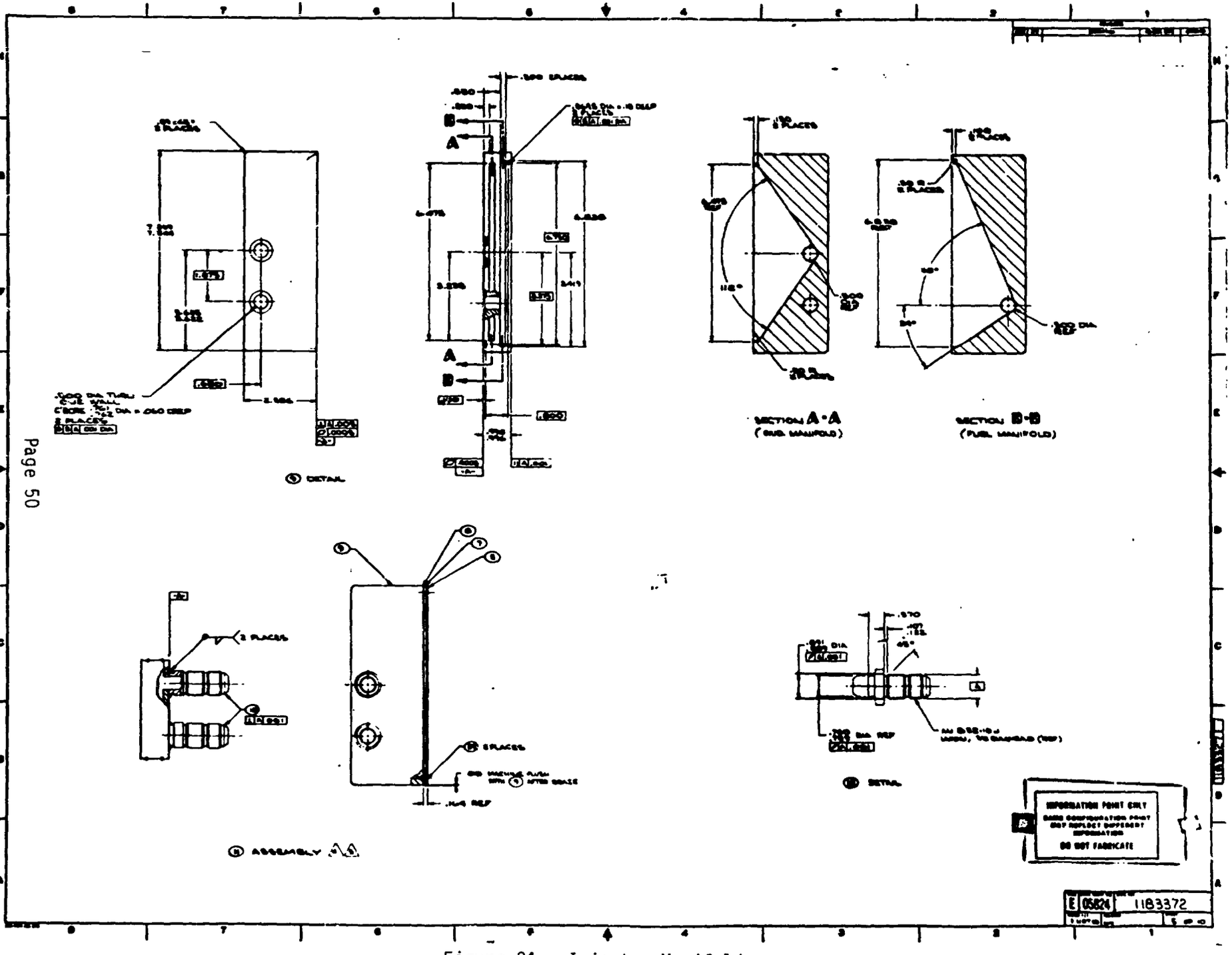

Figure 24. Injector Manifold

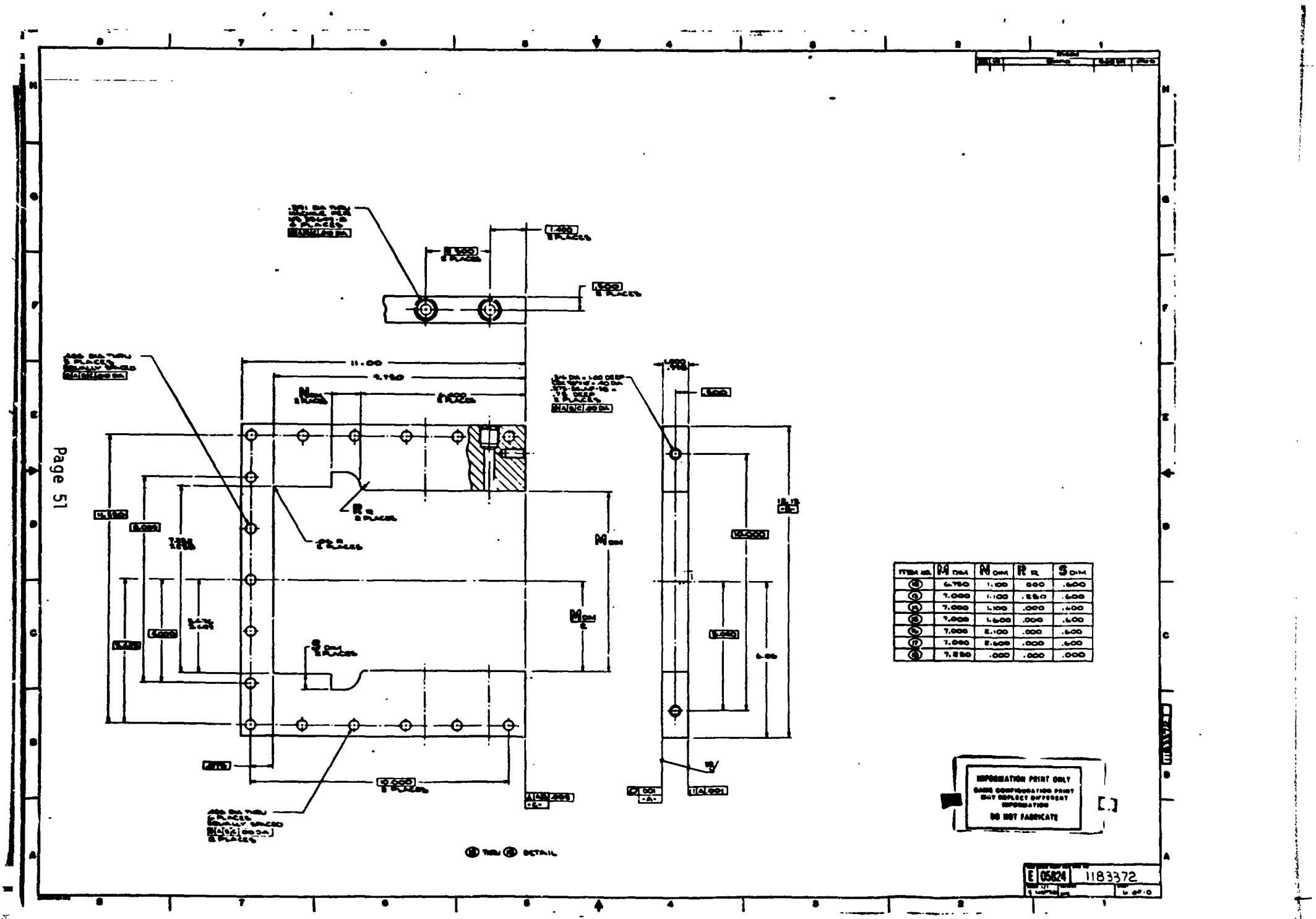

Figure 25. Cavity and Chamber Geometry

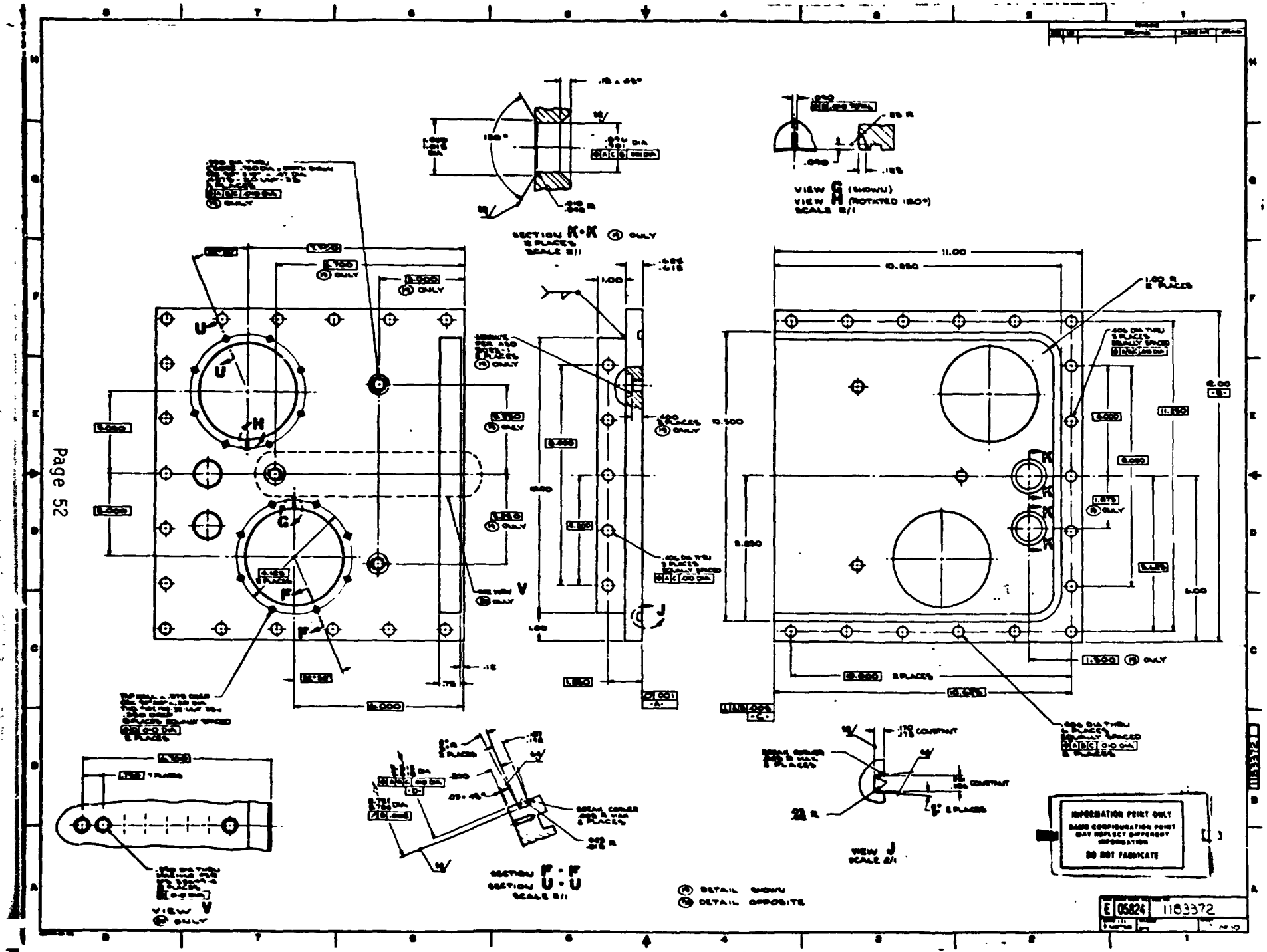

Figure 26. Chamber Side Plates

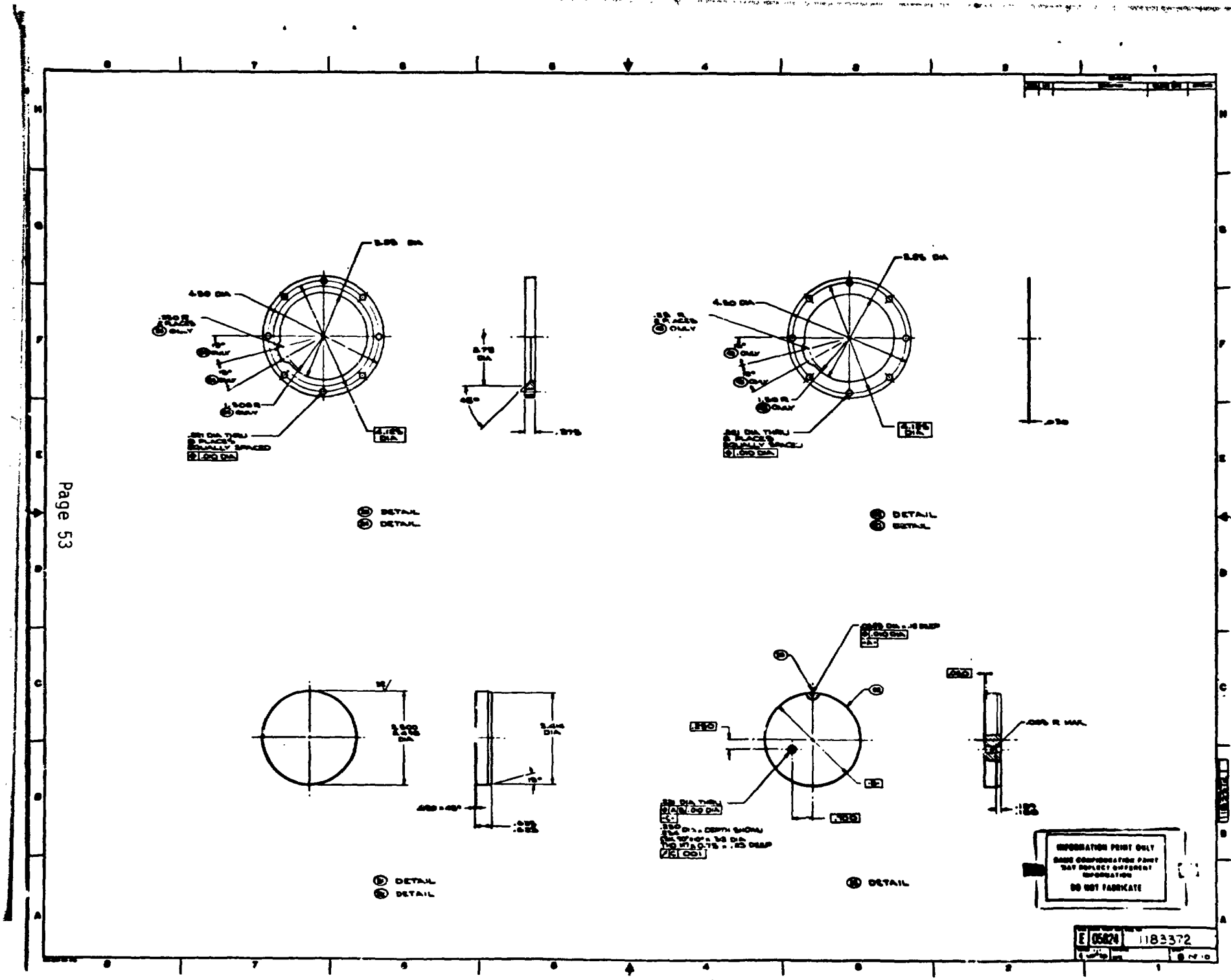

Figure 27. Quartz Windows

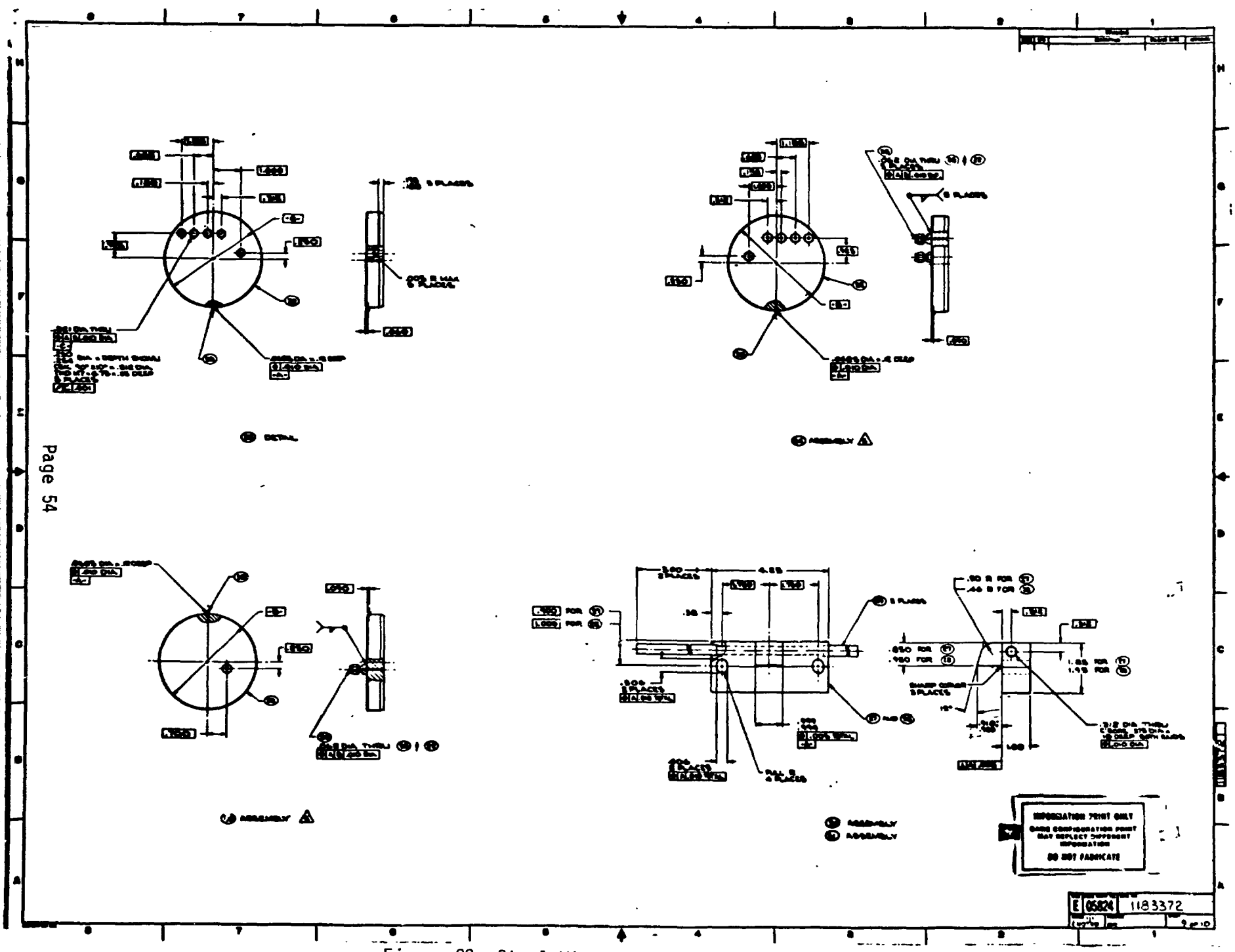

Figure 28. Steel Windows with Instrumentation

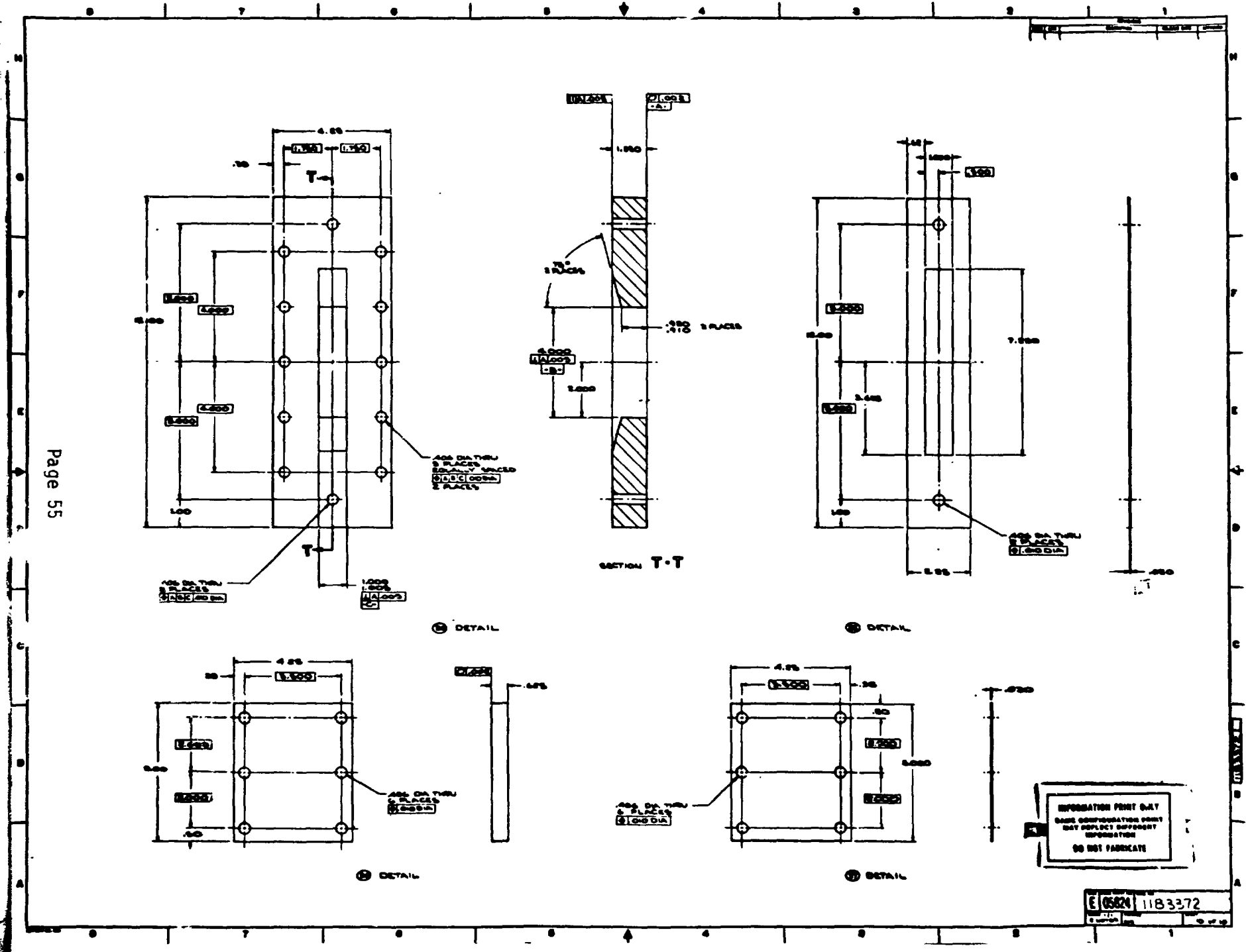

Figure 29. Chamber End Closure

VIII, Hardware, Instrumentation, Test Facility (cont.)

MAJOR PARTS LIST

Description	Quantity	Drawing No.
Chamber	5	1183372-10 thru -14
Side plates	2	1183372-17, -18
Injector	2	1183372-29
Throat inserts	2+	1183372-39, -49
End plate	1+	1183372-25
Steel instrumentation windows	3	1183372-59, -69, -79, -89
Steel windows	2	1183372-34, 35
Quartz windows	4*	1183372-20

+ Complete unit, two pieces per unit
* Or as required due to discoloration or breakage

Five cavity configurations were fabricated--i.e., five chamber pieces--and two more were anticipated by reworking two of the five. Variations in cavity length, inlet radius, and overlap (the distance the injector protrudes into the cavity beyond the chamber wall) were as follows:

VARIATIONS IN CAVITY CONFIGURATION

Item No.	Injector Overlap (in.)	Cavity* Length (in.)	Inlet Radius (in.)	Cavity Width (in.)
12	0.25	0.5	0	0.60
13	0.125	0.5	0.25	0.60
14	0.125	0.5	0	0.60
15	0.125	1.0	0	0.60
16	0.125	1.5	0	0.60
17**	0.125	2.0	0	0.60
18	0.125	0	0	0

* Measured from injector face
** Not fabricated, available by machining Item 16

Item 17 was not made while Item 15 was obtained by adding 0.5-in. blocks to the Item 14 cavities rather than by rework procedures.

Perturbation of the combustion field was accomplished with 2.0 grain RDX bombs located approximately at midchamber. Overpressures were ample (to 100% of P_c) and shrapnel damage to the face was not experienced.

VIII, B, Hardware, Instrumentation, Test Facility (cont.)

Early efforts to perturb the flow with a shock tube system that utilized a gaseous nitrogen source upstream of a calibrated burst disc failed to achieve satisfactory overpressures.

Instrumentation included low and high frequency pressure transducers as well as thermocouples. The high frequency (Kistler 601 or 601A) transducers could be located as follows: chamber, 3 places; injector manifolds, 2 places; acoustic cavities, 5 places (on the steel instrumentation windows). Low frequency pressure transducers could be located as follows: chamber, 7 places; injector, 2 places; propellant tanks, 2 places. High and low frequency instruments were also located on the shock tube system. Thermocouple instrumentation included: injector manifolds, 2 places; flow meters, 2 places; heat exchangers, 2 places; acoustic cavities, 4 places (on the steel instrumentation window). Not all the instrumentation could be used simultaneously because of the limited number of recording channels.

Low frequency response parameters were recorded on a Consolidated Electronics Corp. direct writing oscillograph. High frequency measurements were recorded on a Sangamo model 3564 analog tape recorder. Operating point determinations and other calculations were made on a Hewlett-Packard 2100A computer.

Testing was performed in the Research Physics Laboratory, Test Bay A-2, at ALRC in Sacramento. Figure 30 shows the chamber as mounted on the test stand. The sea level test stand includes two 40-gallon run tanks, with propellant lines to the thrust chamber instrumented for pressure, temperature, and flow rate measurements. Half-inch valves were independently actuated and close-coupled to the injector. Gaseous nitrogen purges were located on both circuits to expel the propellants on shutdown. Sequencing of various engine functions and controls was done by the Hewlett-Packard 2100A computer.

Test Stand, 2-D Testing

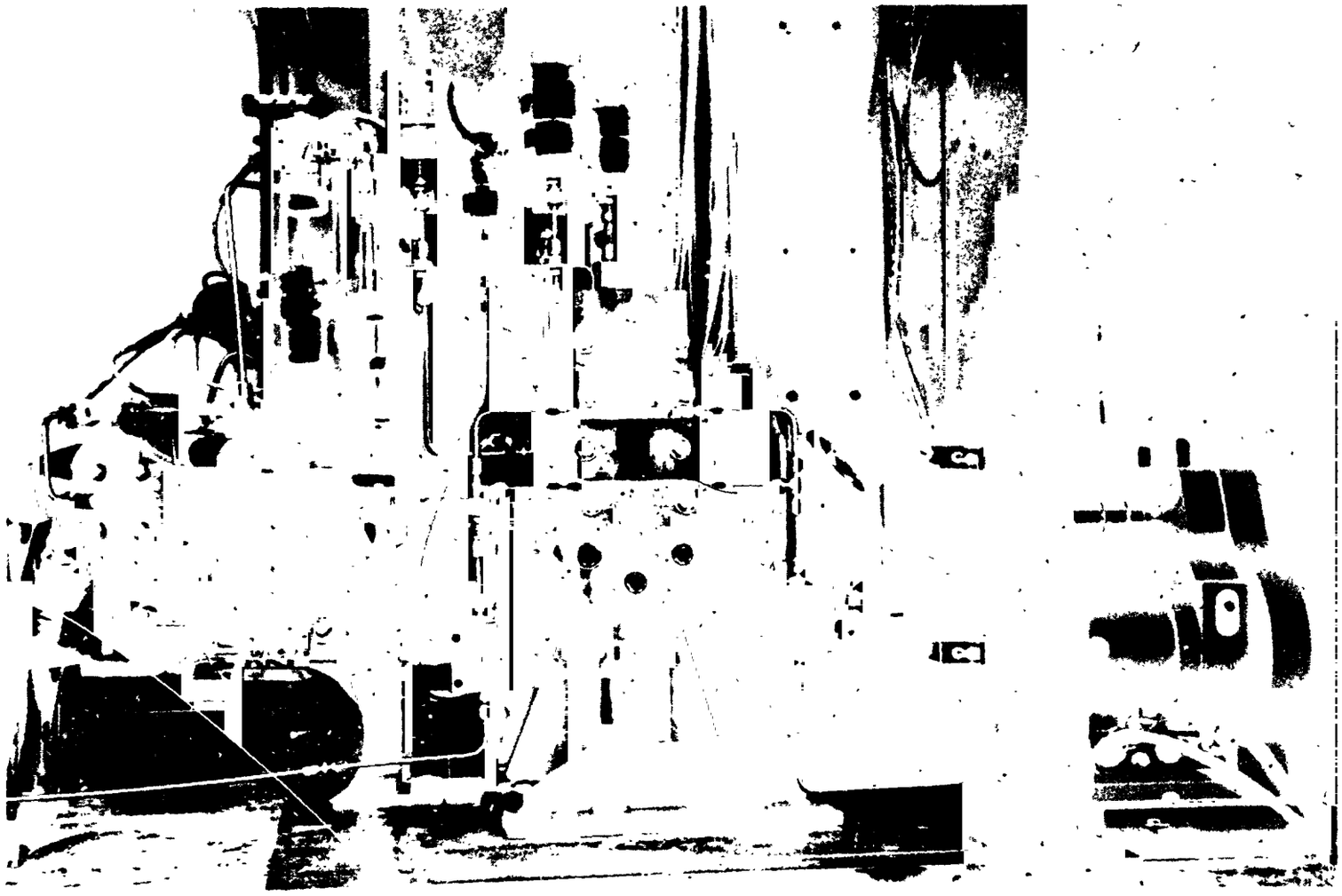

Figure 30

VIII, Subscale (Photographic) Testing (cont.)

C. TEST SUMMARY

The test matrix was laid out in terms of series and sequences in accordance with recent NASA-JSC programs; each series represents a particular test objective, each sequence a single hardware configuration. Consecutive test numbers were assigned, however, following ALRC's customary approach. The test matrix is summarized below:

TEST MATRIX

Series Sequence	Item No.	Operating Point	Notes
			Series I - Checkout
I-1	14	Nominal	Checkout, balance system, evaluate shock tube apparatus, sequence, etc.
			Series II - Cavity Tune Investigation
II-1	14	Box	Baseline configuration 0.5-in. cavities.
II-2	16	Box	1.5-in. cavities
II-3	18	Box	No cavities
II-4	15	Box	1.0-in. cavities
			Series III - Inlet Radius Investigation
III-1	13	Box	0.25-in. radius
			Series IV - Overlap Investigation
IV-1	12	Box	0.25-in. overlap

The operating point "box" referred to above describes the "corners" of the chamber pressure/mixture ratio matrix, as well as the nominal point in the center of the box:

P_c (psia)	O/F (-) 1.40	1.65	1.90
100	x		x
125		x	
150	x		x

The propellants were nitrogen tetroxide (N_2O_4) and monomethyl hydrazine (MMH). The fuel was heated in ten of the early tests but when no sensitivity to fuel temperature was observed in repeat testing, the procedure was discontinued.

The entire test program is summarized in Table I, which gives the operating point conditions, propellant temperatures, stability result, camera settings, and pertinent remarks for each of the tests.

Bomb and shutdown (FS_2) initiation were simultaneous. The stability results as based on CPIA 247 can be briefly described:

STABILITY RESULTS

Cavity Configuration	Stability Results
Square-edged inlet:	
0-in. cavity	Unstable
0.5-in. cavity	Stable at high P_c only
1.0-in. cavity	Stable
1.5-in. cavity	Stable
Rounded inlet	Unstable
0.25-in. Overlap	Stable

In all cases the indicated result refers to postbomb behavior. No spontaneous instabilities were experienced. The instabilities were always the first width (1W) mode. Postbomb ringdown back to stable operation involved both the 1W and the 2W modes however, the latter with the 1.0 and 1.5-in. cavities.

D. TEST SERIES DESCRIPTION

Sequence I-1. This was the first sequence of tests, conducted for the purpose of checking out, balancing, and sequencing the system. The first test, number 101, was 2.0 sec duration; this proved too long--heat marks were observed on the cavity lip--and the duration was subsequently reduced to 0.8 sec. Also the throat area on the first test was 2.24-in.^{2}, which proved too large and was therefore reduced to 2.00-in.^{2} Test 102 was run under the revised conditions. Test 103 was the first firing to be bombed; a 1W (first width) mode instability resulted and the quartz viewing window was shattered.

TABLE I

ACOUSTIC CAVITY PROGRAM
2-D INJECTOR (X-DOUBLET) TESTS
0C82-536-XXX

Test No.	Date	O/F	Pc (psia)	To (F)	T_f (F)	Bomb	Stable	Frame Rate	Shutter	f/Stop	Process	Roll No.	Remarks
								SERIES I -- Checkout Sequence 1 -- 0.5 in. Cavities					
101	5/7/76	1.63	101	73	72	No	Yes	--	--	--	--	--	Checkout; 2.24 in.^{2} throat; burn marks on aft corner of cavity
102	5/11/76	1.71	121	82	82	No	Yes	--	--	--	--	--	Balance with 2.00 in.^{2} throat
103	5/11/76	1.88	135	82	82	Yes	No	--	--	--	--	--	Quartz window shattered
								SERIES II -- Cavity Tune Investigation Sequence 1 -- 0.5 in. Cavities					
104	5/13/76	1.80	134	91	224	Yes	No	--	--	--	--	--	Steel window and Pc_6 replaced by Pc_3 but not labelled (tests 104-109)
105	5/13/76	1.43	110	100	240	Yes	No	--	--	--	--	--	Premature bomb
106	5/13/76	--	--	--	--	--	--	--	--	--	--	--	Malfunction
107	5/13/76	1.86	110	92	239	Yes	No	--	--	--	--	--	
108	5/13/76	1.40	161	92	251	Yes	Yes		--	--	--	--	
109	5/13/76	1.89	159	92	236	Yes	Yes	--	--	--	--	--	
110	5/14/76	1.66	136	82	232	No	Yes	3000	1/20	f/3.3	Normal	1	Light meter reading 14 with 2 ND filters; ASA 150 color film
111	5/14/76	1.41	163	84	251	Yes	Yes	3000	1/20	f/3.3	Normal	2	
112	5/14/76	1.65	137	85	240	Yes	No	3000	1/20	f/3.3	Normal	3	
113	5/14/76	1.90	160	85	245	Yes	Yes	3000	1/20	f/3.3	Normal	4	
114	5/14/76	1.24	112	87	236	Yes	No	3000	1/20	f/3.3	Normal	5	

TABLE I (cont.)

Test No.	Date	O/F	Pc (psia)	To (F)	T_f (F)	Bomb	Stable	Frame Rate	Shutter	f/Stop	Process	Roll No.	Remarks
								SERIES II -- Cavity Tune Investigation Sequence 1 -- 0.5 in. Cavities (cont.)					
115	6/1/76	1.51	139	75	74	Yes	No	11,000	1/10	f/3.3	Push 1	6	Repeat 110-114 at high frame rate
116	6/1/76	1.61	136	73	73	Yes	No	11,000	1/10	f/3.3	Push 1	7	
117	6/1/76	1.62	161	75	75	No	Yes	11,000	1/10	f/3.3	Push 1	8	No bomb
118	6/1/76	1.63	161	75	75	Yes	Yes	11,000	1/10	f/3.3	Push 1	9	Bomb premature ~ 0.1 sec
119	6/1/76	1.63	111	77	77	Yes	No	11,000	1/10	f/3.3	Push 1	10	
								Sequence 2 -- 1.5 in. Cavities					
120	6/14/76	1.61	137	86	85	Yes	Yes	6,000	1/10	f/3.3	Normal	11	Al and Mg shavings in cavity
121	6/14/76	1.37	112	87	85	Yes	Yes	6,000	1/10	f/3.3	Normal	12	Al and Mg shavings in cavity
122	6/14/76	1.85	111	86	85	Yes	Yes	6,000	1/10	f/3.3	Normal	13	Al and Mg shavings in cavity; window pitted
123	6/14/76	1.38	163	83	82	Yes	Yes	6,000	1/10	f/3.3	Normal	14	
124	6/14/76	1.48	111	87	228	Yes	Yes	6,000	1/10	f/3.3	Normal	15	Heated fuel
								Sequence 3 -- 0 in. Cavities					
125	6/17/76	1.63	136	82	78	Yes	No	6,000	1/10	f/3.3	Normal	16	
126	6/17/76	1.38	112	87	82	Yes	No	6,000	1/10	f/3.3	Normal	17	
127	6/17/76	1.37	168	85	85	Yes	No	6,000	1/10	f/3.3	Normal	18	
128	6/17/76	1.84	112	84	83	Yes	No	6,000	--	f/3.3	Normal	19	7241 Film, strobe
129	6/17/76	1.75	163	83	82	Yes	No	2,000	--	f/5.5	Normal	20	7241 Film, strobe
130	6/17/76	1.82	163	84	84	Yes	No	2,000	--	f/5.6	Normal	21	7241 Film, strobe
								SERIES III -- Inlet Radius Investigation Sequence 1 -- Rounded Inlet Cavities					
131	6/25/76	1.67	140	88	88	Yes	No	5,000	--	f/8	Normal	22	7241 Film; strobe; early bomb
132	6/25/76	1.47	163	88	88	Yes	No	5,000	--	f/11	Normal	23	7241 Film; strobe; fuel flow meter erroneous post bomb
133	6/25/76	1.65	113	88	88	Yes	No	6,000	1/10	f/3.3	Normal	24	7242 Film
134	6/25/76	1.66	138	88	88	Yes	No	6,000	1/10	f/3.3	Normal	25	
135	6/25/76	1.54	164	88	88	Yes	No	6,000	1/10	f/3.3	Normal	26	

TABLE I (cont.)

Test No.	Date	O/F	Pc (psia)	To (F)	T_f (F)	Bomb	Stable	Frame Rate	Shutter	f/Stop	Process	Roll No.	Remarks
							SERIES II -- Cavity Tune Investigation (cont.) Sequence 4 -- 1.0 in. Cavities						
136	6/29/76	1.63	137	79	76	Yes	Yes	6,000	1/10	f/3.3	Normal	27	Al blocks in cavity, NaCl used as tracer
137	6/29/76	1.37	112	80	80	Yes	Yes	6,000	1/10	f/3.3	Normal	28	NaCl smears window
138	6/29/76	1.86	112	80	80	Yes	Yes	6,000	1/10	f/3.3	Normal	29	Al used as tracer
139	6/29/76	1.40	164	80	80	Yes	Yes	6,000	1/10	f/3.3	Normal	30	
140	6/29/76	1.85	161	80	80	Yes	Yes	6,000	1/10	f/3.3	Normal	31	
							SERIES IV -- Overlap Investigation Sequence 1 -- 0.25 in. Overlap						
141	7/1/76	1.35	128	75	76	Yes	Yes	6,000	1/10	f/3.3	Normal	32	Ox valve nut entirely open: low P_c, low O/F
142	7/1/76	1.62	122	78	80	Yes	Yes	6,000	1/10	f/3.3	Push 1	33	Repeat; 7241 film
143	7/1/76	1.38	111	80	80	Yes	Yes	6,000	1/10	f/3.3	Push 1	34	7241 Film
144	7/1/76	1.40	163	80	80	Yes	Yes	6,000	1/10	f/3.3	Push 1	35	7241 Film
145	7/1/76	1.63	85	80	80	Yes	Yes	6,000	1/10	f/3.3	Normal	36	Intentional low P_c

VIII, D, Test Series Description (cont.)

Sequence II-1 began the investigation of cavity tune--i.e., length --effects, starting with the same hardware configuration used in the checkout test sequence. The first six tests (104 through 109) were conducted around the operating point box, with the result that the unit was bomb-stable at high chamber pressure but could otherwise be bombed unstable. Steel windows replaced the quartz viewing windows in these tests, and the bomb initiation was delayed, because of the inferred danger of breakage. The following group of tests (110 - 114) again utilized the quartz windows; the high speed camera was used for the first time, at 3000 frames per second with a 1/20 shutter wide open. Sequence II-1 was concluded with five tests (115 - 119) in which the camera was operated at the highest frame rate available, 11,000 frames per second, to obtain a better time resolution of events observed in the first movies. Stability results for these five tests were unchanged from previous testing.

Sequence 2 of Series II utilized the 1.5-in. deep cavity configuration. Aluminum and magnesium shavings were sprinkled into the cavity to provide tracers of the fluid motion; after three tests pitting of the quartz windows was noticed and the procedure was discontinued. All five firings (No. 120 - 124) were bomb-stable, including one low P_c test conducted with heated fuel.

In Sequence 3, the zero cavity depth configuration was evaluated. Although there were no cavities in this unit, there was a notch in the chamber wall corresponding to the cavity entrance, due to maintenance of the nominal 0.125-in. overlap at the cavity lip. The configuration could be bombed unstable all around the operating point box. On three of the tests a strobe was used for illumination, to stop motion in the flow field; electrical problems precluded a long sequence of flashes, but a small and sometimes random number was obtained.

VIII, D, Test Series Description (cont.)

Series III consisted of one sequence of tests (No. 131 - 135) of the rounded inlet configuration. In every test the bomb resulted in instability. Use of the strobe was again attempted on two of the tests, with limited success.

The Cavity Tune Investigation (Series II) was continued with a series (No. 136 - 140) of tests in which the cavity depth was 1.0-in. This configuration was created by adding 0.5-in. long blocks to the 1.5-in. cavity unit tested earlier. Salt (NaCl) was tried as a tracer and was found to leave white streaks on the windows. Although the streaks could be easily washed off with water, the practice was discontinued. All tests were stable.

The final series of tests, Series IV, investigated the effect of overlap with a configuration having a 0.25-in. overlap rather than the nominal 0.125-in. found on all other cavities. The unit proved bomb-stable, even at a chamber pressure of 85 psia.

E. PHOTOGRAPHIC RESULTS

The high speed movies were taken with a Red Lake Hycam 16 mm high speed motion picture camera. This device uses a rotating prism to transfer the image from the optical system to the film plane and is capable of frame rates to 11,000 pictures per second. A rotating slit shutter provides shutter openings of 1/2.5 to 1/50. The effective exposure time is the product of the shutter opening and the reciprocal of the frame rate. Most of the present movies were taken at 6000 frames per second with a 1/10 shutter, giving an exposure time of (1/10) x (1/6000) or 16.7 μsec. Two lenses were used: a 75mm Cosmicar and a 55mm Pentax.

Sufficient illumination was achieved by backlighting with a 1000W tungsten lamp focused through a Fresnel lens and with additional back and front lighting supplied by banks of 650W tungsten movie lights. A ground glass was

used as a diffusing screen for the back lighting. Total illumination significantly exceeded the combustion light.

Ektachrome 7242 film was used for most of the tests; the remaining few were taken with 7241 film. Exposure and development was generally normal. In the high frame rate tests, the film was deliberately underexposed and overdeveloped; the gain in frame rate was judged to be not worth the loss of color balance.

Examination of the movies, frequently on a frame-by-frame basis, was done with a time-motion study (TMS) projector; the image was focused actual size on a sheet of graph paper, allowing measurements to be taken directly.

Typically a firing would appear as follows. First comes a fuel lead, which is the result of test stand plumbing rather than intentional design. The oxidizer circuit then chugs as it comes up to pressure, no doubt because each greater injection of oxidizer causes a momentary rise in chamber pressure which in turn reduces the flow and so on -- the sequence repeating until steady flow is established. Some combustion products flow directly into the cavity (Figure 31, Sketch "a"), as evidenced by a zone of blue coloration indicative of the OH, NH, and CH radicals. With the establishment of steady flow, alternate layers of fuel and oxidizer in the chamber are apparent, as shown in Sketch "b" on Figure 31. The fuel appears gray and the oxidizer orange. These layers extend over the distance visible, about 2.0 in., and streaks on the chamber wall imply this condition of poor mixing exists to the throat. The zone of blue coloration exists between propellant layers and also at a 45° angle in the cavity, as shown by the arrow in Sketch "b". Flow of unburned propellant into the cavity is minimal but does occur with some configurations, frequently in a cyclical manner. Recirculation of gases in the cavity is inferred (Figure 31, Sketch "c") on the basis of tracer

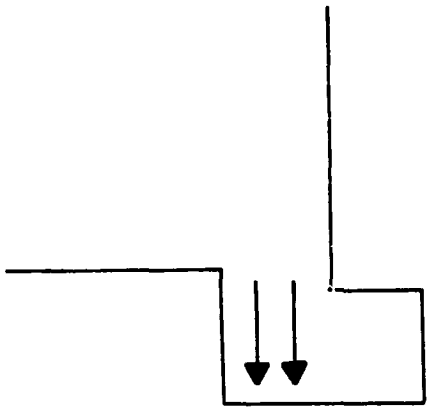

Sketch "a"

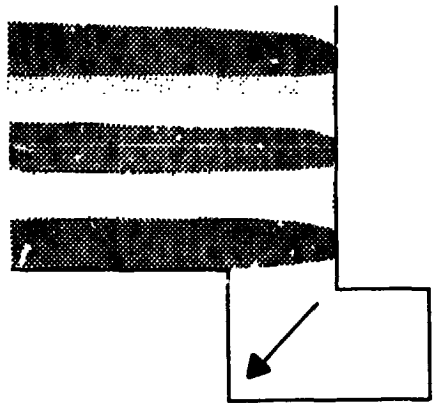

Sketch "b"

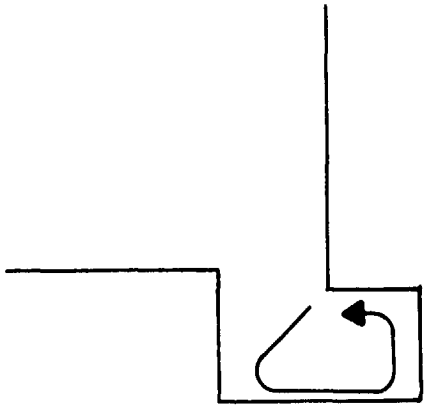

Sketch "c"

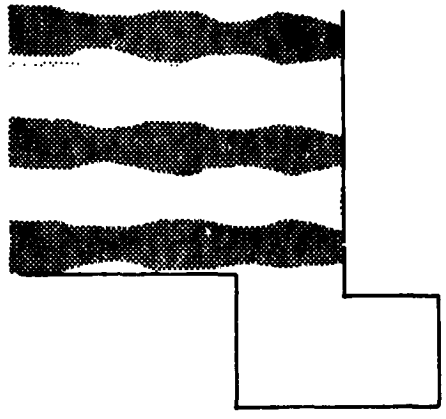

Sketch 'd"

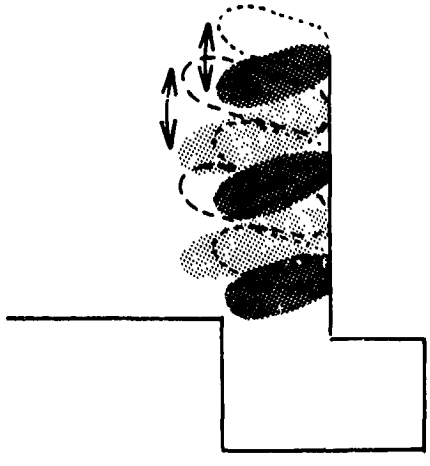

Sketch "e"

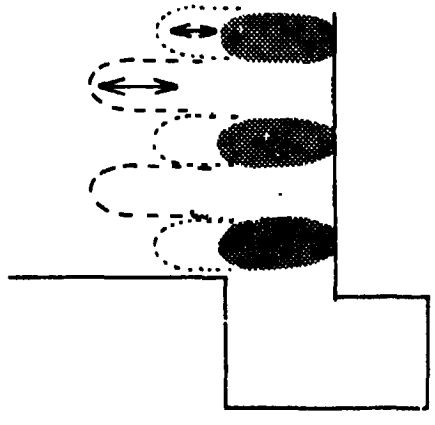

Sketch "f"

Figure 31. Sketches Illustrating Flow Behavior

or other particle motion; velocities up to 250 ft/sec are calculated for the particles; presumably the gas velocity is greater.

The bomb causes the propellant streams to be bowled over; in some cases flow is stopped right at the injector face. Intense flame light is produced for a moment. Some uncombusted propellant is swept into the cavity, at a 45° angle. Behavior thereafter varies with cavity configuration. The longer cavities and the 0.25-in. overlap configuration damp the perturbation in 3-4 msec, based on the high frequency pressure response data; during this time the propellant streams display some thickening and thinning (Figure 31, Sketch "d"), which is probably an indication of instantaneous adjustments to the flow rate. The 0.5-in. cavity, when it damps the perturbation, requires 12 or 13 msec to do so. During this interval, the propellant streams are foreshortened and oscillate both axially and in the direction of the width mode.

When the unsteady combustion remains undamped -- as with the rounded inlet, zero cavity, or 0.5-in. cavity configuration at low chamber pressure -- the propellant streams remain foreshortened, wavering back and forth (Figure 31, Sketch "e") as well as oscillating axially (Figure 31, Sketch "f"). The wavering and length variation both have a periodicity corresponding to the 1W mode frequency. The length of the streams typically varies by 0.5 in., with the minimum length ranging from 0.4 to 1.5 in. Some flow of propellant into the cavity occurs, in a cyclical manner, and with the 0.5-in. cavity the outer fuel stream breaks into small puffs which occur at the 1W frequency and are perhaps a manifestation of jet interaction.

Photographs illustrating some of the above points are reproduced in Figures 32 and 33. Unfortunately many of the events of interest can be best understood by normal projection of the motion pictures -- particle or

Selected Frames Of High Speed Movies

FUEL LEAD (TEST 117)

OXIDIZER FLOW (TEST 115)

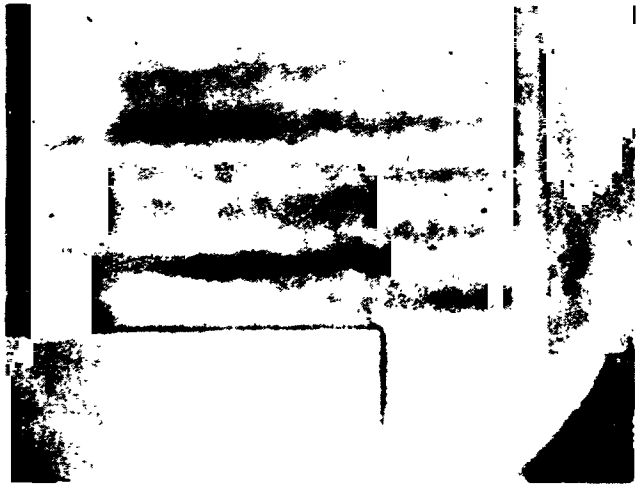

STABLE COMBUSTION (TEST 112)

FLOW STOPPAGE DUE TO BOMB (TEST 112)

Figure 32

Selected Frames Of High Speed Movies

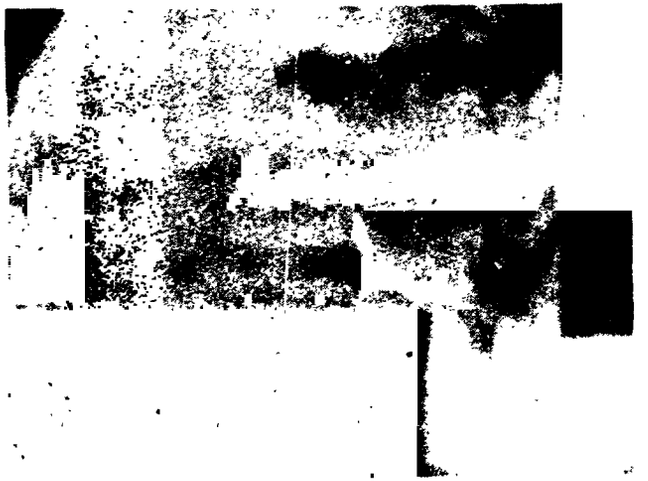

COMBUSTION OF PROPELLANT BLOWN INTO CAVITY. NOTE LAYER ON WALL (TEST 115)

UNSTABLE COMBUSTION
0.5-IN. CAVITY (TEST 115)

UNSTABLE COMBUSTION, ROUNDED INLET CAVITY (TEST 133)

UNSTABLE COMBUSTION, ZERO CAVITY CONFIGURATION (TEST 125)

Figure 33

tracer action, recirculation, zones of blue coloration, flickering of light colored zones, much of the transient response, and all aspects of cyclic behavior. Isolated or single frames do not convey a sense of the motion involved nor do they reproduce the manner of coloration observed.

F. ANALYTICAL RESULTS

Analysis of the subscale test results centers on (1) modeling the various cavity geometries tested, and (2) correlating the experimental results with the models to infer the cavity gas acoustic velocity and parameters describing the cavity inlet resistance and damping characteristics.

1. Cavity Model

The generalized cavity geometry shown in Figure 34 is considered for modeling purposes. It consists of a short ($\Delta X \simeq 0$) entrance section, Zone II, in which energy losses are attributed to viscous flow and nonlinear pressure drop, and a constant area section, Zone I, in which losses are due to viscous flow, heat conduction to the wall, and energy absorption by the gas due to nonequilibrium effects. The losses in Zone I are characterized by a single damping parameter, δ, and in Zone II by a single resistance parameter, R. Both terms are based on empirical data in the literature.

The method of approach is as follows. The pressure amplitude ratio P_1'/P_2' between planes 1 and 2 is defined by the linear wave equation in terms of δ, the sound speed, C, and the cavity length, ℓ. The acoustic admittance at plane 2, denoted G_2, is defined in terms of the same parameters. The pressure amplitude ratio P_2'/P_3' between planes 2 and 3 is calculated from the continuity and momentum equations in terms of R and G_2 and an inertance parameter x. The admittance G_3 is calculated from the same parameters.

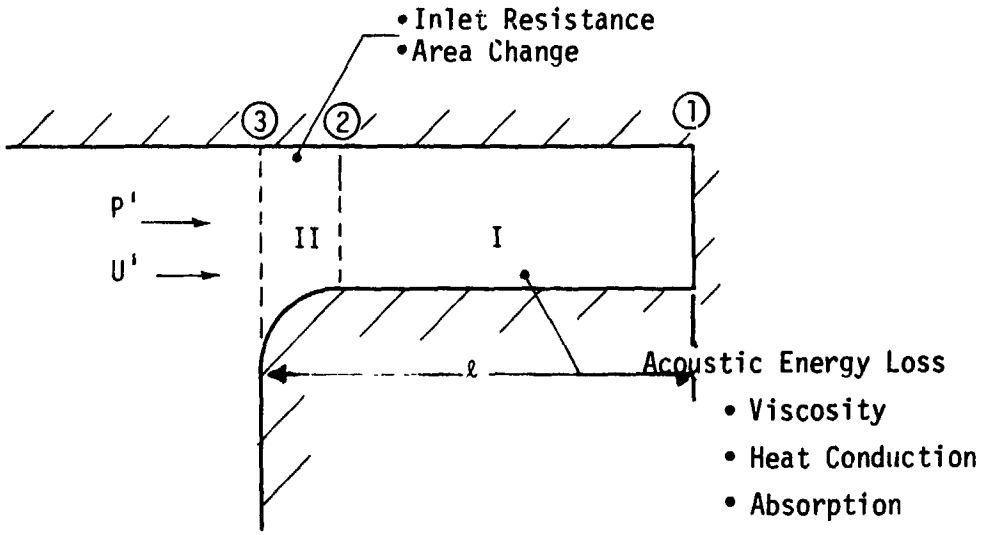

Figure 34. Acoustic Cavity Model

VIII, F, Analytical Results (cont.)

The ratio P_1'/P_3' can thus be determined, from the product of P_1'/P_2' and P_2'/P_3'. This is a measured quantity as well, i.e., the indicated responses of transducers located at the back and at the entrance of the cavity. Hence the assumed values of δ, R, and C can be checked against measured data. The admittance G_3 is an input to the Injector Face Acoustic Resonator (IFAR) model described in Section VII which is used to predict stability of three-dimensional -- i.e., round -- combustors. The IFAR program lacks the capability of rectangular analysis; hence it cannot be applied to the 2-D hardware. The admittance G_3 however can be used as an indicator of stability trends, as discussed subsequently.

The damping parameter δ is related to the frequency response bandwidth and can be determined for a round tube from the following equation[1]:

$$\delta = \frac{C}{\pi}\left[\frac{(\pi\mu)}{r}\right]^{1/2}\left[\left(\frac{1}{\gamma}\right)^{1/2} + \left(\frac{\lambda}{\mu C_v}\right)^{1/2}\left(\frac{\gamma-1}{\gamma}\right)\right]\left(\frac{f}{P}\right)^{1/2}$$

where μ is the viscosity, r the tube radius, γ the ratio of specific heats, λ the gas thermal conductivity, C_v the specific heat at constant volume, f the frequency, and P the pressure. However, comparison of the predicted and measured values of δ show a large discrepancy at the higher frequencies of interest; for this reason it is best to estimate δ from experimental (bandwidth) data when available.

The inlet resistance R is based on Ingard's experimental work,[2] in which the oscillatory velocity through an orifice was measured as a function of driven pressure amplitude. At high sound pressure levels (SPL > 140 db) the sound pressure amplitude was found to be proportional to the square of velocity. Resistance, defined as the real part of the ratio of pressure amplitude to flow rate amplitude,

---

1. Blair, D. W., Eriksen, E., and Berge, G. K., Acoustic Absorption Coefficients of Combustion Gases, AIAA Journal, Vol. 2, No. 2, Feb. 1964.
2. Ingard, U. and Ising, H., Acoustic Nonlinearity of an Orifice, Journal of the Acoustic Society of America, Vol. 42, No. 1, 1967.

VIII, F, Analytical Results (cont.)

$$R = \frac{P'}{\dot{W}'}$$

where: $\dot{W}' = \rho A u'$

Since $u \sim \sqrt{\frac{P}{\rho}}$, R can thus be written as

$$R = \sqrt{P'} / (A\sqrt{\rho})$$

The parameter $RA\sqrt{\rho}$ is plotted in Figure 35 as a function of sound pressure amplitude. Hence, the value of R can be selected on the basis of the experimentally determined sound pressure level.

The pressure ratio across planes 1 and 2 is based on the linear wave equation:

$$P_1'/P_2' = \left(\cosh^2 \frac{\delta \ell}{c} - \sin^2 \frac{\omega \ell}{c}\right)^{-1/2}$$

where ω is the angular frequency. The acoustic admittance is defined by the equation:

$$C_2 = \frac{g_c A}{c} \left[\frac{\sinh \frac{\delta \ell}{c} \cosh \frac{\delta \ell}{c} + i \sin \frac{\omega \ell}{c} \cos \frac{\omega \ell}{c}}{\cosh^2 \frac{\delta \ell}{c} - \sin^2 \frac{\omega \ell}{c}}\right]$$

where g_c is the gravitational constant and A is the cross-sectional area.

The pressure ratio across planes 2 and 3 is

$$P_2'/P_3' = \left[1 + (R^2 + x^2)(G_{2r}^2 + G_{2i}^2) + 2(RG_{2r} - xG_{2i})\right]^{-1/2}$$

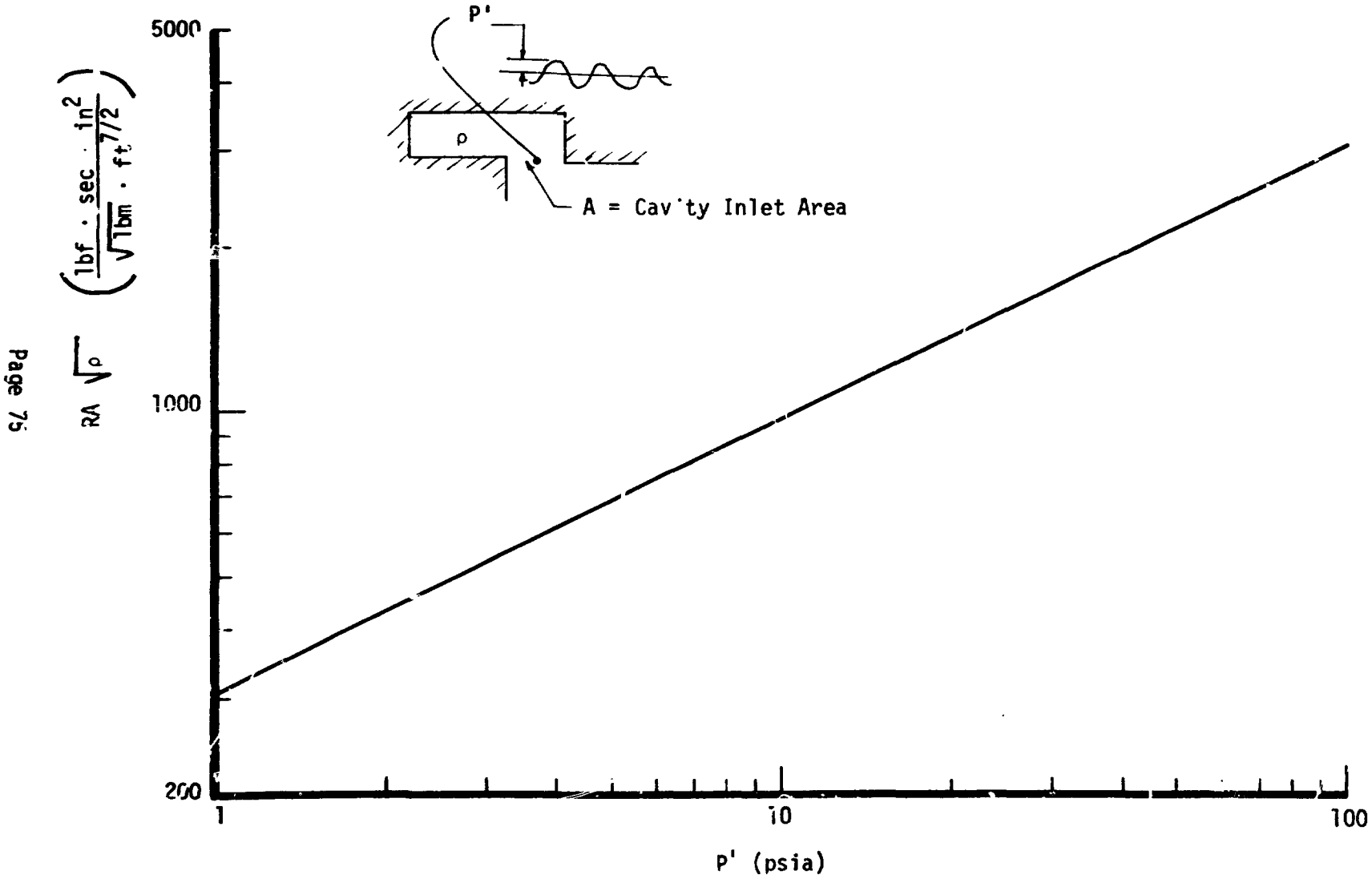

Figure 35. Cavity Inlet Resistance Correlation

where χ is an inertance parameter and the subscripts r and i refer to the real and imaginary parts of the complex G function. The admittance at plane 3 is written as

$$G_3 = \frac{G_2}{1 + (R + i\chi)\, G_2}$$

The pressure ratio and admittance equations form the basis of the Cavity Acoustics Program (CAP) which is ancillary to the IFAR Program. Inputs to the program include cavity geometry, sound speed, damping parameter δ and resistance R. Output includes the pressure ratio P_1'/P_3' and the admittance G_3.

2. Experimental Data

Experimental data pertinent to the above analysis comprise the cavity gas temperature measurements, from which the sound speed is calculated, and the ratio of pressures determined at the back and entrance of the cavity. These are discussed in detail below.

Also measured, in the hopes of characterizing the energy release profile, were the chamber pressures in two axial rows. One row was at the chamber centerline, with seven transducers located every 0.70 in. starting 0.30 in. from the injector face. The other row was near the cavity entrance, with five transducers located every 0.10 in., starting 0.10 in. from the face. The latter row, which was installed in a steel instrumentation window, was of primary interest. Unfortunately the measurements were not consistent with expectations, even after correcting the bias in the instrumentation, by sealing and pressurizing the chamber for a tare reading. Figure 36 shows the profiles over the forwardmost inch of the chamber. The

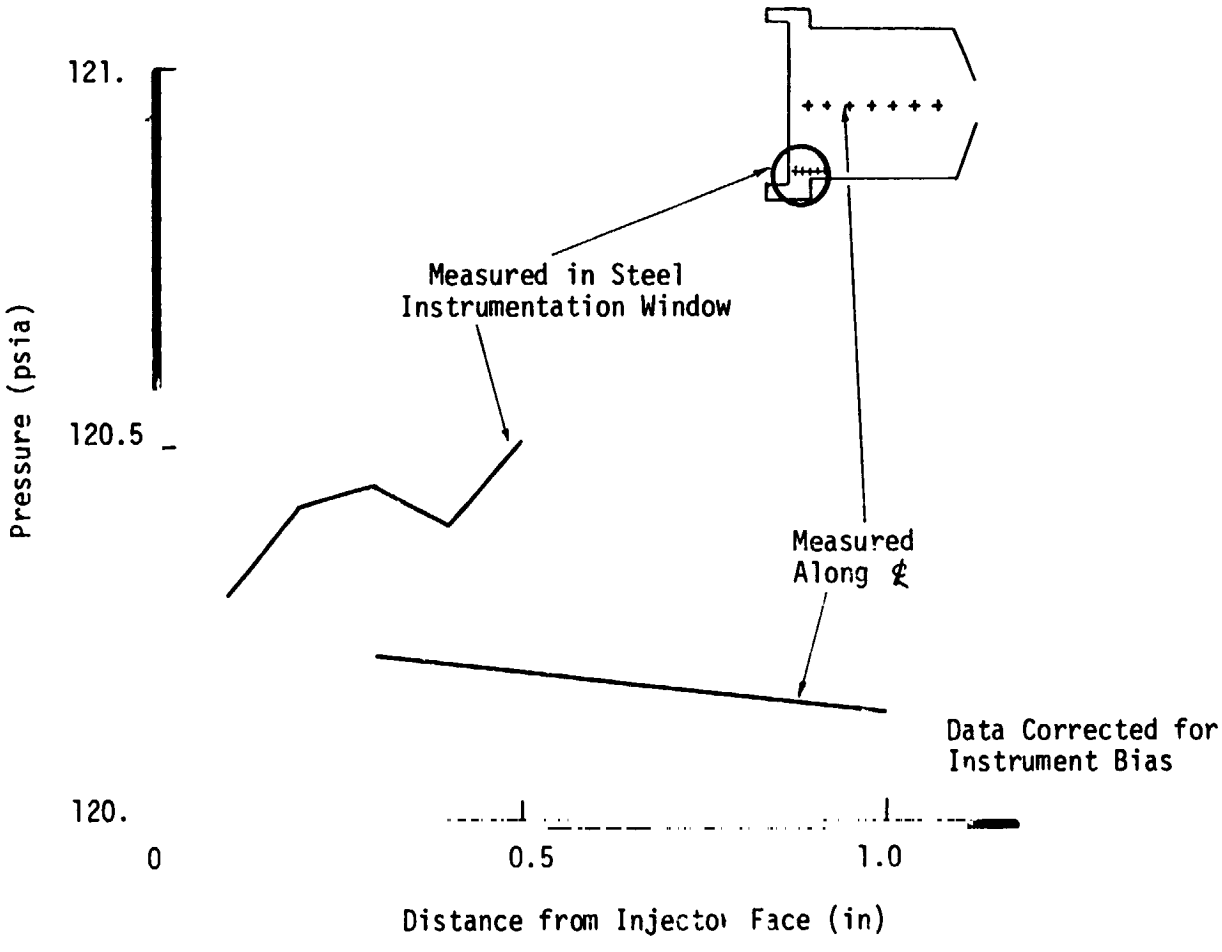

Figure 36. Pressure Profiles for 2D Chamber

window row shows an upward trend, amounting to 0.2 psi, and reads about 0.2 psi higher than the centerline row. This was typical of several tests and is presumably the result of local flow effects. Since the pressure profiles were not considered indicative of energy release characteristics the measurements were discontinued after a few tests.

Cavity gas temperatures were measured by thermocouple probes inserted at various locations as shown by Figure 37. Steady-state temperatures were not obtained because of insufficient firing duration; typical responses are shown in Figure 38 for three early tests. The 2.0 sec duration was unique to the first test; because of burn marks on the cavity edge the duration was reduced to 1.0 sec on all subsequent tests. The indicated temperatures in the 0.75 to 0.85 sec time frame -- that is, near the end of the test -- are plotted in Figure 39 as a function of distance into the cavity. It should be noted that the thermocouple immersion depth was altered during the testing; the shorter depth resulted in lower temperatures, probably because of reduced convection nearer the wall in combination with increased thermocouple lead losses. In general the figure shows that the 0.25 in. overlap and rounded inlet configurations promote higher cavity gas temperatures than the 0.125 in. square-edged inlet. Also, a trend of decreasing temperature into the cavity is evident, and the longer the cavity the lower the temperature at the back wall. Whether this is actually the case or the result of increased thermal capacitance of the gas mass and increased heat transfer to the wall is unclear.

Pressure amplitude ratios of various component frequencies were obtained by filtering the PCAV1 and PCAV2 records. The amplitude ratio PCAV2/PCAV1 for the first three width modes is given in Table II, along with other pertinent information for each test. Correlation of the pressure amplitude ratios is discussed below. The amplitude ratio is designated as positive when the filtered PCAV1 and PCAV2 waves are in phase, and negative when they

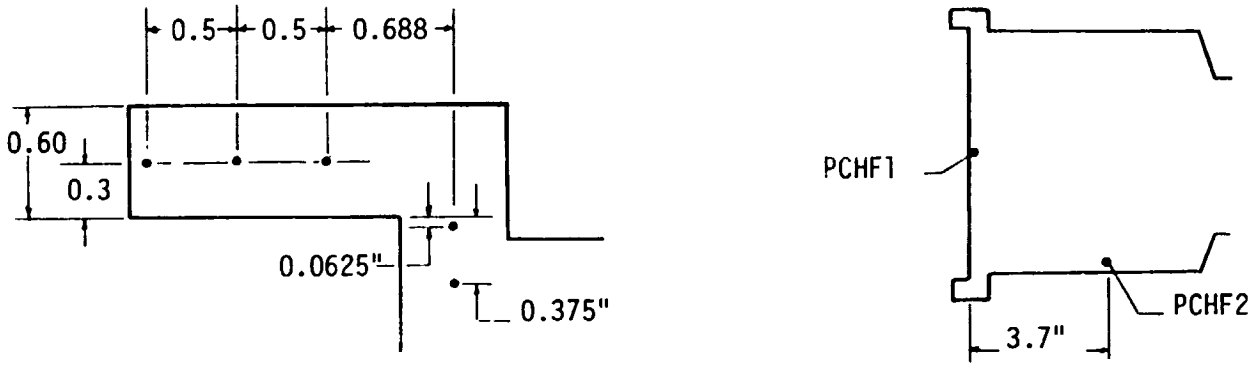

INSTRUMENTATION PORT LOCATIONS

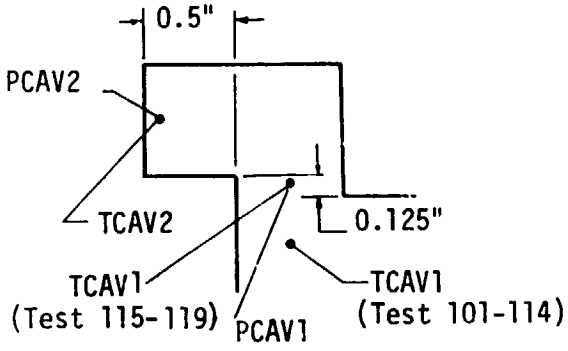

0.5" CAVITY

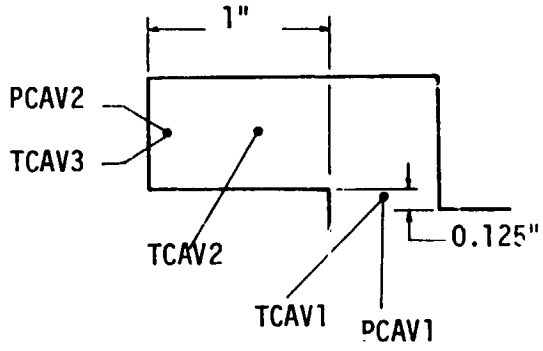

1.0 CAVITY

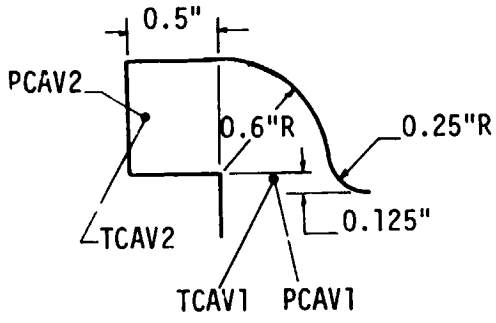

ROUNDED INLET

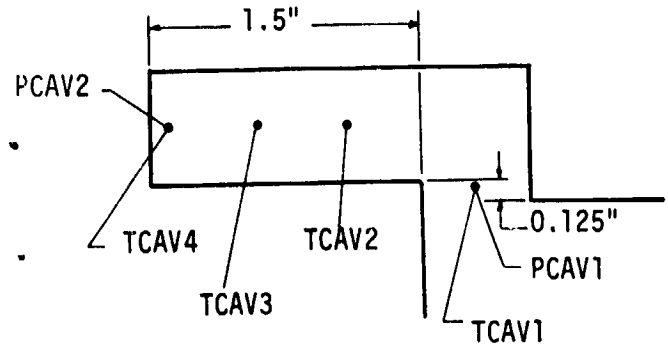

1.5" CAVITY

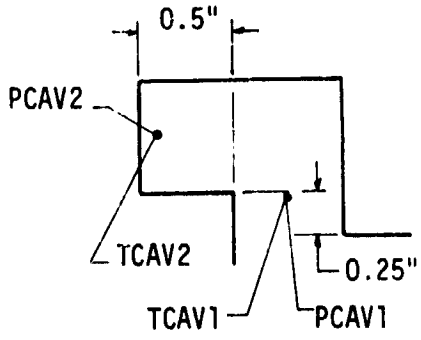

1/4" OVERLAP

Figure 37. Cavity Instrumentation

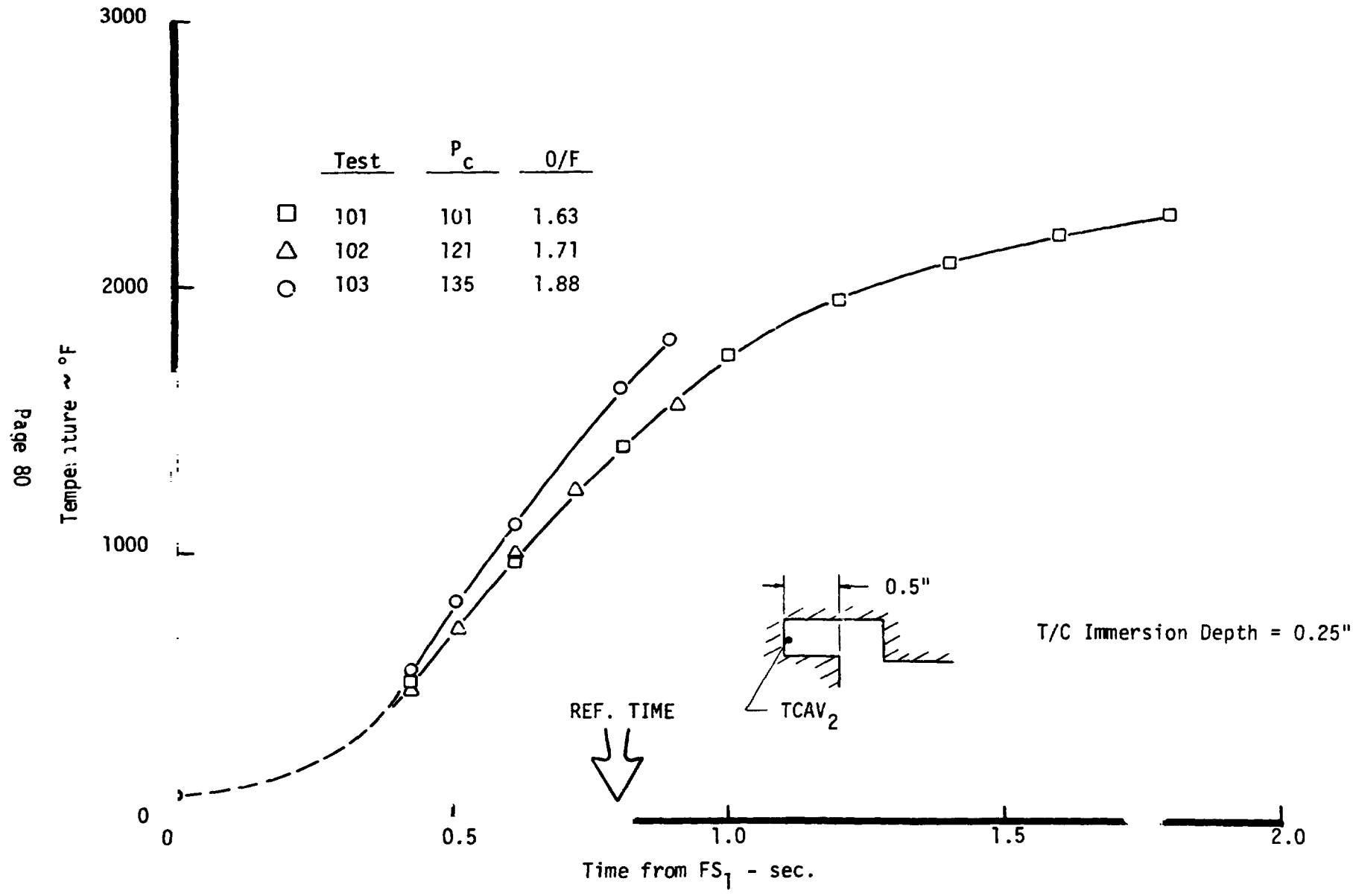

Figure 38. Indicated Temperature Response of Cavity Thermocouple

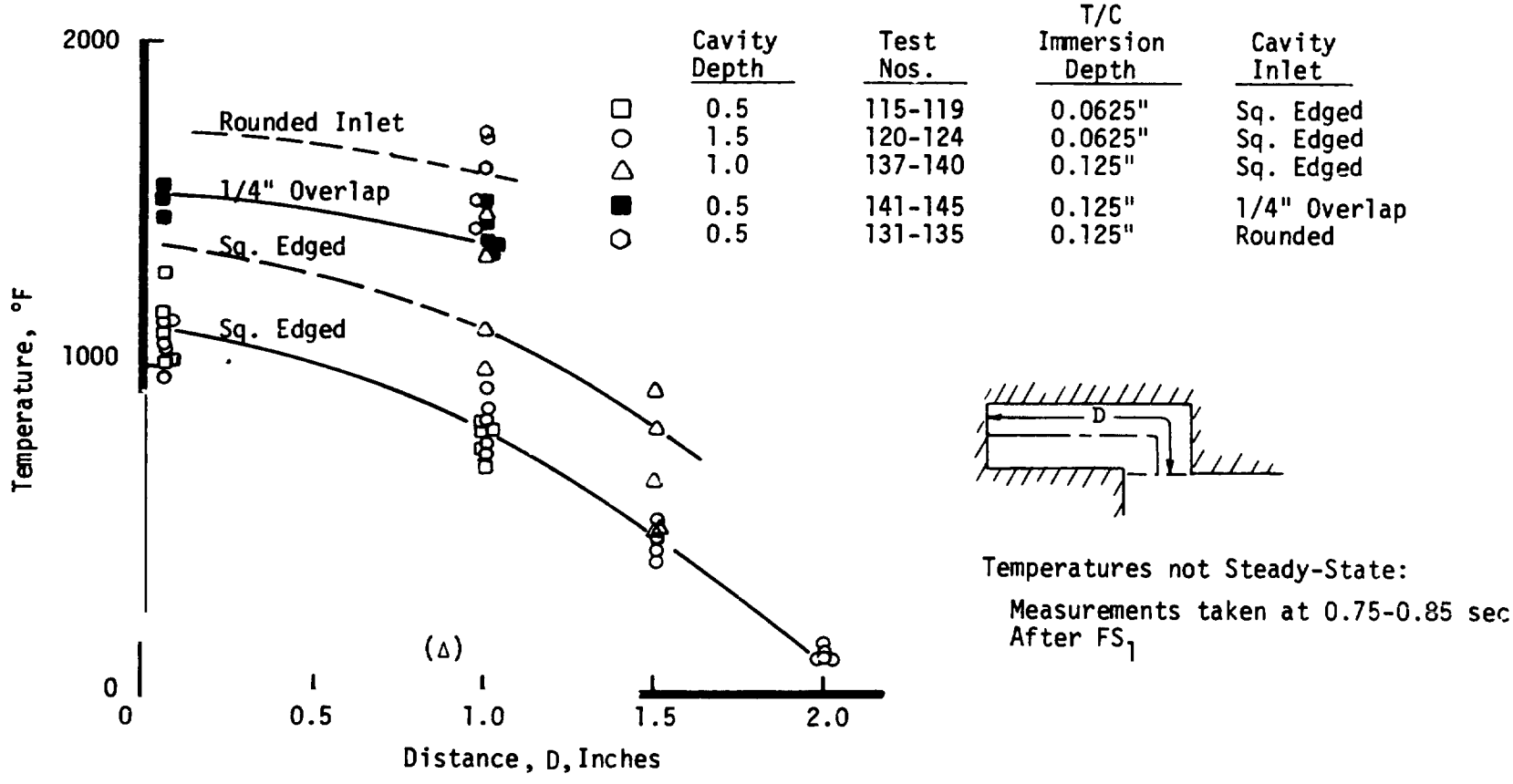

Figure 39. Indicated Gas Temperatures

TABLE II

2D CAVITY TEST RESULTS

Test No.	MR	P_c (psia)	T_f (°F)	CAVITY Depth (in)	CAVITY Inlet Config.	Bomb	Damp Time (ms)	Stab.	FREQUENCY Predom. Comp.	FREQUENCY f_{1W}(Hz)	PCAV1 PK-PK Comp.Amp. (PSI) 1W	PCAV1 PK-PK Comp.Amp. (PSI) 2W	PCAV1 PK-PK Comp.Amp. (PSI) 3W	Cav. Press. Comp. Amp. Ratio 1W	Cav. Press. Comp. Amp. Ratio 2W	Cav. Press. Comp. Amp. Ratio 3W	Cavity Gas Temperatures (°F) TCAV1	TCAV2	TCAV3	TCAV4
101	1.63	101	72	0.5"	Sq.Edged	No	-	S	1W	-	-	-	-	-	-	-	1209	1402	-	-
102	1.71	121	82			No	-	S	1W	-	-	-	-	-	-	-	1444	1392	-	-
103	1.88	135	82			Yes	-	US	1W	2750	*	*	*	*	*	*	1407	1699	-	-
104	1.80	134	224			Yes	-	US	1W	2850	*	*	*	*	*	*	1449	1180	-	-
105	1.43	110	240			Yes	-	US	1W	2875	42	17	*	+1.20	+1.71	*	-	-	-	-
106							Malfunction													
107	1.86	110	239			Yes	-	US	1W	2825	42	12	5	*	*	*	1427	1125	-	-
108	1.40	161	251			Yes	15	S	1W	2650	-	-	-	+1.14	*	*	685	1515	-	-
109	1.89	159	236			Yes	9	S	1W	2670	-	-	-	*	+1.50	*	586	1426	-	-
110	1.66	136	232			No	-	S	1W	-	-	-	-	-	-	-	550	1542	-	-
111	1.41	163	251			Yes	13	S	1W	2650	*	*	*	+1.25	*	*	479	1551	-	-
112	1.65	137	240			Yes	-	US	1W	2700	41	8	*	+1.20	*	*	602	1547	-	-
113	1.90	160	245			Yes	11	S	1W	2700	-	-	-	+1.20	*	*	628	1434	-	-
114	1.20	112	236			Yes	-	US	1W	2850	41	11	6	+1.20	+1.73	*	667	1388	-	-
115	1.51	139	74			Yes	-	US	1W	2725	43	9	*	+1.22	+1.79	*	1090**	750	-	-
116	1.61	136	73			Yes	-	US	1W	2725	46	*	*	+1.18	*	*	1165	800	-	-
117	1.62	161	75			No	-	S	1W	-	-	-	-	-	-	-	1008	832	-	-
118	1.63	161	75			Yes	10	S	1W	2690	-	-	-	+1.23	-	*	1021	811	-	-
119	1.63	111	77			Yes	10	US	1W	2750	44	13	*	*	*	*	1290	687	-	-
120	1.61	137	85	1.5"	Sq.Edged	Yes	4	S	3W	2825	-	-	-	+1.30	-2.70	*	1074	817	530	125
121	1.37	112	85	1.5"		Yes	4	S	3W	2830	-	-	-	+1.70	-2.20	-1.13	1242	866	510	133
122	1.85	112	85	1.5"		Yes	4	S	3W	2900	-	-	-	+1.69	-2.73	-1.16	980	727	400	117
123	1.38	163	82	1.5"		Yes	4	S	*	*	-	-	-	*	*	*	1059	937	490	143
124	1.43	111	228	1.5"		Yes	4	S	*	*	-	-	-	*	*	*	1251	759	435	126
125	1.63	136	78	No Cavity		Yes	-	US	1W	3250	280	70	****	-	-	-	-	-	-	-
126	1.38	112	82			Yes	-	US	1W	3300	310	70	****	-	-	-	-	-	-	-
127	1.37	168	85			Yes	-	US	1W	3320	330	80	****	-	-	-	-	-	-	-
128	1.84	112	83			Yes	-	US	1W	3150	290	55	****	-	-	-	-	-	-	-
129	1.75	163	82			Yes	-	US	1W	3250	330	85	****	-	-	-	-	-	-	-
130	1.82	163	84			Yes	-	US	1W	3300	330	80	****	-	-	-	-	-	-	-
131	1.67	140	88	0.5"	Rounded	Yes	-	US	1W	2800	65	*	*	+1.18	*	*	***	70	-	-
132	1.47	163	88	0.5"	Rounded	Yes	-	US	1W	2750	53	*	*	+1.10	*	*	***	71	-	-
133	1.65	113	88	0.5"	Rounded	Yes	-	US	1W	2875	50	17	7	+1.13	+1.67	*	***		-	-
134	1.66	138	88	0.5"	Rounded	Yes	-	US	1W	2750	50	*	*	+1.13	*	*	***	1493	-	-
135	1.54	164	88	0.5"	Rounded	Yes	-	US	1W	2725	60	*	*	*	*	*	***	1415	-	-
136	1.63	137	76	1.0"	Sq.Edged	Yes	9	S	1W	2500	-	-	-	+1.20	*	*	***	-	-	-
137	1.37	112	80	1.0"	Sq.Edged	Yes	7	S	*	3000	-	-	-	+1.26	*	*	***	1473	810	-
138	1.86	112	80	1.0"	Sq.Edged	Yes	6	S	*	2650	-	-	-	+1.19	*	*	***	988	508	-
139	1.40	164	80	1.0"	Sq.Edged	Yes	7	S	*	2670	-	-	-	+1.25	*	*	***	1340	932	-
140	1.85	161	80	1.0"	Sq.Edged	Yes	6	S	*	2500	-	-	-	+1.25	*	*	***	1104	647	-
141	1.35	128	71	0.5"	1/4" Overlap	Yes	6	S	*	2750	-	-	-	+1.30	+1.52	*	***	1378	-	-
142	1.62	122	76	0.5"		Yes	6	S	*	2750	-	-	-	+1.32	*	*	***	1492	-	-
143	1.38	111	83	0.5"		Yes	6	S	*	2800	-	-	-	+1.32	*	*	1510	1368	-	-
144	1.40	163	80	0.5"		Yes	6	S	*	2550	-	-	-	+1.33	*	*	1460	1447	-	-
145	1.63	85	80	0.5"		Yes	6	S	*	2500	-	-	-	+1.32	*	*	1558	1388	-	-

*Information Unavailable or Intufficient for Determination

**Changed TCAV1 Position & T/C Immersion Depths

*** T/C Malfunction

**** Estimated from Non-Filtered Playbacks, 3W Component Amplitudes Not Estimated

are out of phase. The phase is determined by the relationship of the component frequency to the cavity resonant frequency, as illustrated by Figure 40. The ratio is positive when the component frequency is less than the cavity's fundamental frequency or between an odd order overtone and the next higher even order overtone. It is negative when the component frequency is between an even order overtone and the next higher odd order overtone.

3. Pressure Ratio Correlations

As noted previously, the purpose of the cavity model was to establish numerical values for several input parameters by correlating experimental results. The parameters include the damping parameter, δ, the inlet resistance, R, and the sound speed in the cavity, c. The pressure amplitude ratio discussed above is the factor to be correlated.

The damping parameter was found to have little effect on pressure amplitude ratio; the dominant element was found to be the sound speed, as illustrated in Figure 41. For this reason, the inlet resistance, R, and damping parameter, δ, were based on the formulations of Blair and Ingard previously described, rather than on test data. The value of the damping parameter was calculated to be $\delta = 314\ sec^{-1}$, for a mean gas pressure of 150 psia, a sound speed of 3300 ft/sec and a gas temperature of 3500°R. Corresponding bandwidth is 100 Hz. The inlet resistance was calculated to be 7400 lbF-sec/lbm-ft^2, based on the amplitudes observed during the instability of the 0.5 in. deep cavity.

The correlations obtained for the various cavity configurations are shown on Figures 42 through 46. Figure 42 shows the amplitude ratio for the 0.5 in. cavity with both sharp edged and rounded entrance configurations Figure 43 shows the ratio for the 0.5 in. cavity with 0.25 in. overlap. Here the measured data are misleading because the inlet transducer was displaced from

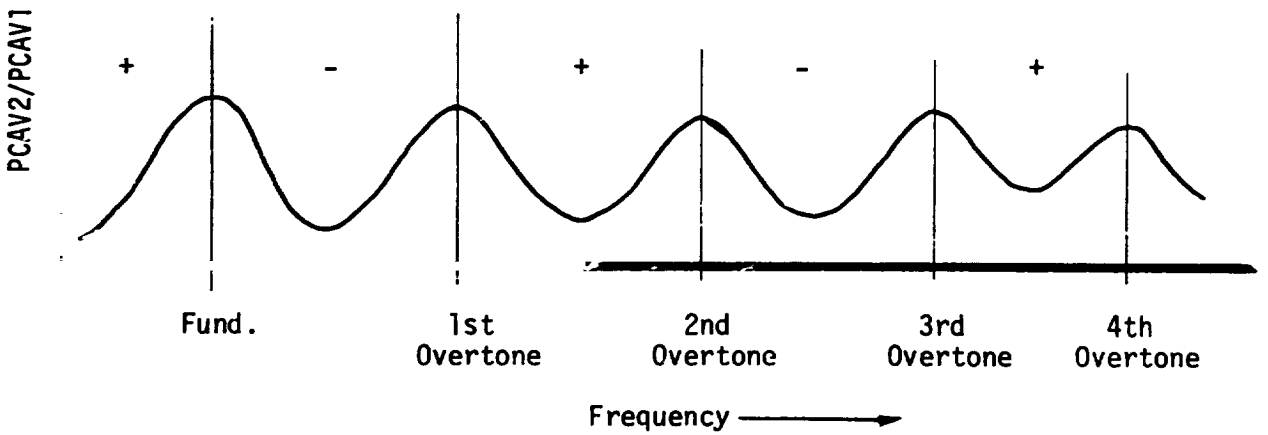

Figure 40. Sign Variation of Cavity Pressure Amplitude Ratio

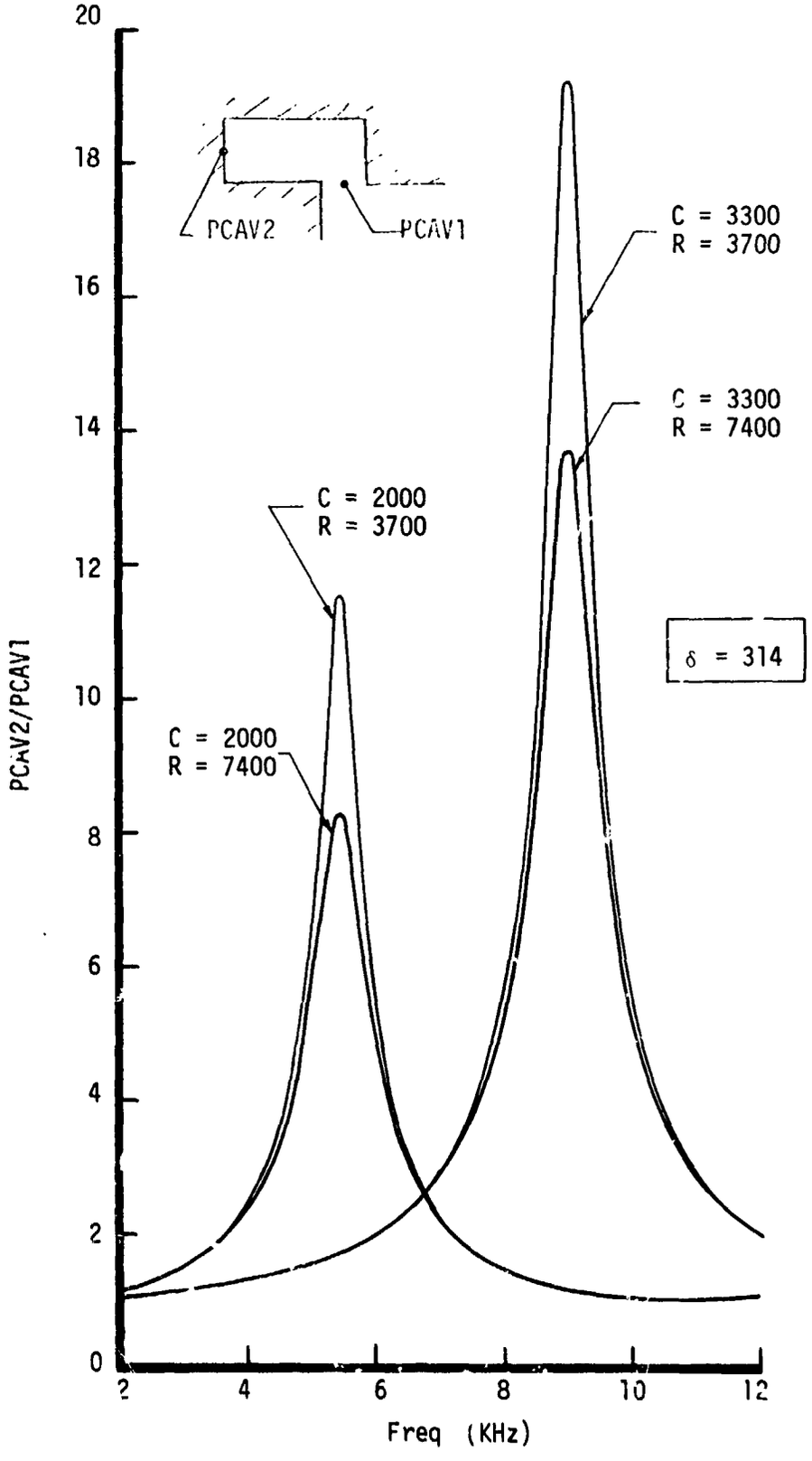

Figure 41. Predicted Effect of Sound Speed and Inlet Resistance or Pressure Amplitude Ratio, 0.5 in. Deep Cavity

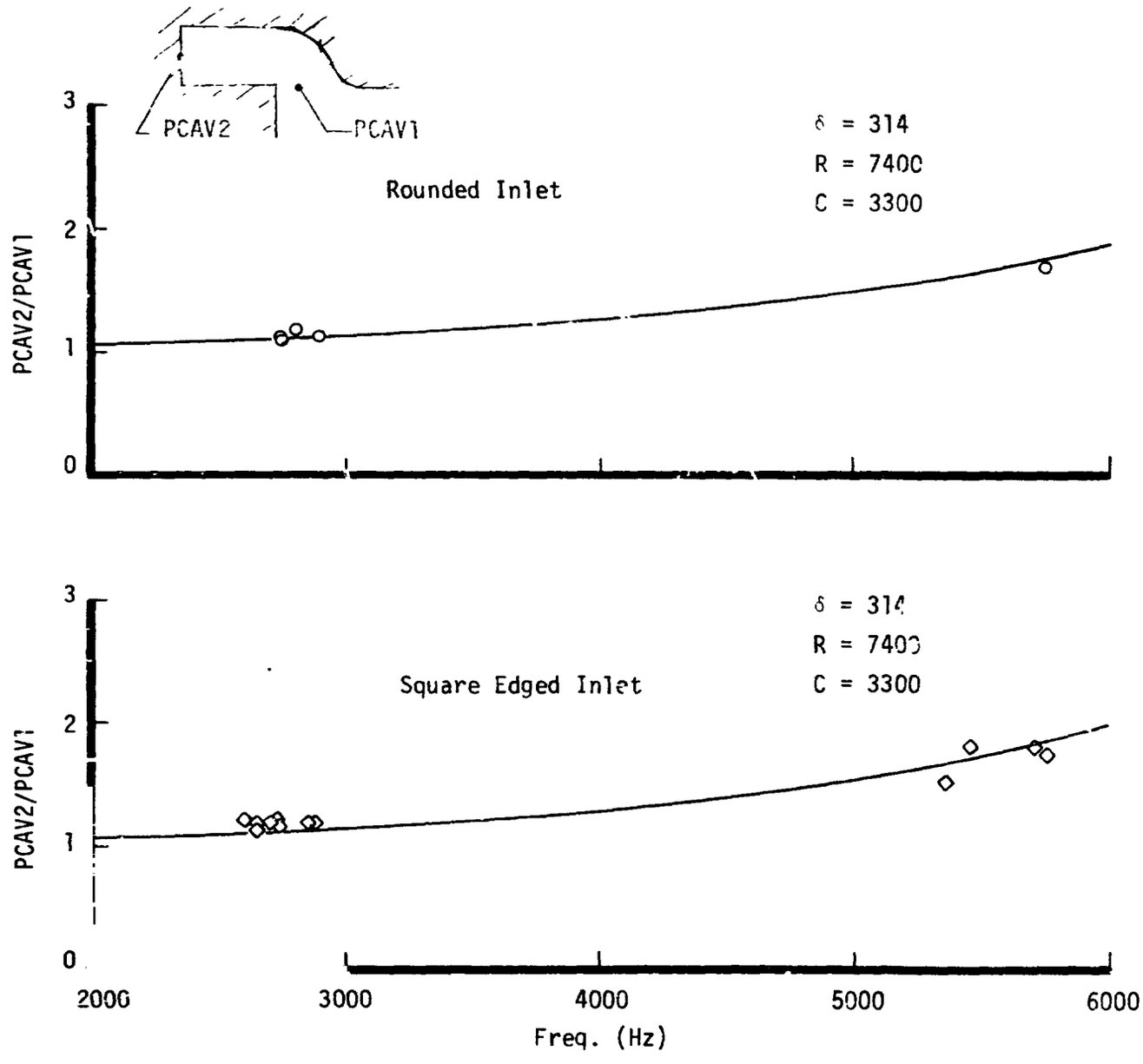

Figure 42 Calculated and Measured Cavity Pressure Amplitude Ratio, 0.5 in. Deep Cavity with 0.125 in. Overlap

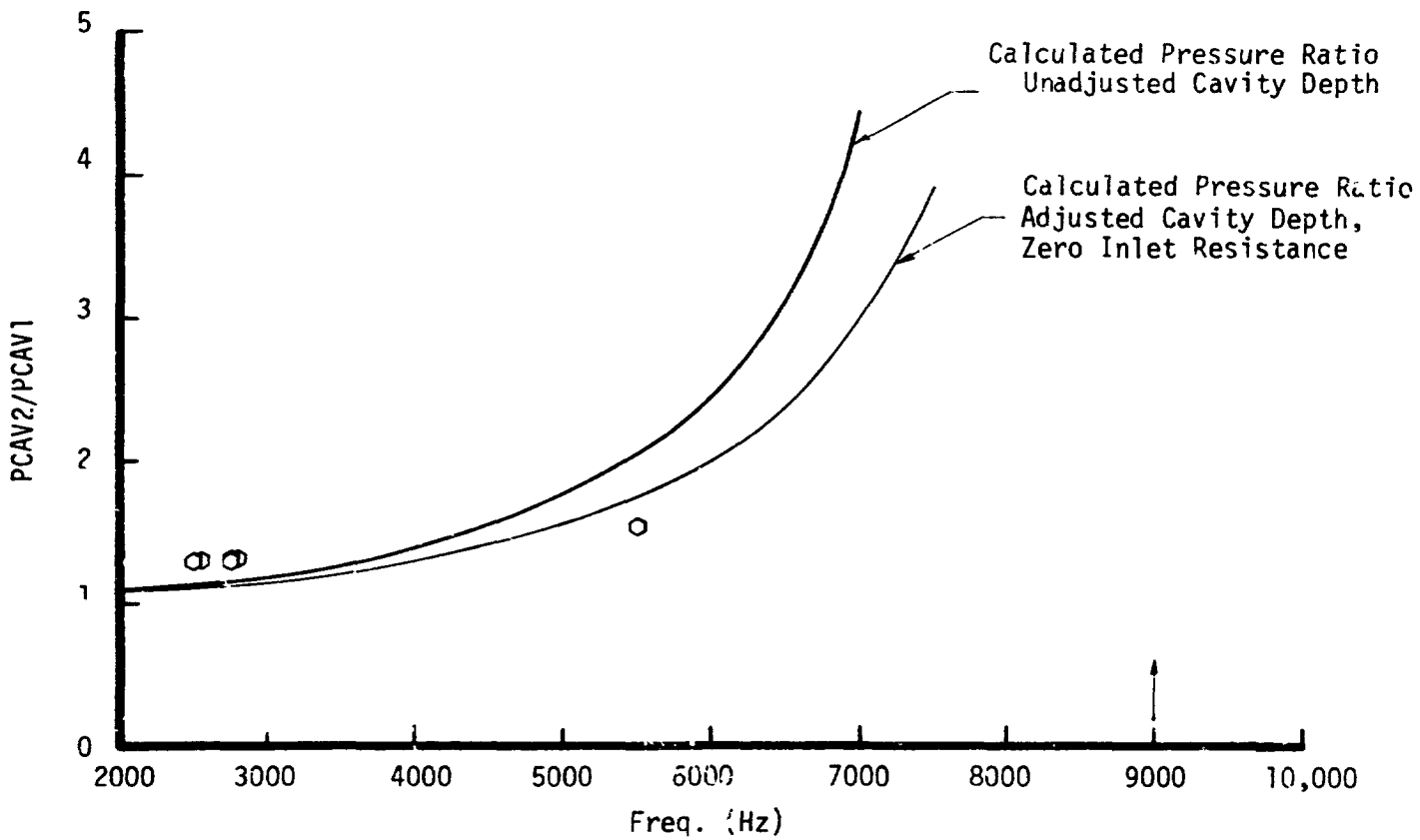

Figure 43. Calculated and Measured Cavity Pressure Amplitude Ratio, 0.5 in. Deep Cavity with 0.25 in. Overlap

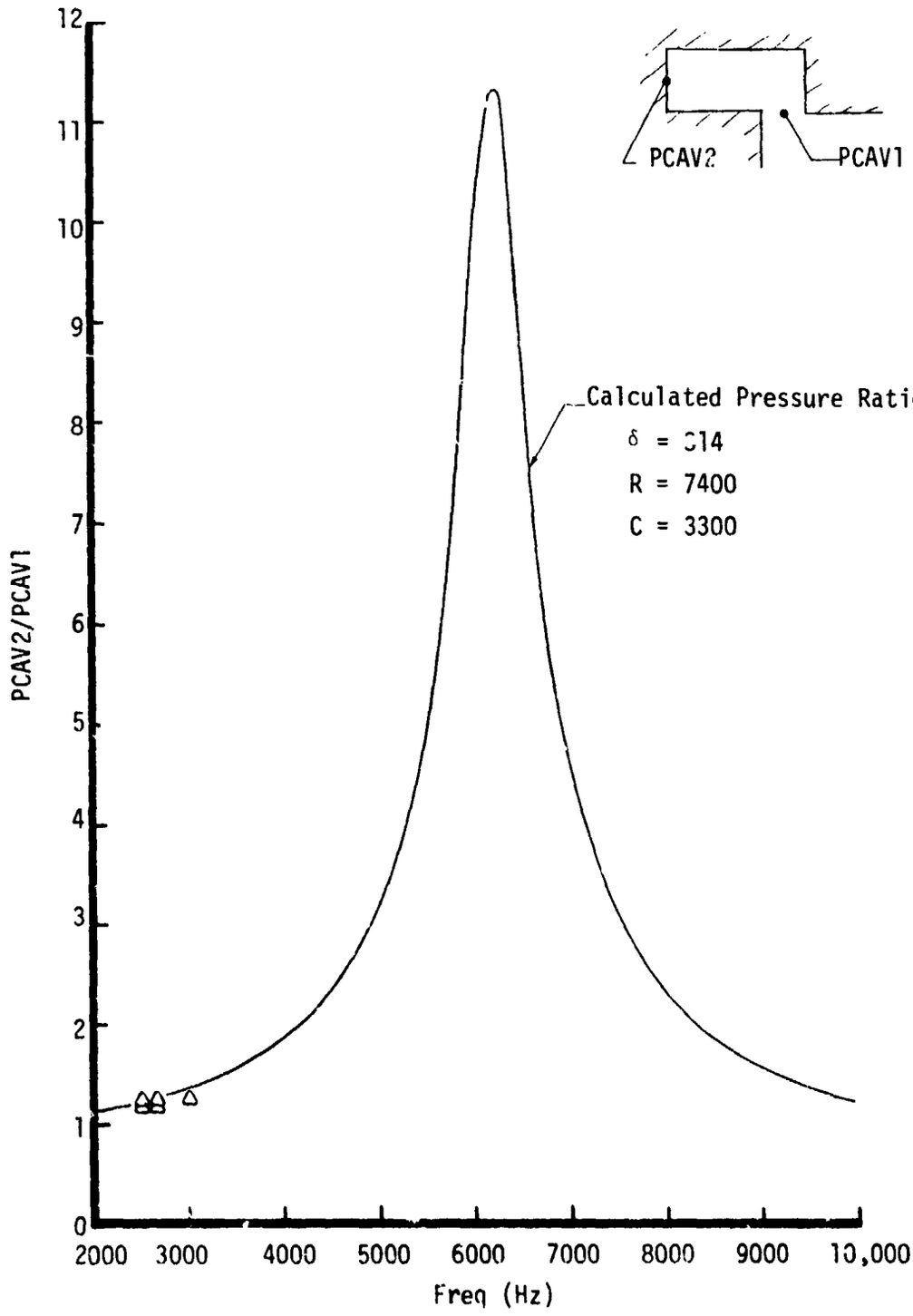

Figure 44. Calculated and Measured Cavity Pressure Amplitude Ratio, 1.0 in. Deep Cavity with 0.125 in. Overlap

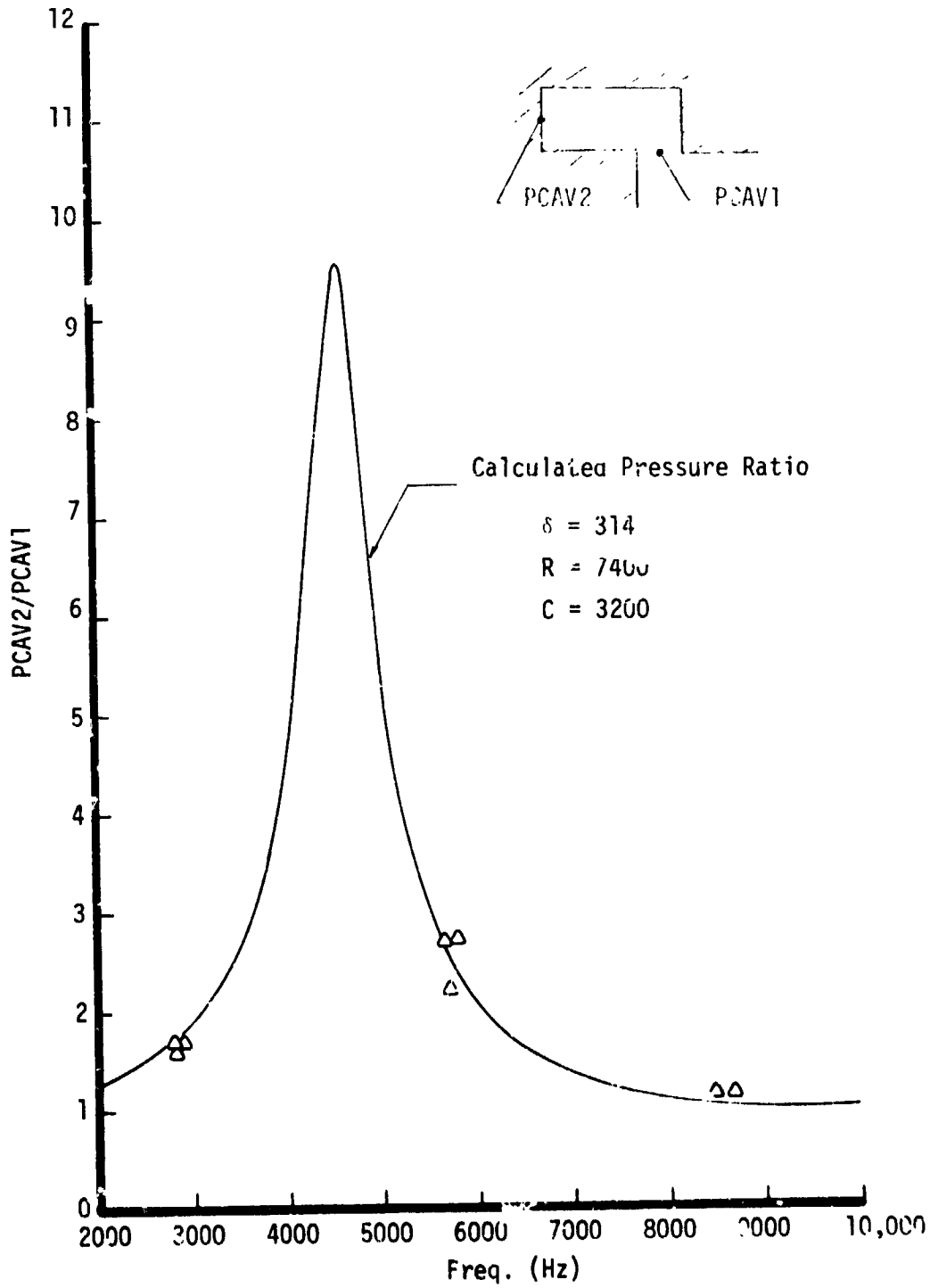

Figure 45. Calculated and Measured Cavity Pressure Amplitude Ratio, 1.5 in. Deep Cavity with 0.125 in. Overlap

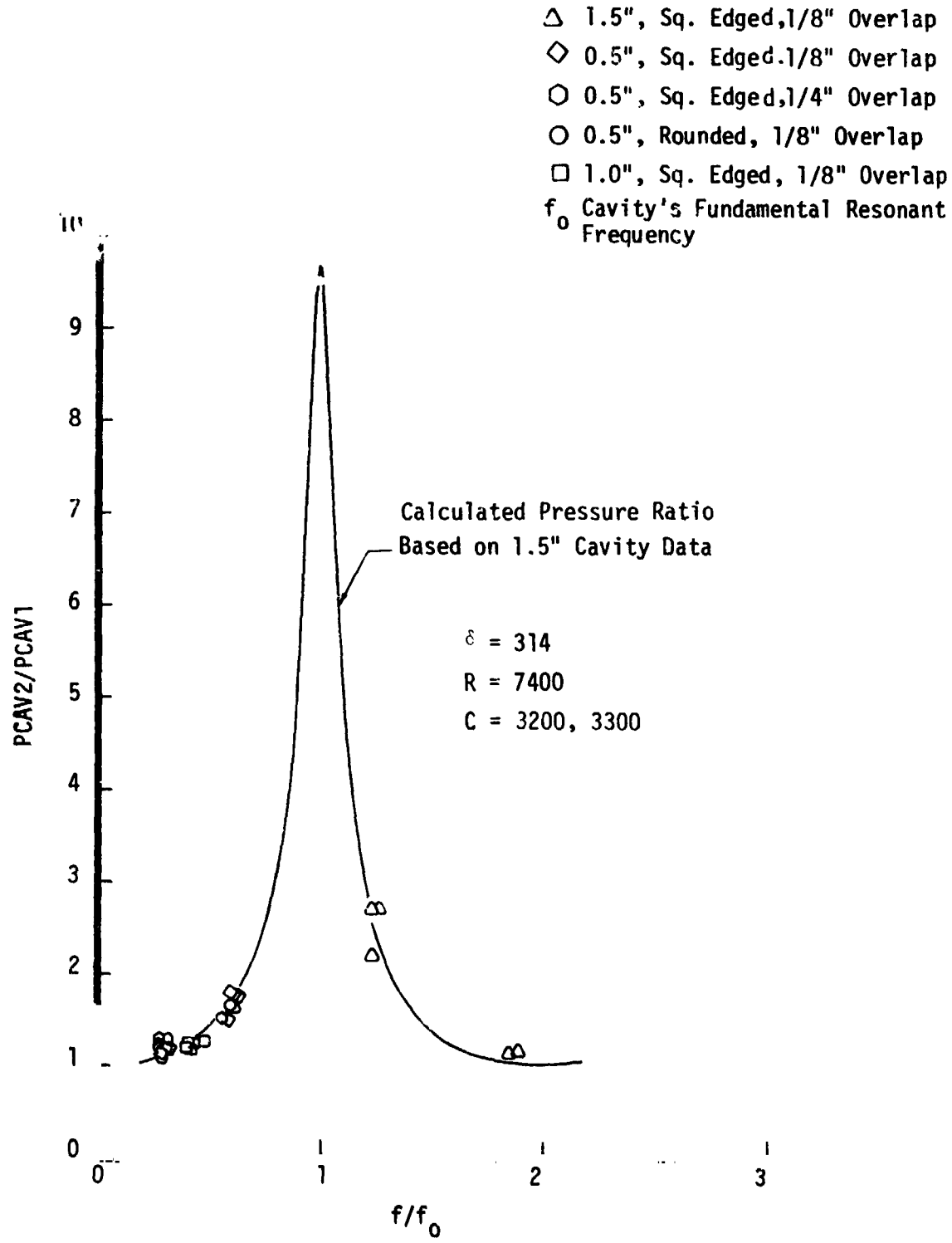

Figure 46. Calculated and Measured Generalized Cavity Pressure Amplitude Ratio

the inlet, as shown in Figure 37; if in the prediction the inlet resistance is ignored and the cavity length adjusted to account for transducer displacement then reasonable correlation is obtained with the measured data. The correlation for the 1.0 in. cavity is presented in Figure 44; band pass data for modes higher than the first width mode were not available for correlation. However, the first three modes are represented in Figure 45 for the 1.5 in. deep cavity. Finally, Figure 46 summarizes all of the above by plotting for all configurations the amplitude ratio versus normalized frequency; that is, the ratio of the component frequency to the cavity resonant frequency. Excellent agreement is obtained, indicating that the choice of parameters within the framework of the analytical model is reasonably correct. Since cavity admittance is formulated from these same parameters, it presumably can be calculated equally well. Most important in such a calculation is that the sound speed be well characterized; in that regard, variations in inlet geometry appear to affect the cavity damping characteristics primarily by changing the sound speed -- i.e., the gas temperature and composition -- rather than by altering the inlet resistance.

4. Stability Correlations

Stability predictions cannot be made for these configurations because the IFAR program, which is used to predict stability, lacks a two-dimensional (rectangular) capability. Nonetheless, the admittance calculated by the CAP subroutine can be used as an indicator of stability trends.

Figures 47, 48, and 49 show the real part of the admittance calculated for the 0.5, 1.0, and 1.5 in. cavities with 0.125 in. overlap, along with typical bomb responses, a summary* of wave component amplitudes and damp times, and for the 0.5 in. cavity a comparison of amplitude versus admittance.

* based on band pass filtering

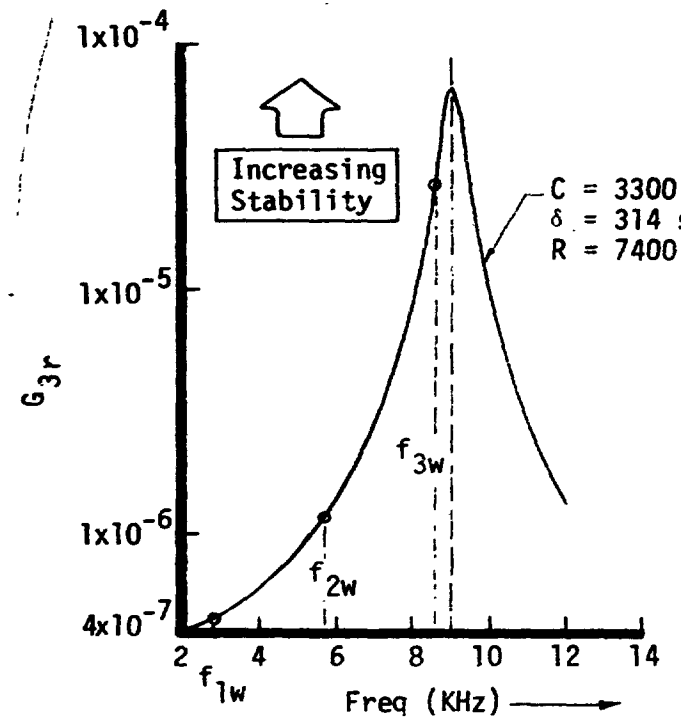

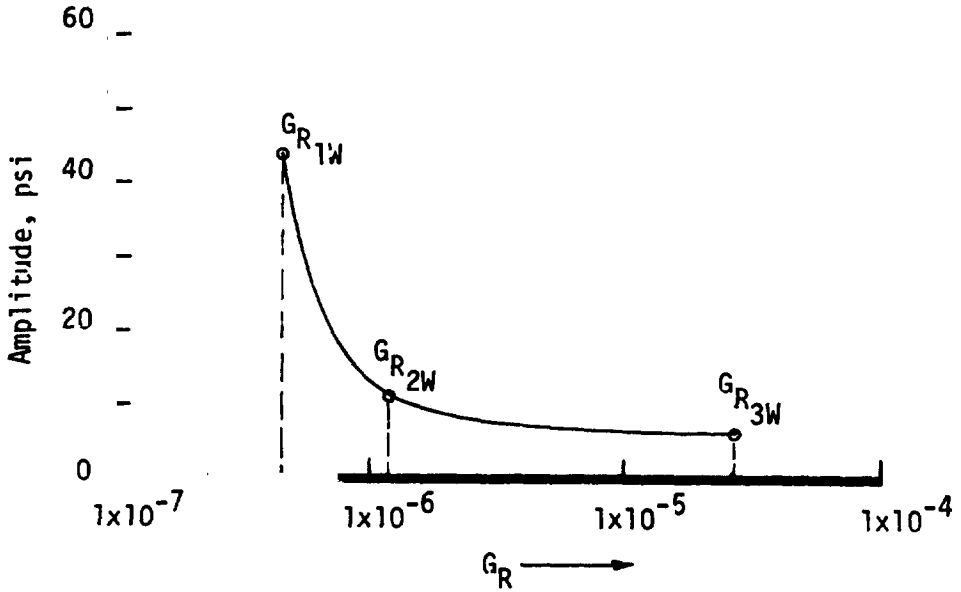

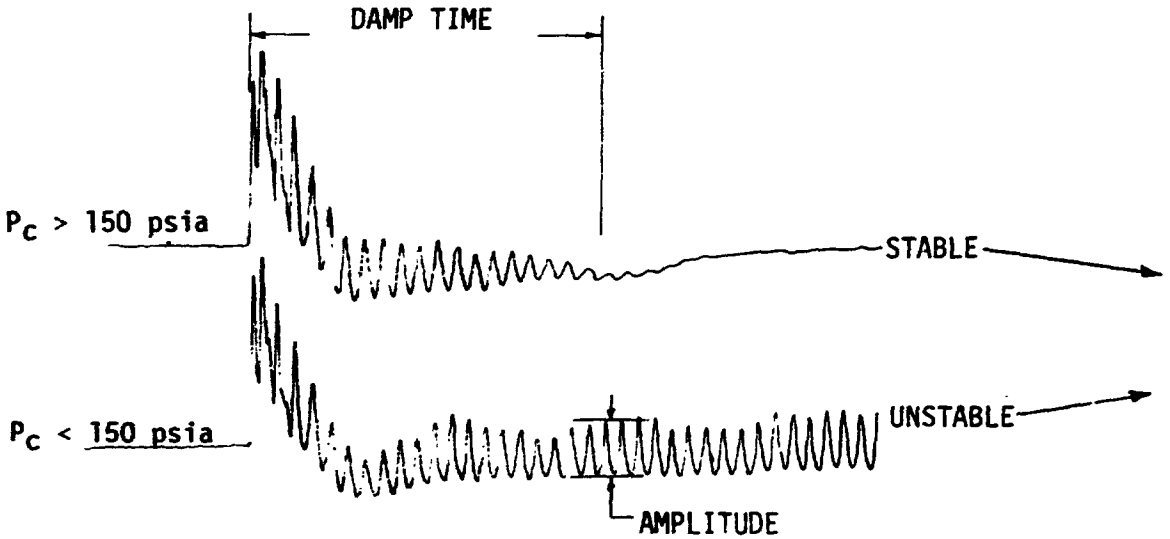

WAVE CONTENTS

Freq.	Avg. Amp.	Avg. Damp Time
1w	-	11 ms
2w	-	
3w	-	
1w	44	N/A
2w	11	N/A
3w	6	N/A

Figure 47 Stability Characteristics for 0.5 in. Deep Cavity

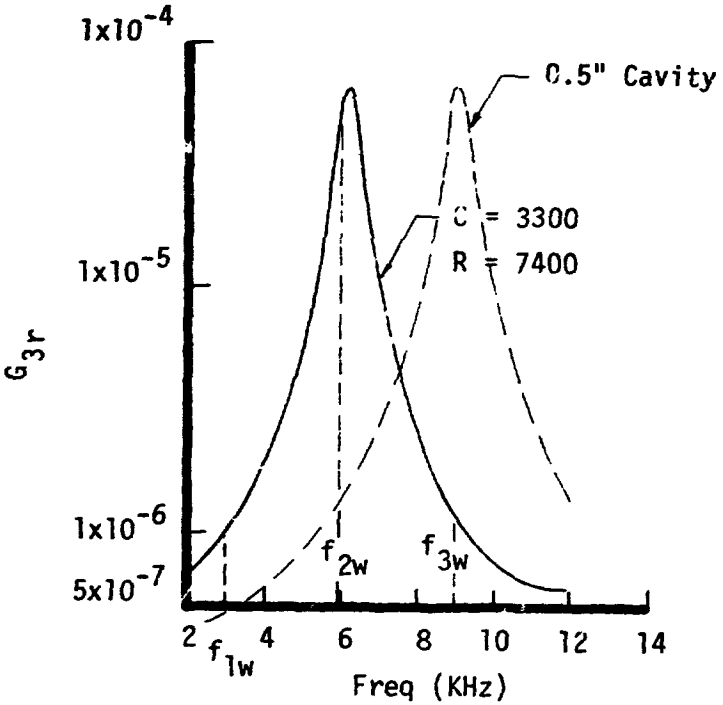

WAVE CONTENTS

Freq.	Avg. Amp.	Avg. Damp Time
1w	-	7 ms
2w	-	
3w	-	

Figure 48. Stability Characteristics for 1.0 in. Deep Cavity

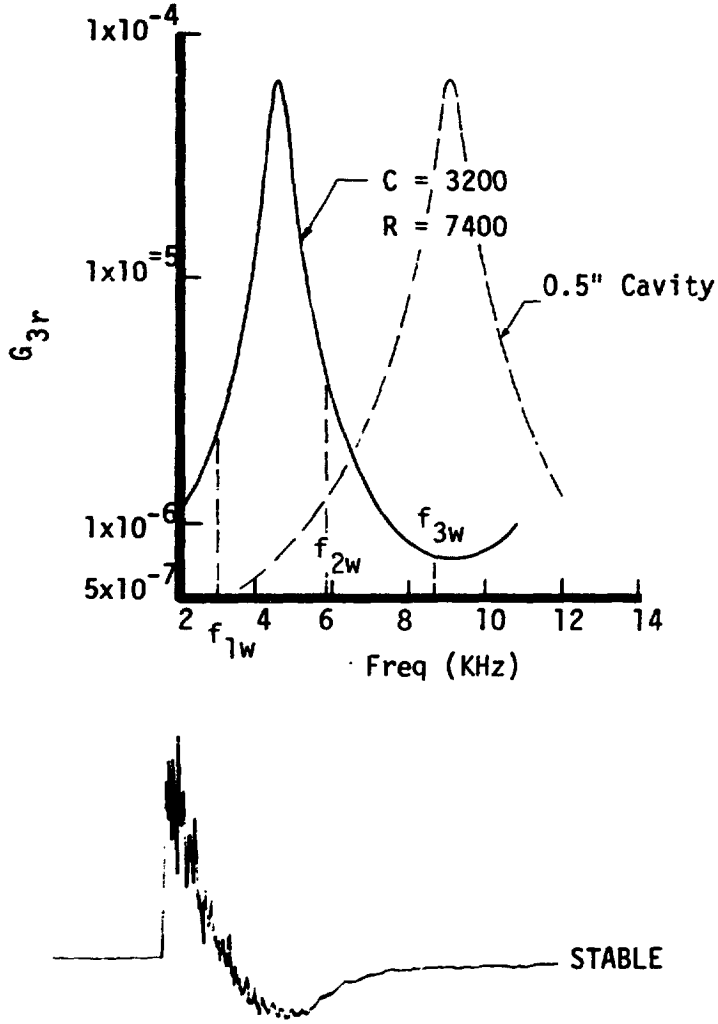

WAVE CONTENTS

Freq.	Avg. Amp.	Avg. Damp Time
1w	-	4 ms
2w	-	
3w	-	

Figure 49. Stability Characteristics for 1.5 in. Deep Cavity

For the 0.5 in. cavity the admittance peak is around 9000 Hz. Hence the 3W mode, about 8400 Hz, is most damped, with successively less damping at the 2W (5600 Hz) and 1W (2800) frequencies. Amplitudes of the component waves are seen to vary inversely with the admittance, being 6, 11, and 44 psi peak-to-peak respectively for the 3W, 2W, and 1W modes. The admittance for the 1.0 cavity peaks around 6000 Hz; hence the 2W mode is most damped. The 1.5 in. cavity admittance peak is between the 1W and 2W modes, and thus the 3W mode is least damped. Successively shorter damp times are noted as cavity length increases and the admittance peak shifts to lower frequencies. Thus the observed stability trends are in agreement with the predicted cavity admittances.

In summary, the data analysis achieved good correlation between the ratio of pressure amplitudes predicted and measured at the back and entrance to the cavity, for all cavity configurations, and showed in a general way the correspondence of actual stability characteristics and predicted admittance values. These accomplishments highlight the progress being made to "reduce" combustion stability to a predictable science.

G. CONCLUSIONS

The movies showed the following:

(1) During stable combustion, the propellant flow from the X-doublet injector is layered -- fuel, oxidizer, fuel, oxidizer, etc. -- over the visible length (2.0-in.), i.e., is not fully mixed or combusted over that distance.

(2) During unstable operation, the combustion couples with the acoustic field. Combustion is complete in 0.4 to 2.0 in., depending on cavity configuration and operating point; this length varies cyclically at the 1W mode frequency, and the propellant streams waver back and forth at the same frequency.

VIII, G, Conclusions (cont.)

(3) During stable combustion, the flow of unburned propellant into the cavity is minimal although it does occur, frequently in a cyclical manner. The combustion products flow into the cavity at a 45° angle, approximately.

(4) During unstable combustion, some cyclic flow of unburned propellant into the cavity occurs; detonation of the bomb causes considerable inflow.

Data analysis showed the following:

(1) The generalized cavity model appears to correctly formulate cavity acoustics, including damping, inlet resistance, and sound speed. Pressure amplitude ratios were closely correlated by the model.

(2) The cavity gas sound speed dominates the analytical predictions; hence assessing the sound speed correctly is of utmost importance.

IX. FULL SCALE (DUAL CAVITY) TESTING

A. INTRODUCTION

Full scale testing was conducted to demonstrate the feasibility of the dual cavity concept, i.e., multimode damping by differently tuned cavities sharing a common entrance. Hardware developed in the Orbit Maneuvering Engine Platelet Injector Program, NAS 9-13133, was used for this purpose. The injector pattern, also from that program, consisted of X-doublet and splash plate elements; it was known to be extremely high performing and unstable in the first three tangential modes as well as in a mixed mode termed resurging, hence was an excellent "instability generator" for evaluating cavity damping effectiveness.

Forty-one firings were conducted, using nitrogen tetroxide and monomethyl hydrazine as propellants. Fifty-eight 6.5 grain RDX bombs were used, some of the firings being double-bombed; double-bombing in effect gives two evaluations per test point and thus yields significant economies.

Five basic cavity configurations, and six additional variations of one of them, were evaluated. These include two dual radial leg concepts, a dual axial leg arrangement, an axial-radial design, and a bitune axial configuration. The six variations, of one of the dual radial units, involved reductions in cavity cross-sectional area. The dual radial and axial radial configurations showed the best damping characteristics.

B. HARDWARE, INSTRUMENTATION, TEST FACILITY

The hardware developed in NAS 9-13133 was modified slightly to accommodate the radial cavity legs: a larger flange was added to the fuel inlet manifold; this flange formed the wall of the radial cavities. A new cavity housing was fabricated as was a spacer plate to bring the injector

face in parallel to the enlarged flange. Also fabricated were 132 blocks that could be inserted into the cavities to change the cavity length or cross-sectional area.

Figure 50 is a photograph of the enlarged flange; it shows also the injector face and axial cavities. The mating cavity housing is pictured in Figure 51. The insertable blocks are shown on Figure 52. Drawings reproduced on Figures 53 through 58 show the top assembly, test assembly, injector, spacer plate, cavity housing, and cavity configuration blocks respectively. The basic parts list is given in Table III.

The mixed element injector developed in NAS 9-13133 combined splash plate and X-doublet elements in concentric rings such that the higher energy release zones associated with the splash plate elements corresponded to zones of low acoustic pressure level for the anticipated acoustic modes, as illustrated in Figure 59. The stability history of this pattern as tested in NAS 9-13133 is summarized in Table IV. The injector was tested five times with bitune cavity configurations of various geometries; spontaneous instabilities occurred each time, with first, second, and third tangential modes as well as resurging in evidence. A third cavity type, installed radially, was added and resulted in stable combustion in five tests conducted over a wide range of operating conditions. Substitution of Aerozine-50 (50% hydrazine, 50% unsymmetrical dimethyl hydrazine) for the fuel resulted in instabilities on the two subsequent tests, however, and reducing the chamber length from the nominal 16 in. to 12 in. also resulted in instabilities.

The injector fabricated for NAS 9-13133 was designated ME 1 and was reworked in that program; the platelet face was machined away and replaced with a different pattern. The face of the injector used in the present program was created (photoetched) from the same artwork and the unit was designated ME 1A. The pressure drops across the face of ME 1A were about 10% higher

Mixed Element Injector

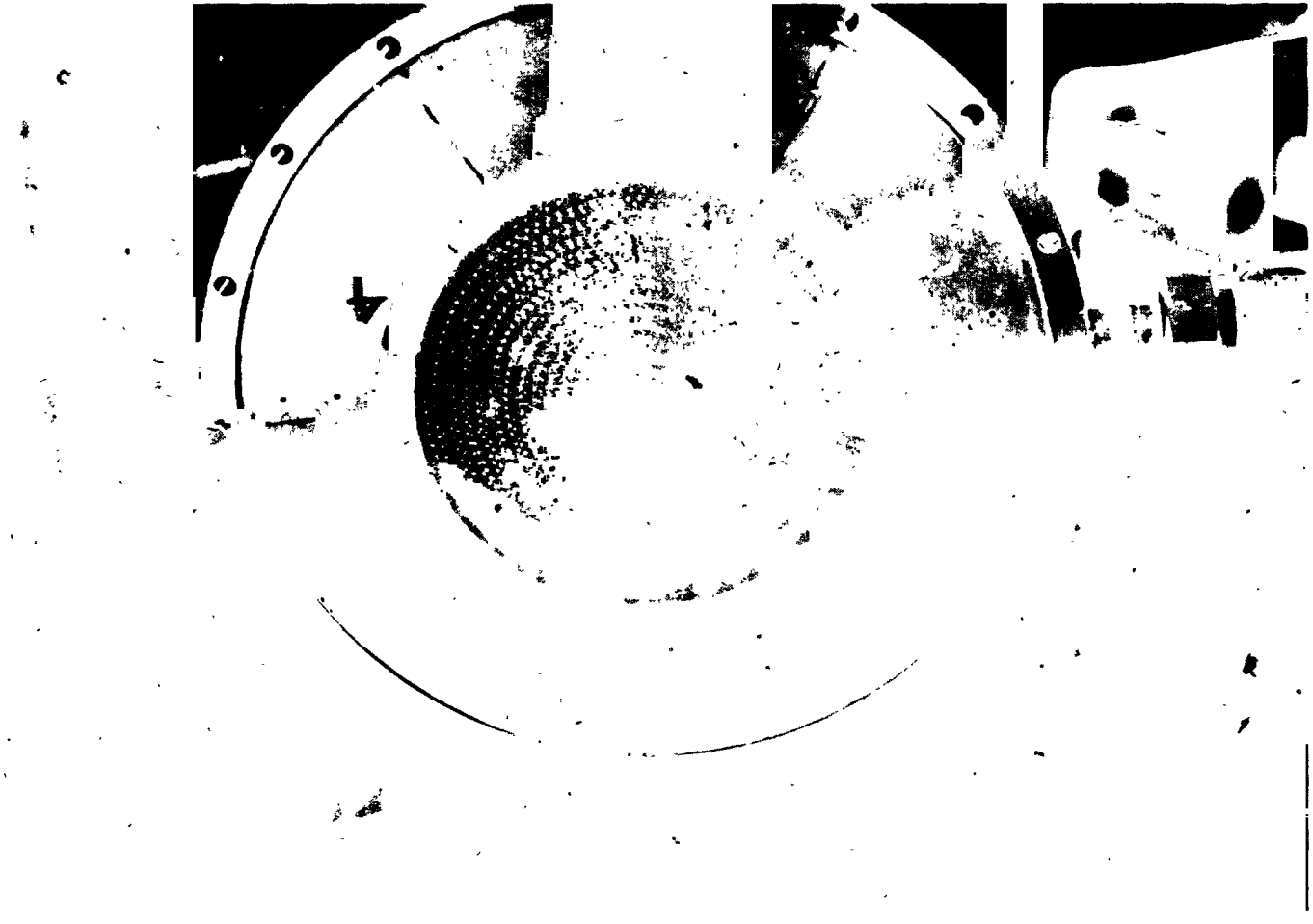

Figure 50

Dual Cavity Housing

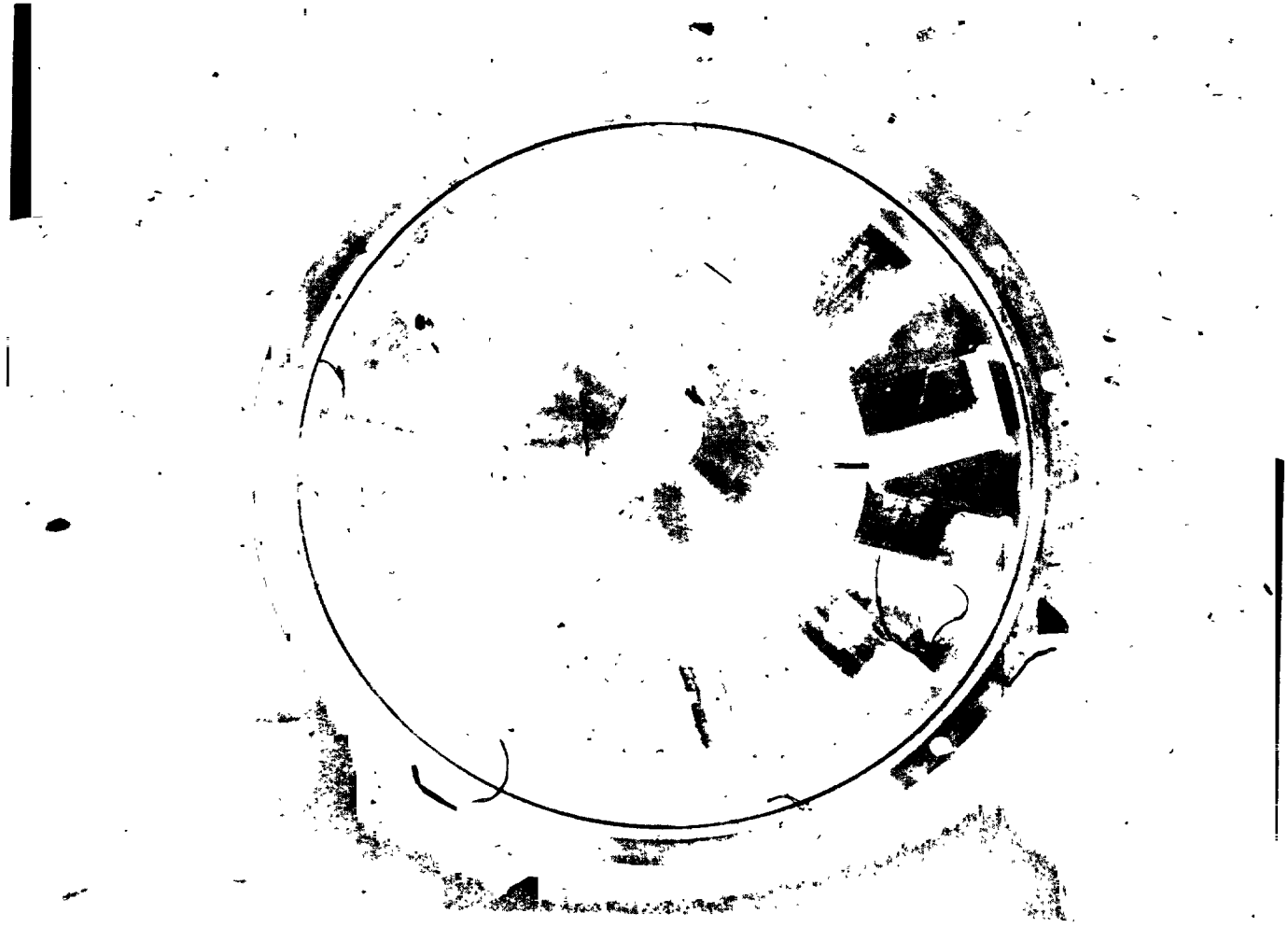

Figure 51

Dual Cavity Hardware

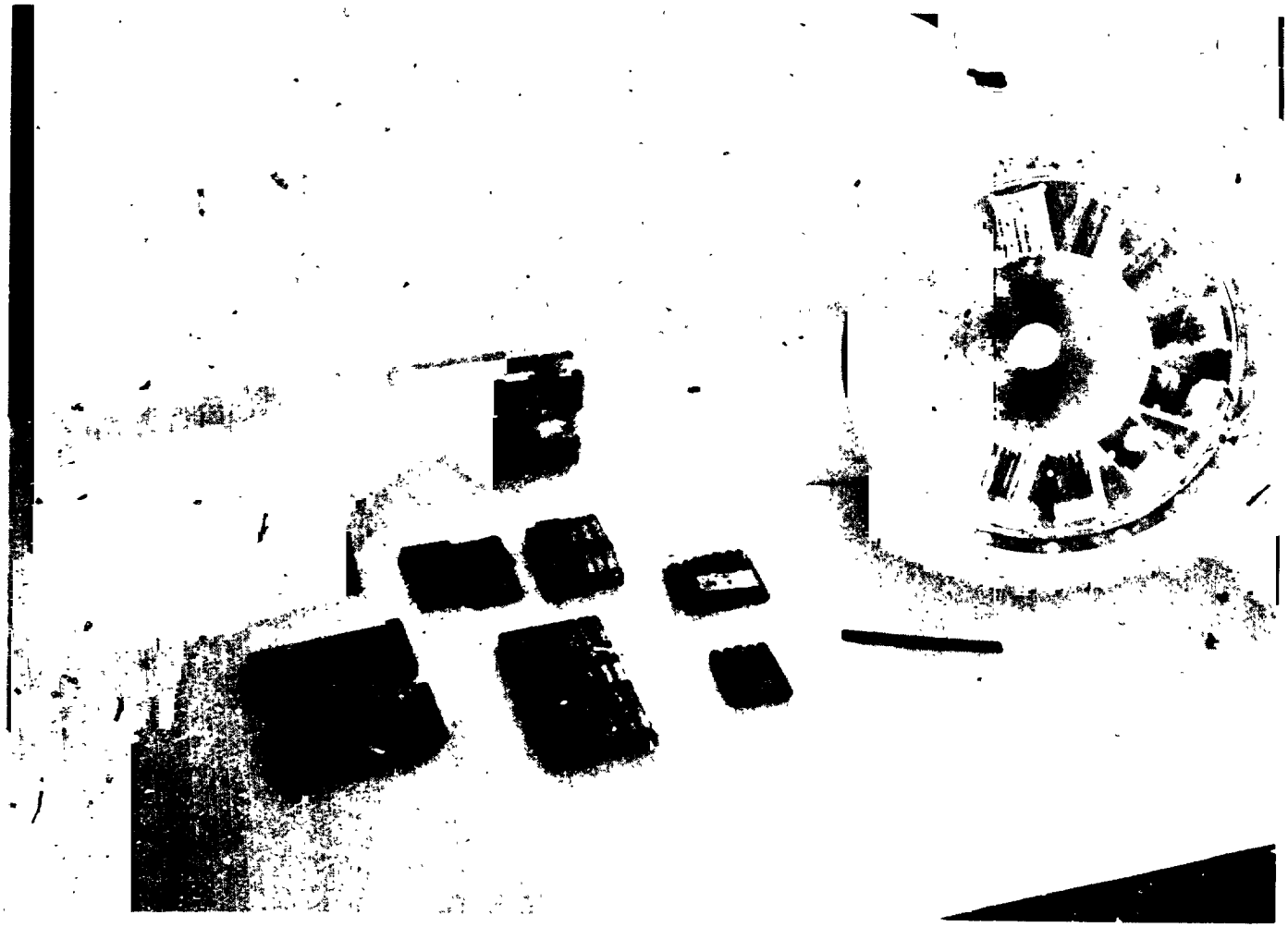

Figure 52

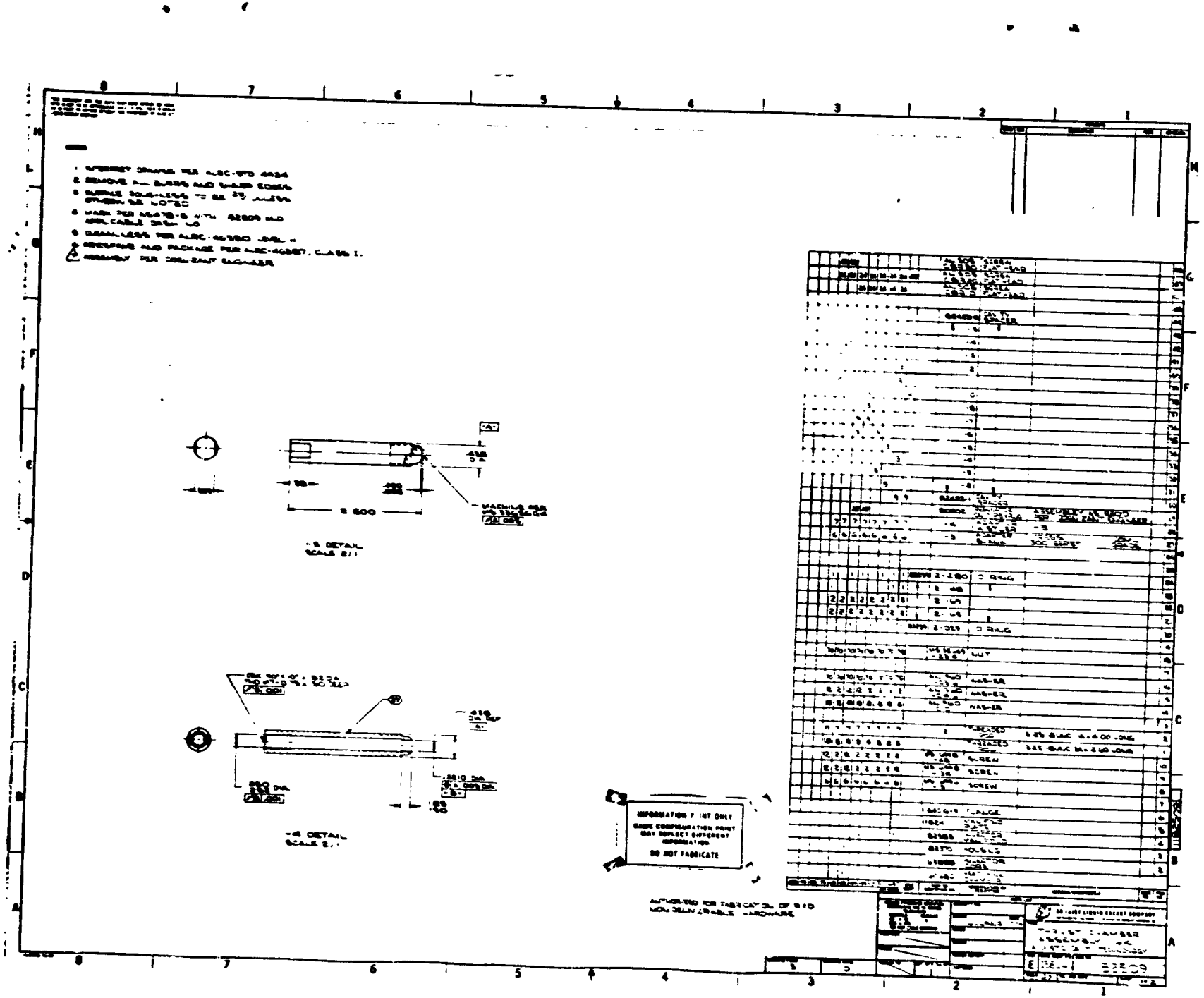

Figure 53. Top Assembly Dash Number

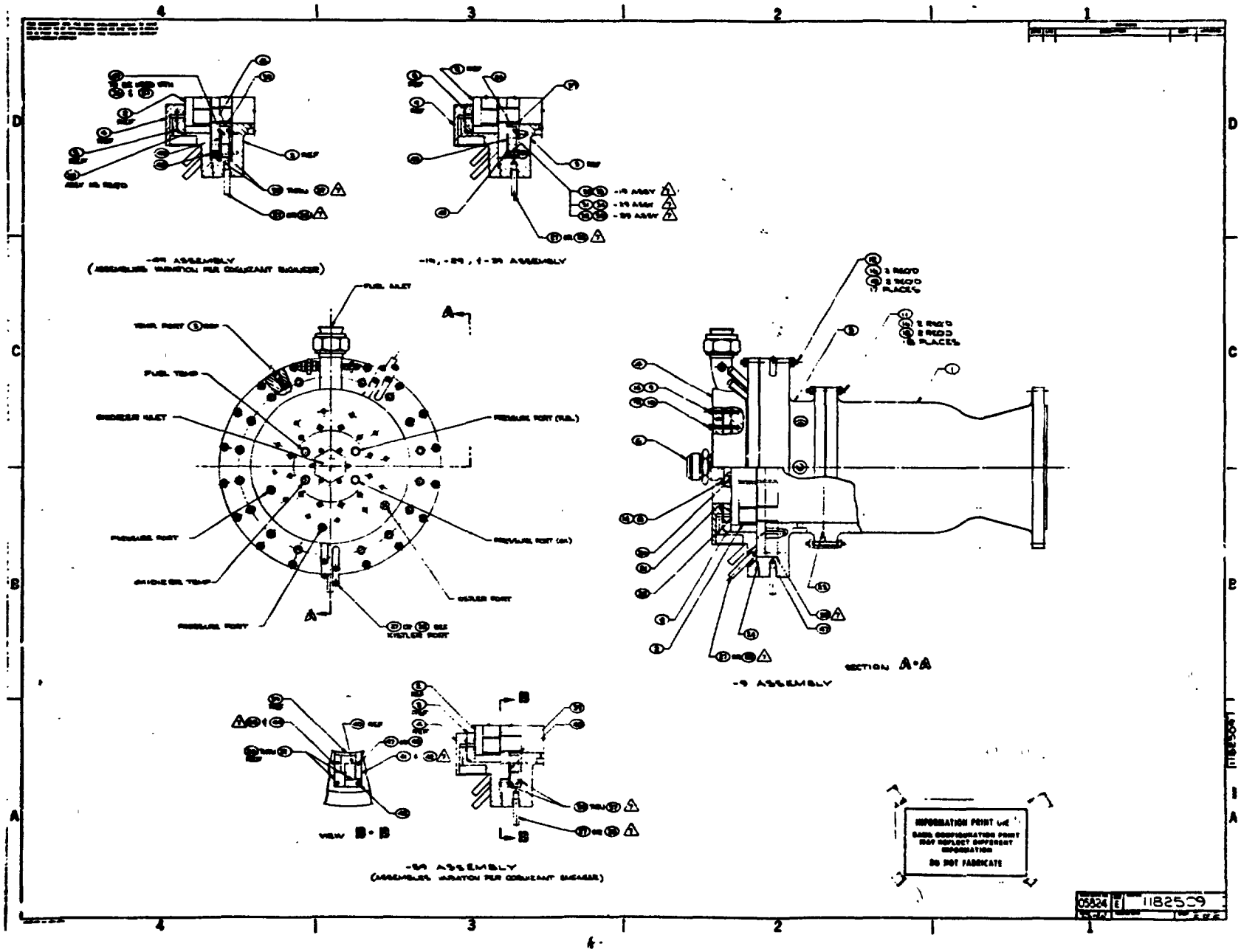

Figure 54. Test Assembly

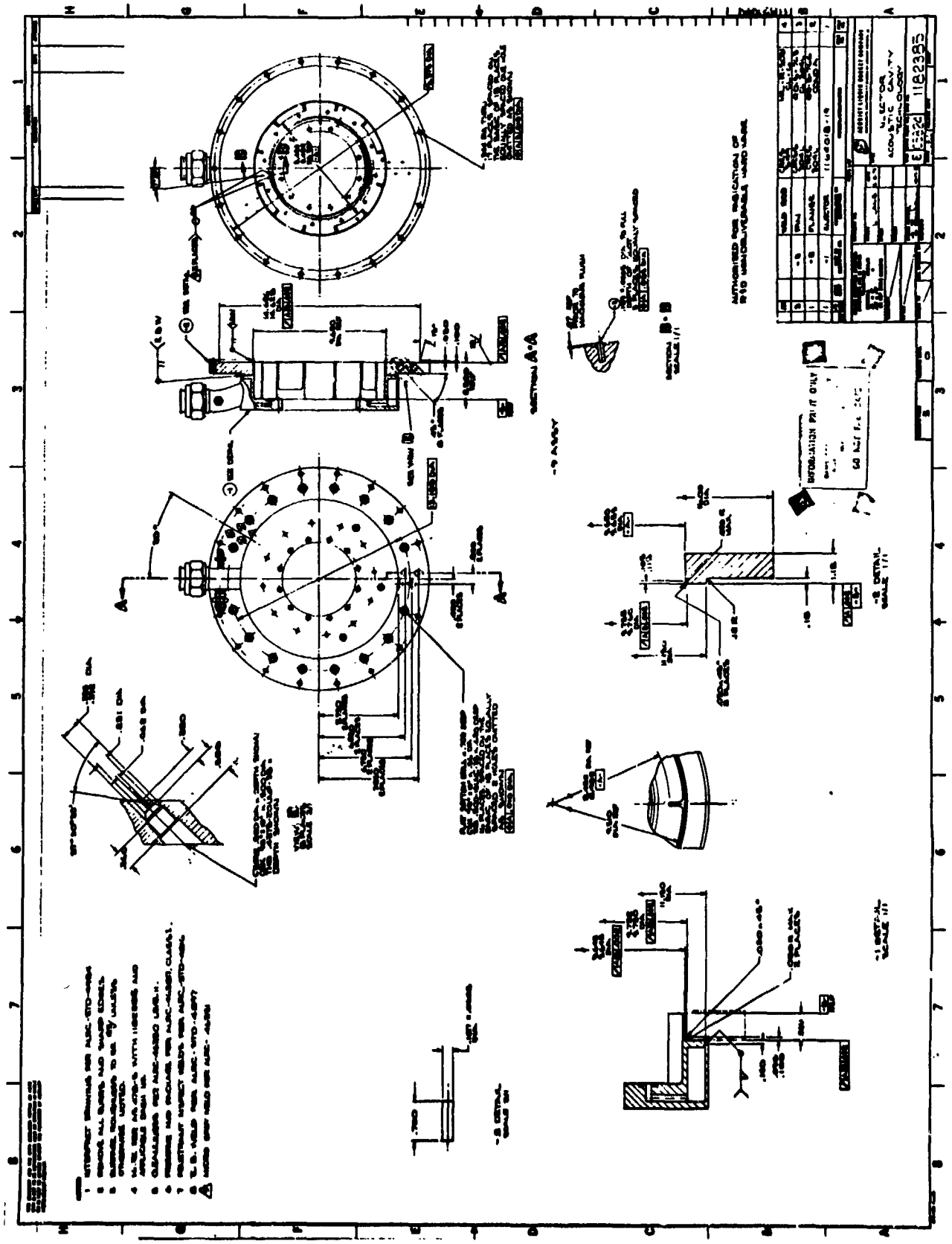

Figure 55. Injector Manifold

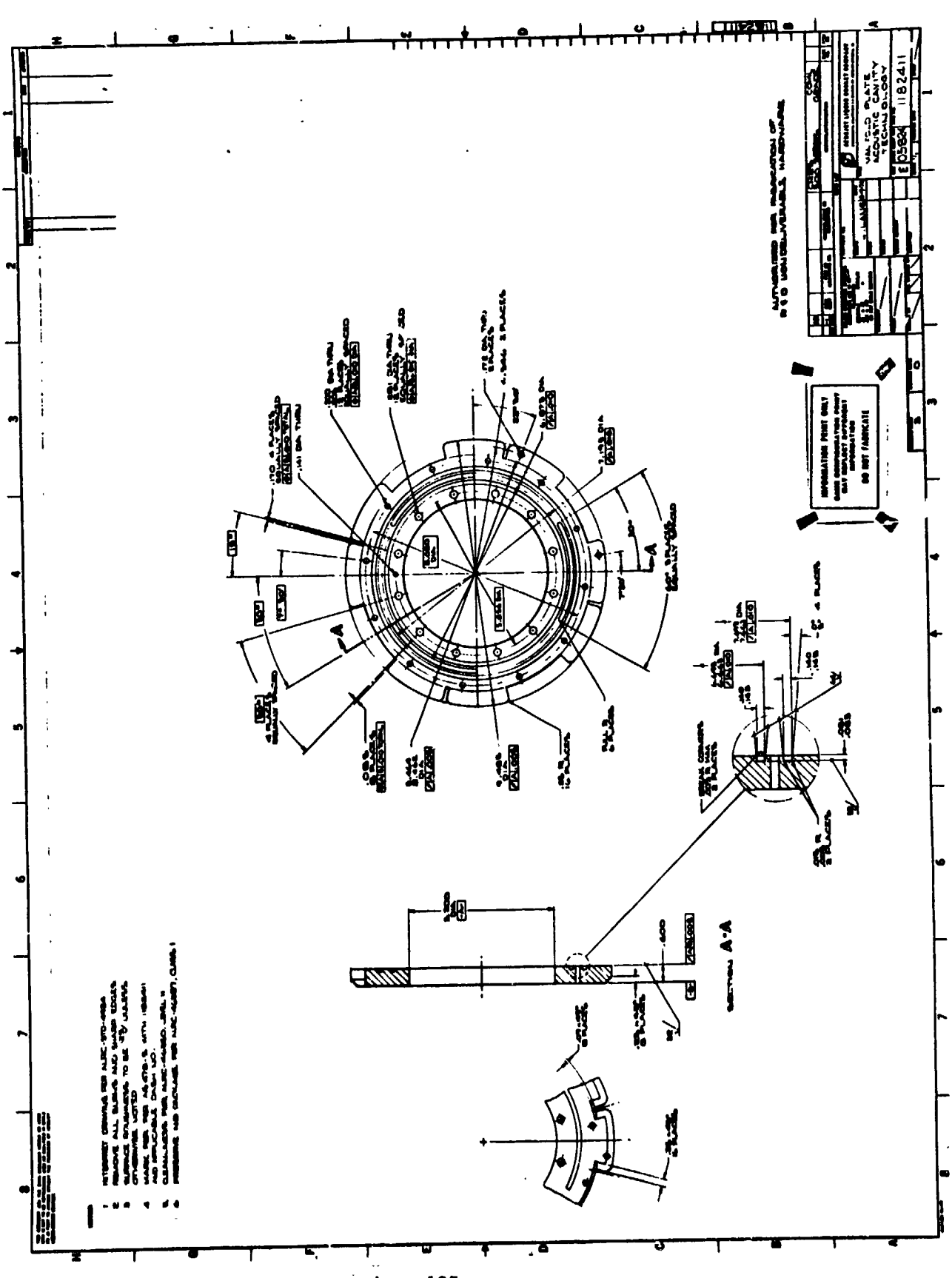

Figure 56. Injector Spacer

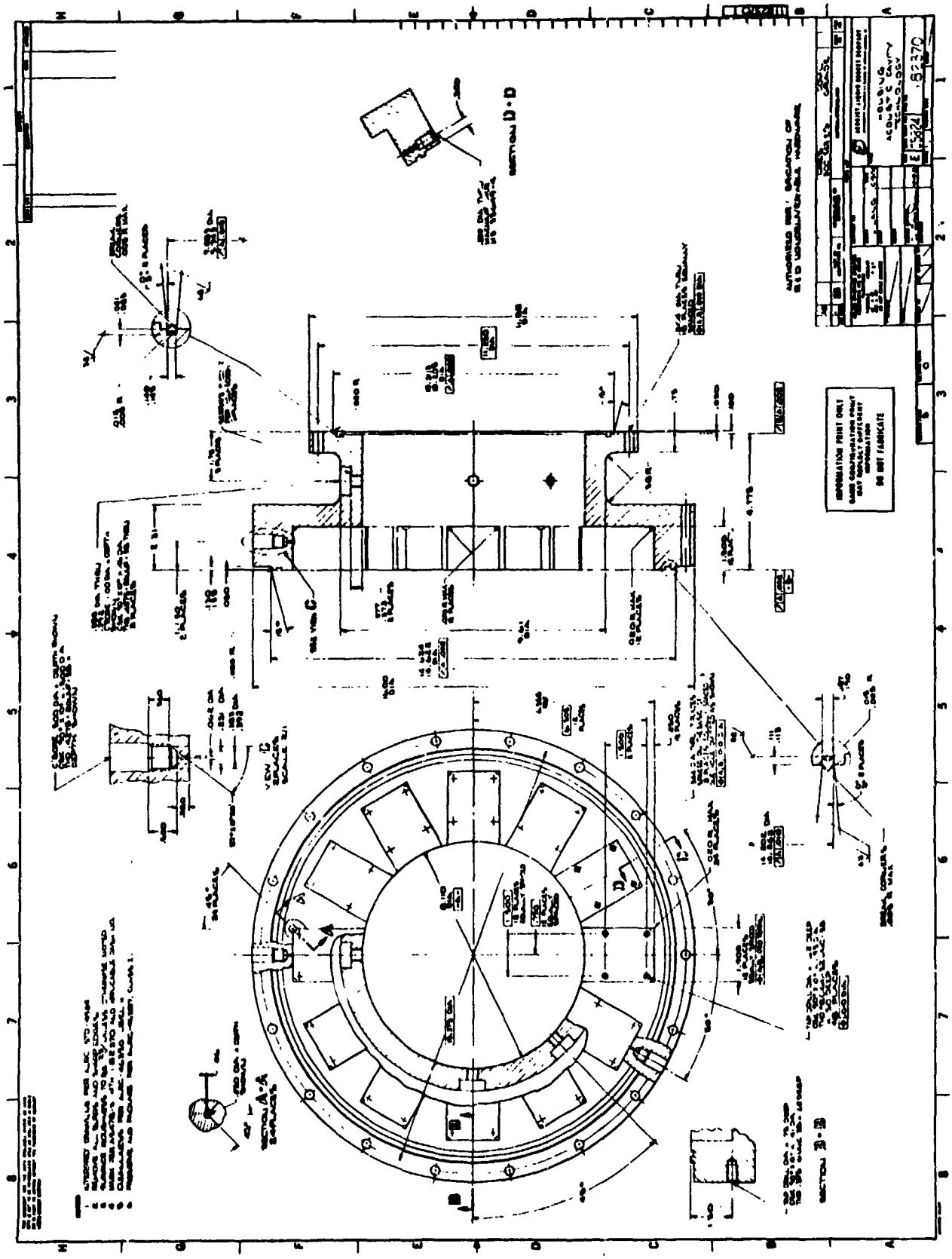

Figure 57. Acoustic Cavity Housing

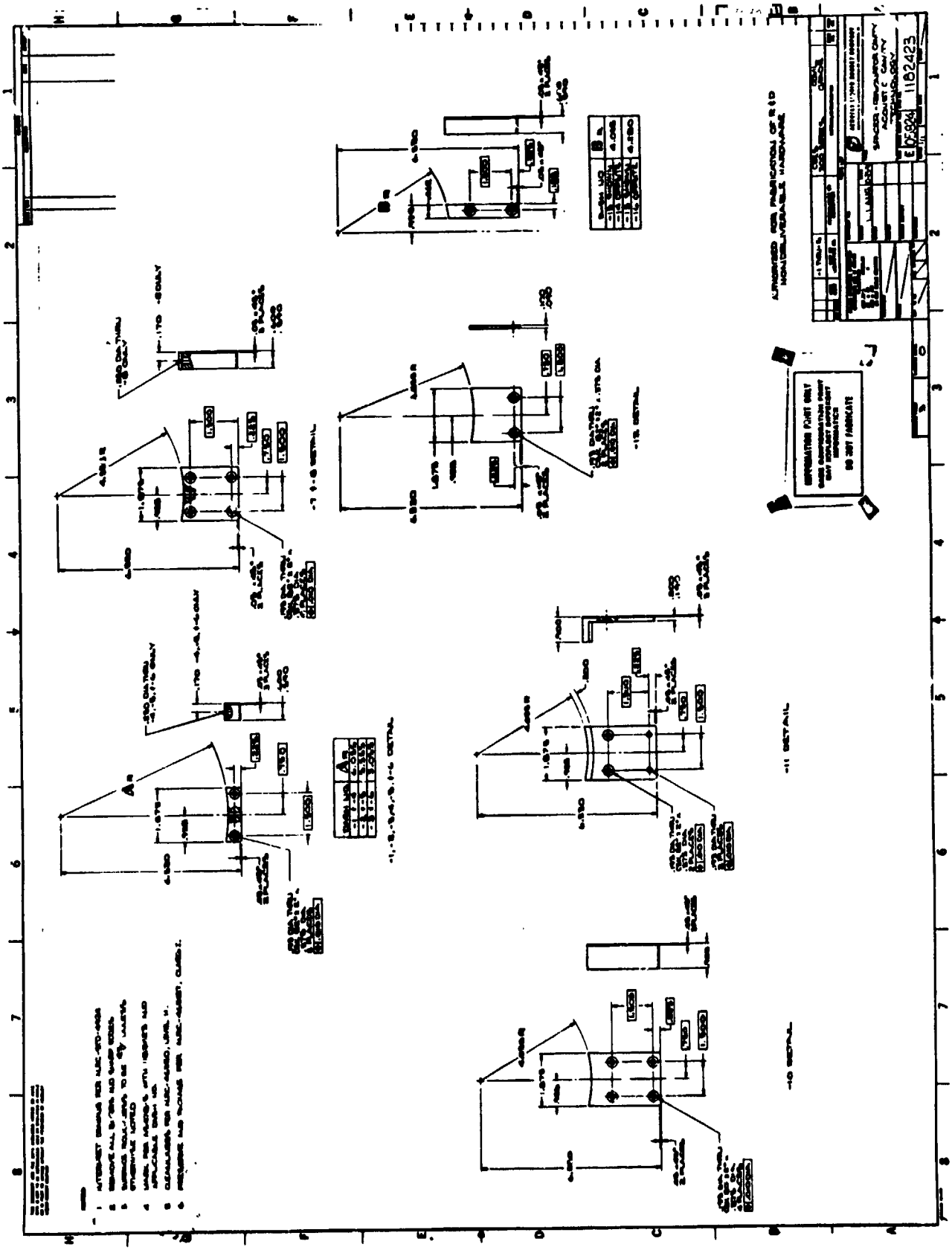

Figure 58. Cavity Configuration Blocks

TABLE III

BASIC PARTS LIST DUAL CAVITY HARDWARE

Description	Qty.	P/N
Heat Sink Chamber	1	1164680
Heat Sink Cavity Housing	1	1182370
Mixed Element Injector Core	1	1163888
Injector Manifold	1	1182385
Injector Manifold Plate	1	1182411
Oxidizer Inlet	1	1164016-9
Cavity Geometry Blocks	*	1182423 1180202
Teflon "O" Ring Seals	1	2-280
" " " "	1	2-148
" " " "	2	2-165
" " " "	2	2-169
" " " "	1	2-029

*As required.

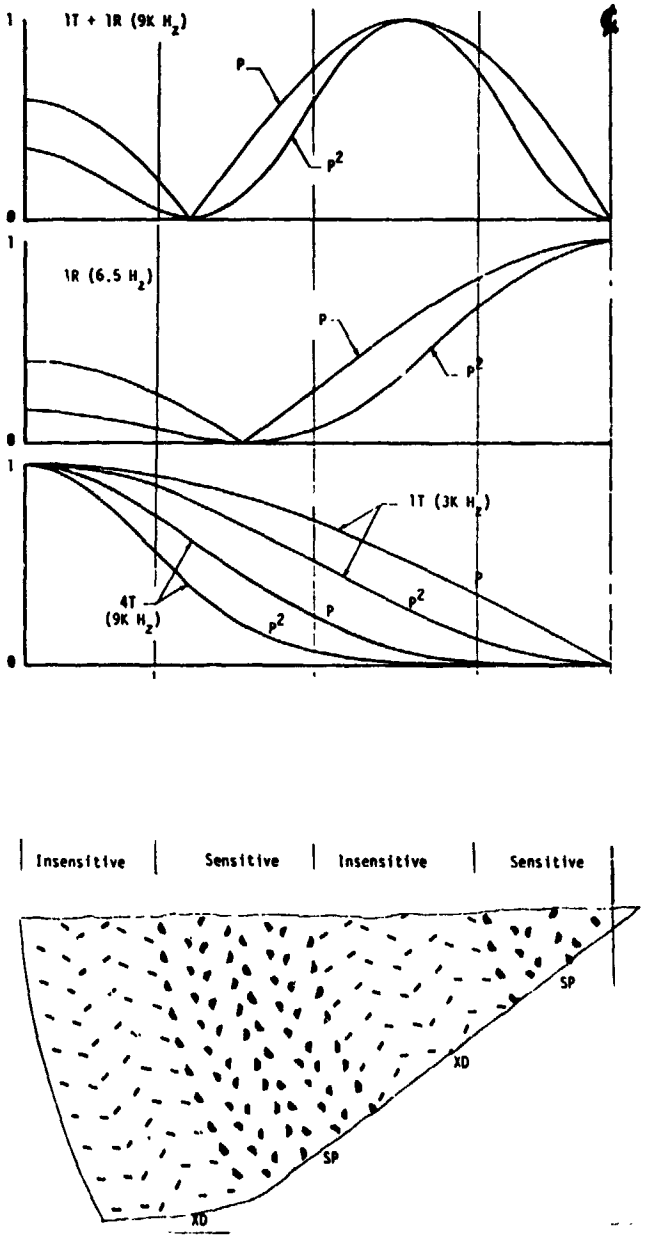

Figure 59. Mixed Element Design Characteristics

TABLE IV

SUMMARY OF OME MIXED ELEMENT TESTING

Test	Pc	O/F	T_{ox}	T_f	Bomb Location	1T Depth (8 cav) (19% A_{face})	3T Depth (4 cav) (20% A_{face})	12 rad. cav (20% A_{face})	Result	Spont.
144	122	1.70	70	70	6	1.5	0.4	-	Resurge → 1T	X
145	123	1.70	70	200	6	1.5	0.4	-	1T, 2T	X
146	123	1.70	70	200	6	1.2	0.4	-	1T, 2T	X
147	120	1.65	70	200	6	1.2	0.6	-	Resurge, 1T, 2T, 3T	X
148	119	1.70	70	200	6	0.95	0.35	-	1T, 2T	X
149	124	1.67	70	200	6	0.95	0.35	1.2		
150	138	1.87	70	200	6	0.95	0.35	1.2		
151	138	1.44	70	200	6	0.95	0.35	1.2		
152	108	1.88	70	200	6	0.95	0.35	1.2		
153	107	1.41	70	200	6	0.95	0.35	1.2		
154	125	1.65	70	200	-	0.95	0.35	1.2	2T	
155	125	1.45	70	200	6	0.95	0.35	1.2	2T	X
168	125	1.64	50	200	2	0.95	0.35	1.2	Resurge 1T	X
169	150	1.65	50	200	2	0.95	0.35	1.2		
170	125	1.64	50	200	2	0.95	0.35	1.2	Resurge	X
171	140	1.84	50	200	2	0.95	0.35	1.2	1T→Resurge	X
172	140	1.65	50	200	2	0.95	0.35	1.2	Resurge, 1T	

Cavity Configuration: Square inlet contour, flat chamber shape, square corner contour, 0.60 in. inlet height, 0.574 in. Cavity Width, 0.126 in. Overlap

All spontaneous instabilities occurred immediately after Pc rise.

No 1L observed except 15 ms of 1400 Hz on Test 144

Tests 154, 155: Aerozine-50 used as fuel

Tests 168-172, 12 in. chamber; all others 16 in.

than those of the earlier injector; performance, however, was comparable, as shown by Figure 60. Stability characteristics of ME 1A were anticipated to be substantially the same as those of ME 1, i.e., highly unstable.

Instrumentation included high and low frequency response devices as listed in Tables V and VI, respectively. Instrumentation locations on the injector back side are specified in Figure 61, and on the chamber in Figure 62.

Testing was conducted in Bay 5 of the ALRC Physics Laboratory in Sacramento. Figure 63 shows the sea level test stand. Heated fuel was supplied from a hot water counterflow heat exchanger located upstream of the valve; the thermal capacitance of the system delayed steady-state injection temperatures until 1.5 sec into the test however. Steady state conditions were maintained for 0.5-sec prior to bomb initiation. Nitrogen purges were activated on shutdown with a 100 psi override. The electrical sequence is given in Figure 64.

C. TEST SUMMARY

The approach to dual cavity testing is illustrated in the logic diagram of Figure 65. Briefly, the intent was to check out the damping effectiveness of the first of the two cavity configurations -- i.e., the dual radial and the axial radial -- selected on the basis of the acoustic modeling effort. If this configuration proved stable, it would undergo (1) operating point testing to investigate the effects of chamber pressure and mixture ratio variations, (2) margin testing involving reductions in cavity cross-sectional area, and (3) statistical testing to obtain a statistically sufficient number of test points. If unstable, the configuration would be tuned by changing cavity leg lengths; if stabilized, it would undergo operating point, margin, and statistical testing.

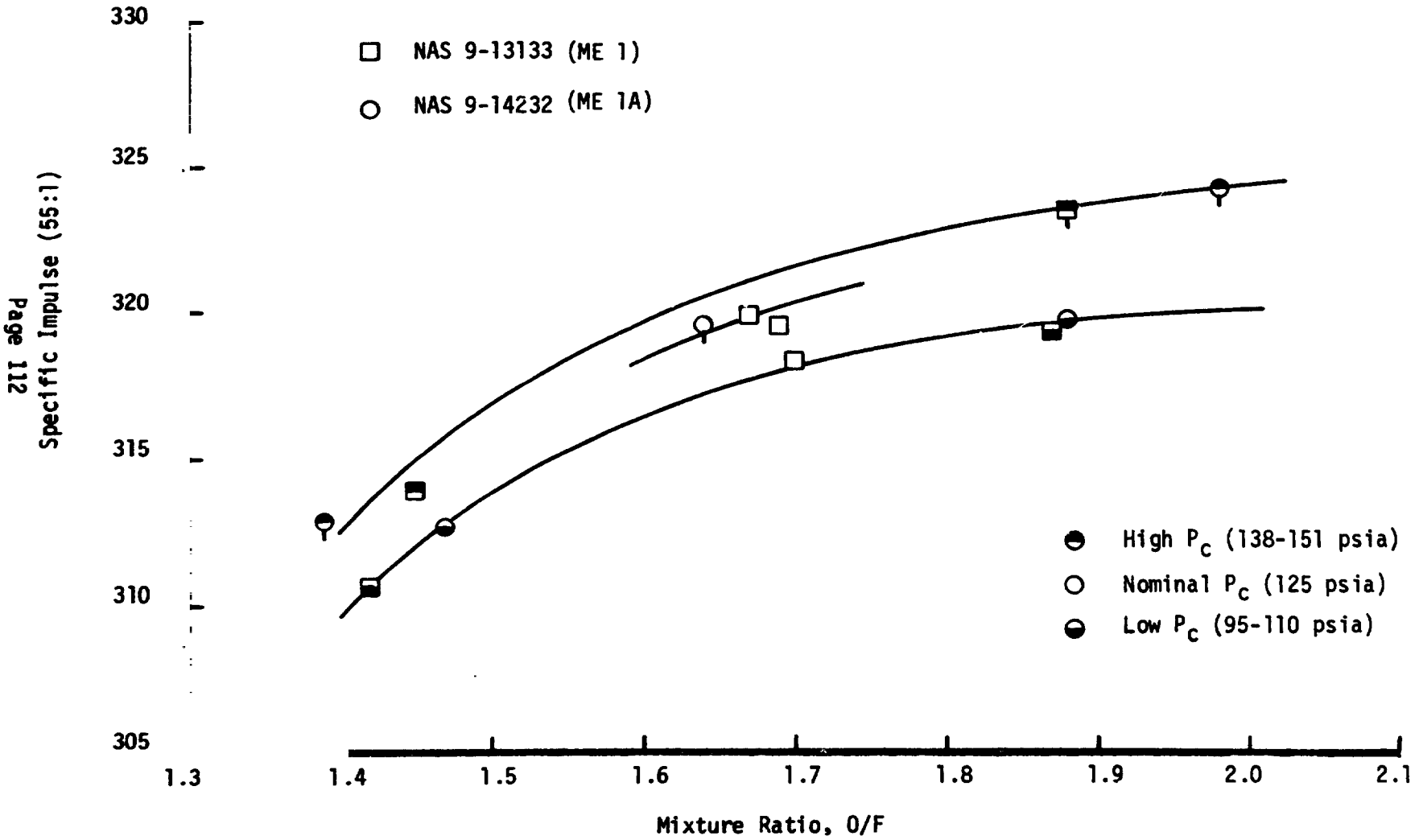

Figure 60. ME1 and ME1A Performance Comparison

TABLE V

HIGH FREQUENCY RESPONSE INSTRUMENTATION

Test Parameter	Symbol	Instrument Make	Instrument Model	Limit	Accuracy	Cavity Type
Axial Cavity Pressure, 320°	P_{AX}-320	Kistler	601	20,000 Hertz	± 0.5%	3T
Radial Cavity #1 Pressure, 270°	$P_{RA1-270}$	"	"	"	"	1T
Radial Cavity #1 Pressure, 60°	P_{RA1-60}	"	"	"	"	"
Radial Cavity #2 Pressure, 60°	P_{RA2-60}	"	"	"	"	"
Radial Cavity #2 Pressure, 270°	$P_{RA2-270}$	"	"	"	"	"
Chamber Pressure, 0°	P_{c-0}	Photocon	307	20,000 Hertz	5%	"
Chamber Pressure, 60°	P_{c-60}	"	"	"	"	"
Chamber Pressure, 270°	P_{c-270}	"	"	"	"	"

TABLE VI

LOW FREQUENCY RESPONSE INSTRUMENTATION

Test Parameter	Symbol	Range	Units	Recorder "O" Graph	Recorder Tape	Recorder Digital
Oxid. Tank Pressure	POT	0-1500	psia	X		X
Fuel Tank Pressure	PFT	0-1500	psia	X		X
Oxid. Injector Pressure	POJ	0-1500	psia	X	X	X
Fuel Injector Pressure	PFJ	0-1500	psia	X	X	X
Chamber Pressure	PC-1	0-1000	psia	X	X	X
Thrust, A & B	FA, FB	0-6000	lbs	X		X,X
Oxid. Flowrate	WO	0-20	lb/sec	X		X
Fuel Flowrate	WF	0-10	lb/sec	X		X
Oxid. Flowmeter Temp.	TOFM	0-100	°F			X
Fuel Flowmeter Temp.	TFFM	0-300	°F			X
Fuel Injector Temp.	TFJ	0-300	°F			X
Oxid. Valve Voltage	VOV			X		
Fuel Valve Voltage	VFW			X		
Injector Purge Valve Voltage	VIPV			X		
1 KHZ Time Code				X		
Axial Cavity Temperature	TA-1					X
	-2					X
	-3					X
	-4					X
Radial Cavity Temperature	TR-1					X
	-2					X
	-3					X
	-4					X
Bomb Trace #1	VB1			X		
Bomb Trace #2	VB2			X		

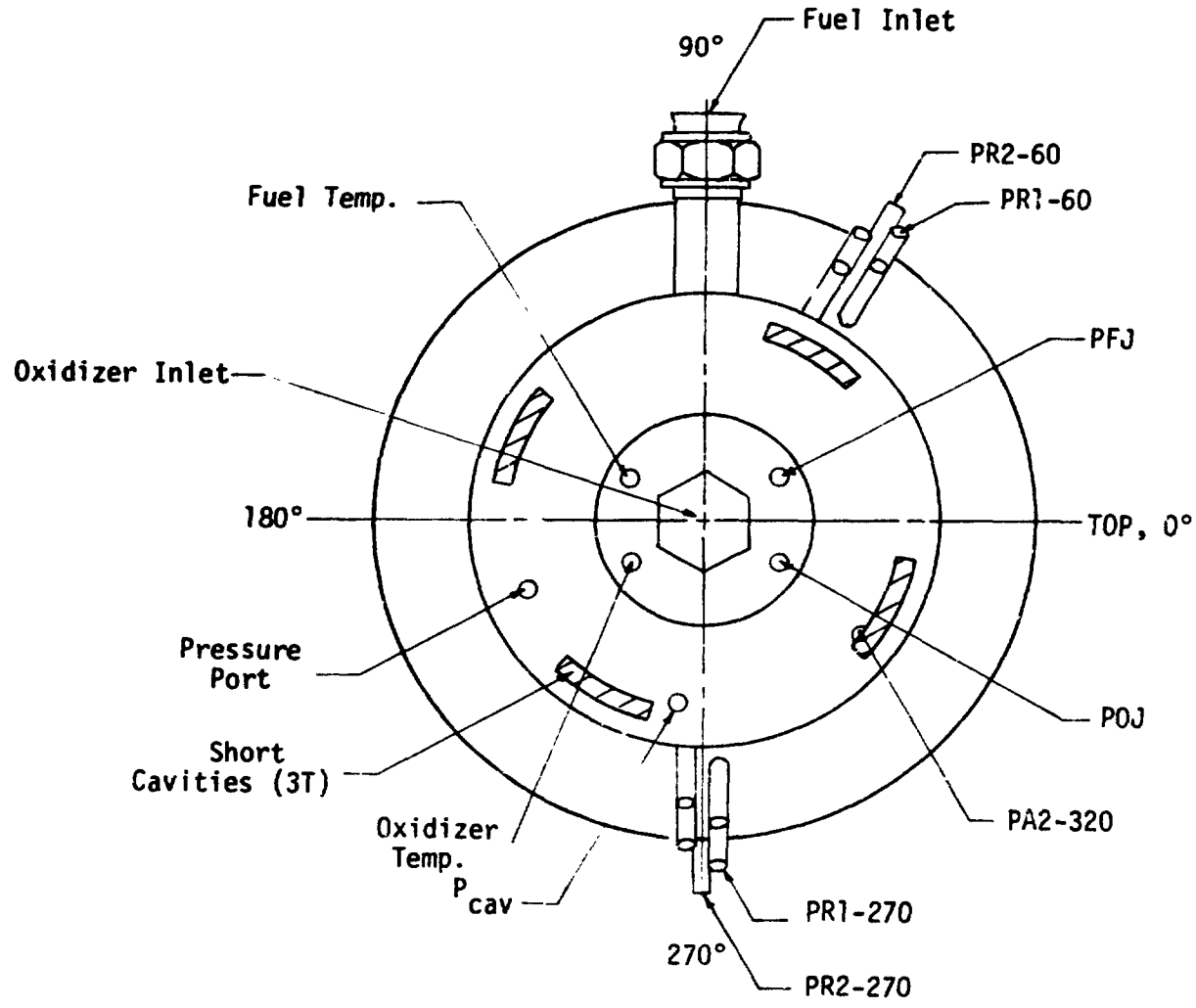

Figure 61. Injector Backside Instrumentation

Engine Assembly Instrumentation

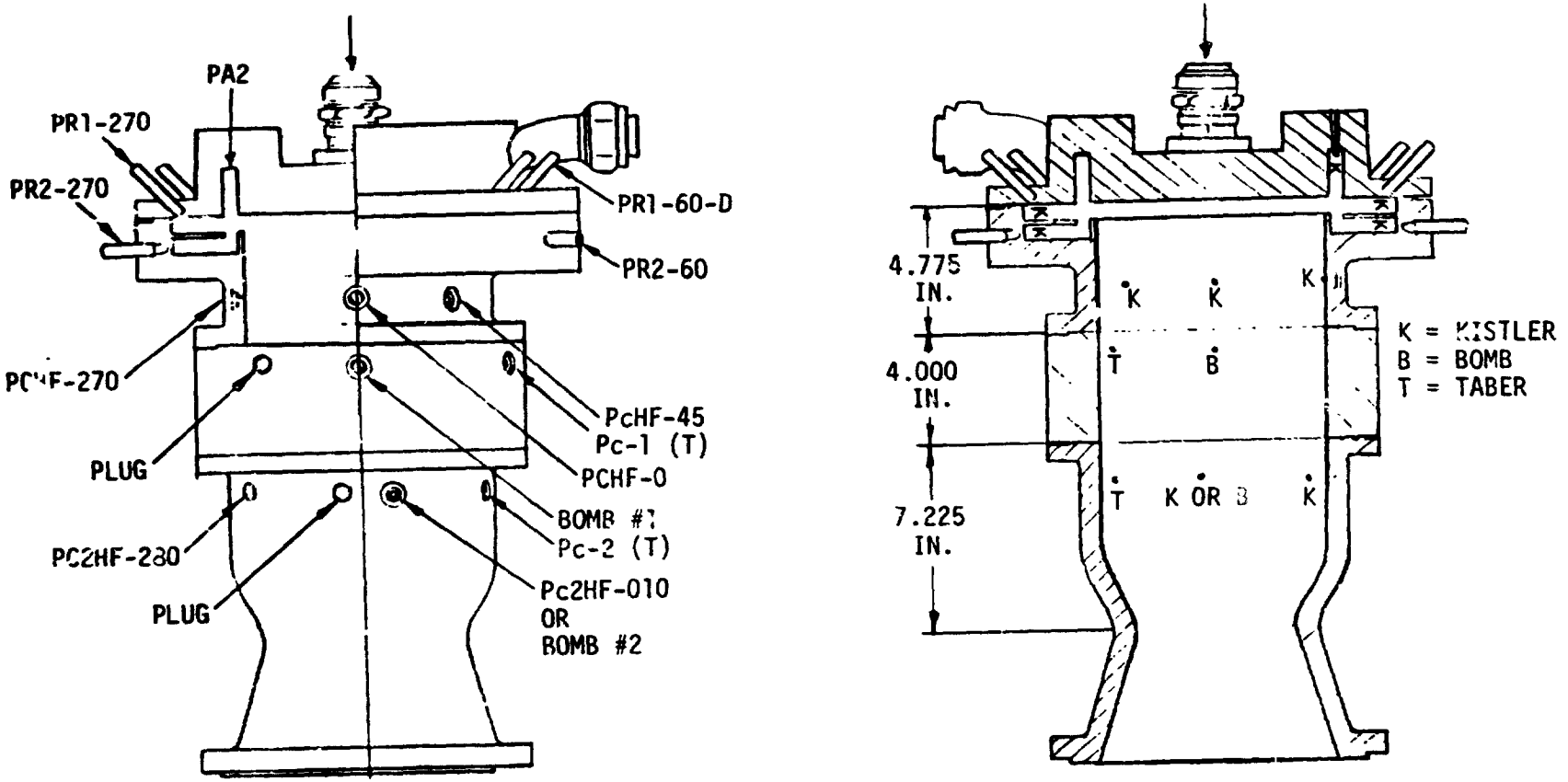

Figure 62

Sea Level Test Facility

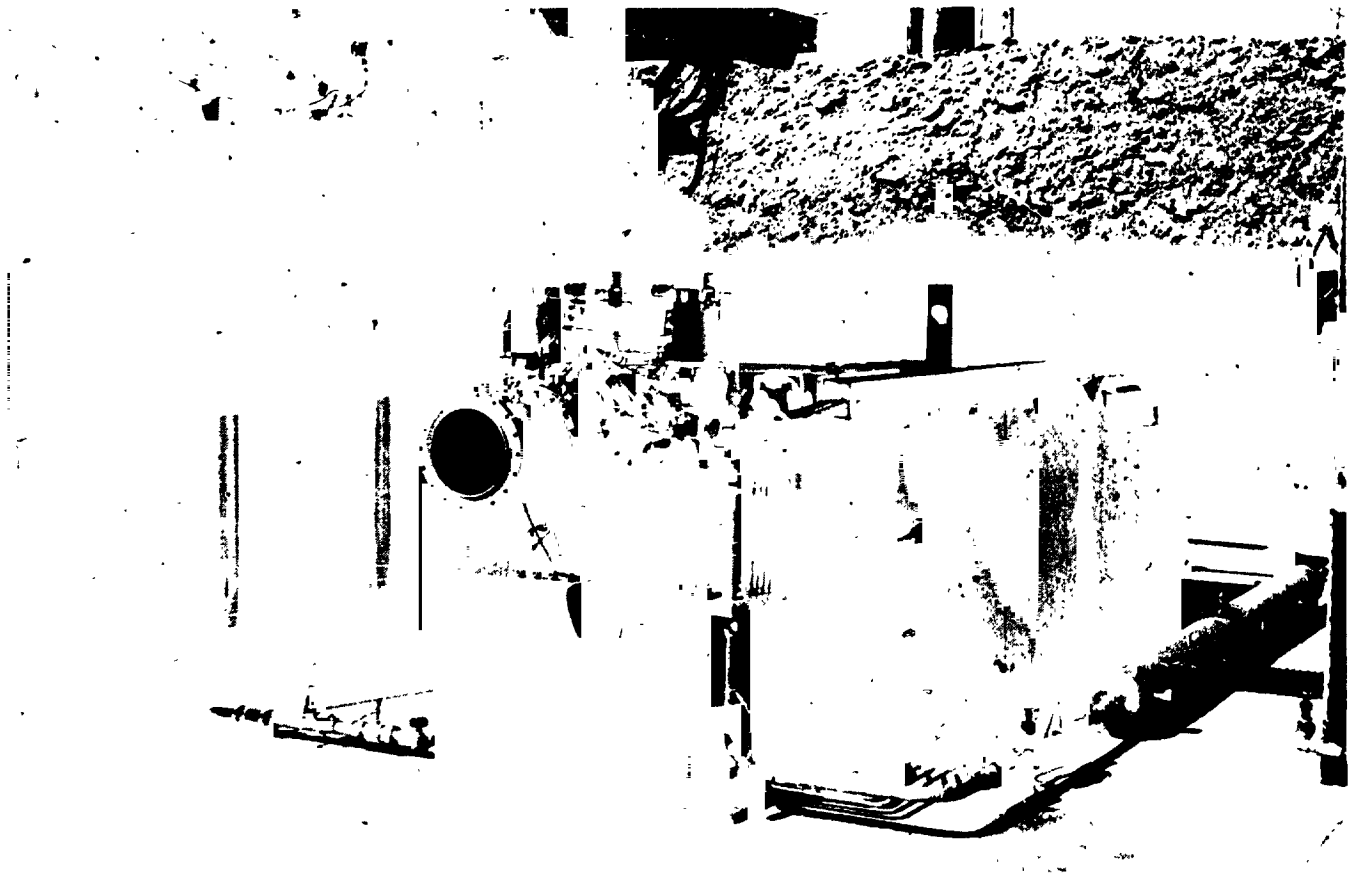

Figure 63

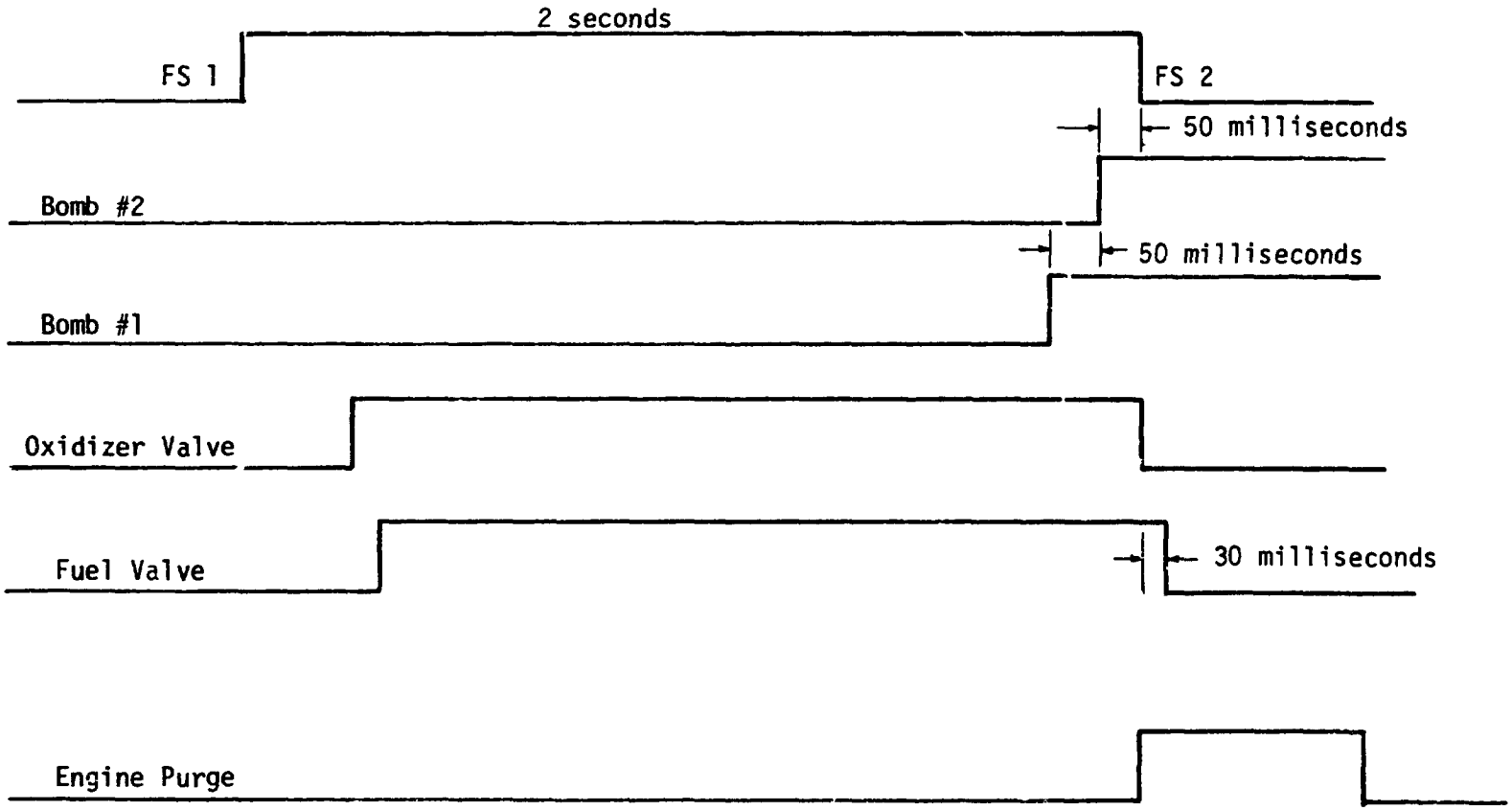

Figure 64. Electrical Sequence

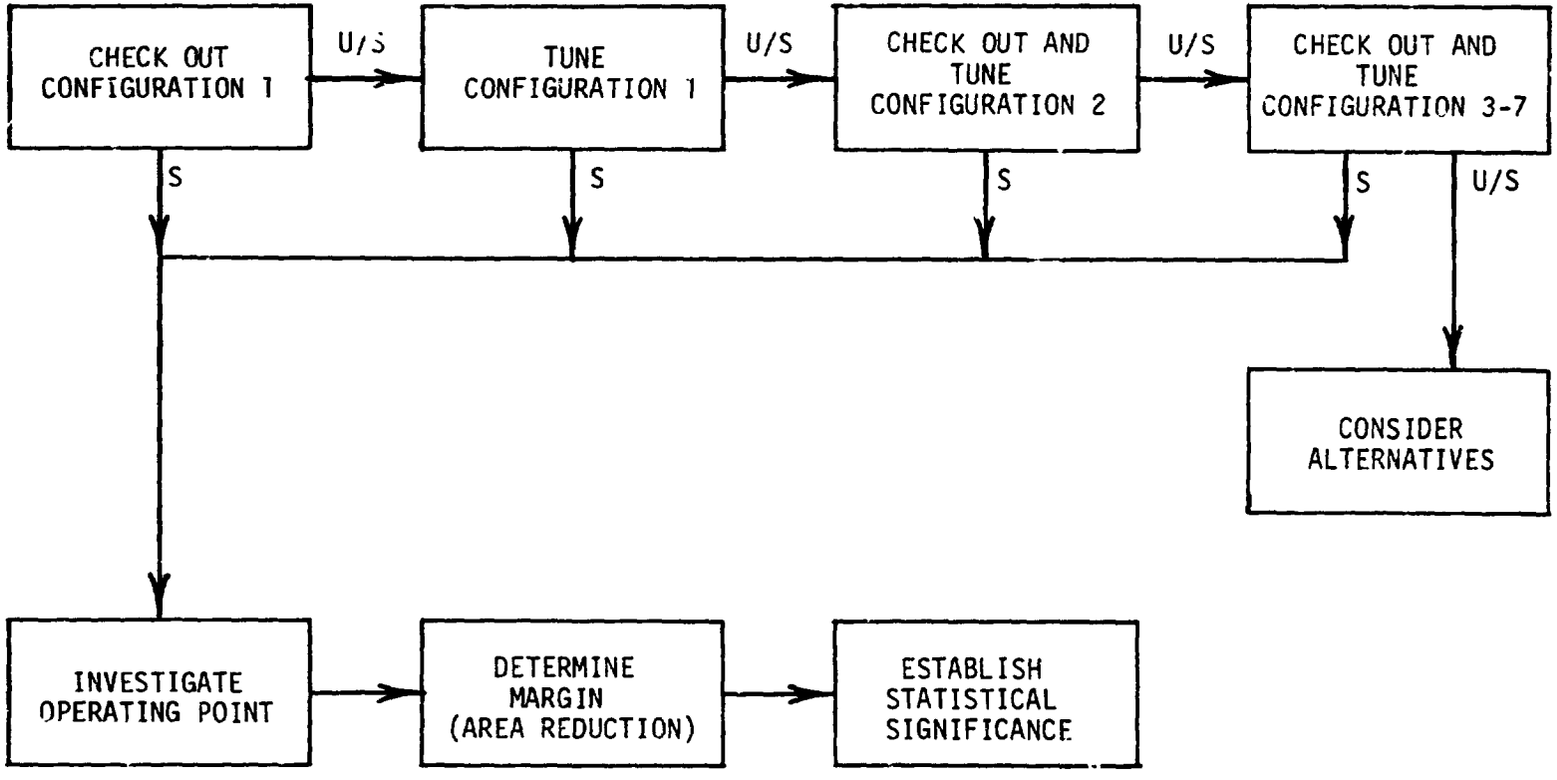

Figure 65. Logic Diagram for Dual Cavity Testing

IX, C, Test Summary (cont.)

If not, the second configuration would be subject to the same procedures. In the event that the second could not be stabilized, a maximum of six additional configurations would be examined.

The first configuration to be tested, the DR1, proved mostly stable through the checkout and operating point testing. The DR2 configuration was then installed, with the objective of improving the marginal tune of DR1. It too was mostly stable through the operating point testing. The AR1 configuration, the alternate design to come out of acoustic modeling, was then evaluated; it proved totally bomb-stable through the operating point testing. At this point, the testing deviated from the logic diagram; some question arose as to the steady-state coolability of the partition between the legs of the dual radial configuration. Thus, the DR1 was evaluated without partitions. It proved bomb-stable, and the suspicion developed that the ME 1A injector might not be as unstable the ME 1. So the bitune configuration, simulating that of earlier testing, was installed, with the result that the injector was indeed unstable. An alternate configuration, the AA1, was then evaluated. Finally the margin testing spelled out in the logic diagram was accomplished, using five area reductions in the legs of the DR1 cavity arrangement.

In all, eleven configurations were tested, as summarized in Table VII. These comprised five basic geometries, as detailed in Figure 66. The stability summary for the entire test series is presented in Table VIII which gives the frequency, amplitude, duration, damp time, etc., for postbomb responses as well as spontaneous events. A brief description of the testing for each geometry is given below.

DR1 Testing. The first ten tests were conducted with the dual radial cavity configuration; single bombs were detonated on seven of the tests.

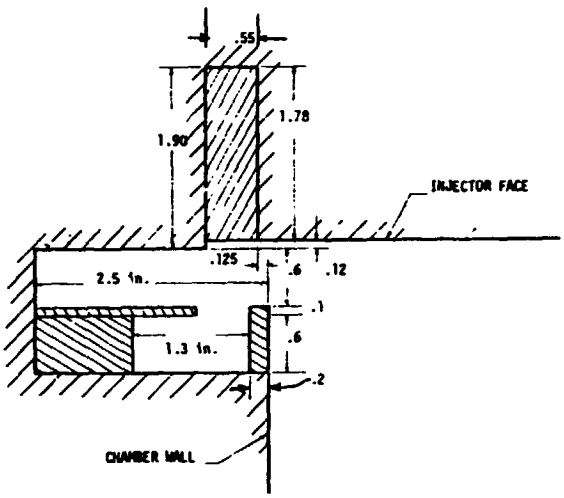

Dual-Radial #1 Cavity (DR1)

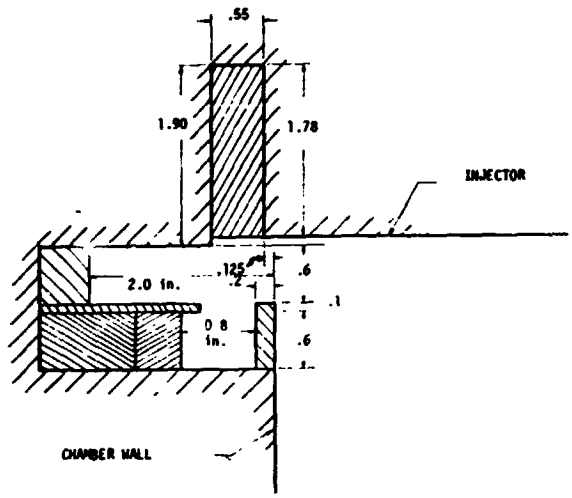

Dual-Radial #2 Cavity (DR2)

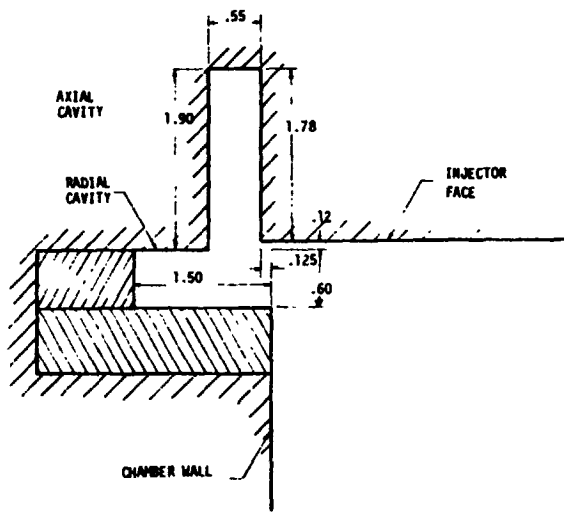

Axial Radial #1 (AR1) Cavity

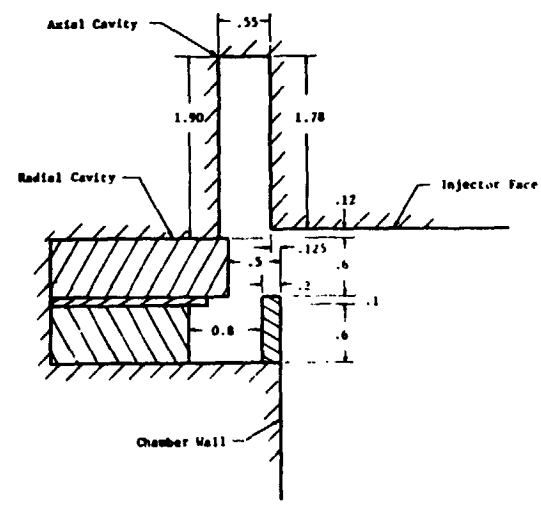

Cavity Configuration #A1

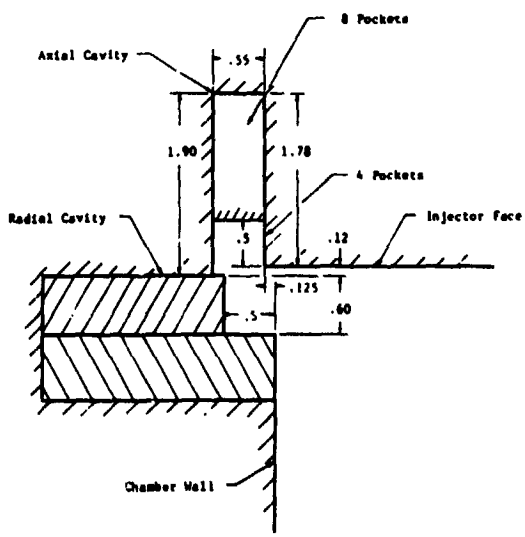

Bitune Cavity Configuration

Figure 66. Basic Cavity Configurations

TABLE VII

Cavity Configuration Test And Bomb Summary

CONFIGURATION TYPE		IDENT	TESTS	BOMBS
Dual Radial	#1	DR 1	10	7
Dual Radial	#2	DR 2	6	7
Axial Radial	#1	AR 1	5	10
Axial Axial	#1	AA 1	2	4
Bitune		Bitune	2	2
Dual Radial #1	No Partition	DR 1 (NP)	2	4
Dual Radial #1	A Reduction	DR 1 A	3	4
Dual Radial #1	B Reduction	DR 1 B	2	4
Dual Radial #1	C Reduction	DR 1 C	3	6
Dual Radial #1	D Reduction	DR 1 D	2	4
Dual Radial #1	E Reduction	DR 1 E	4	6
7 CONFIGURATIONS			41 TESTS	58 BOMBS

TABLE VIII

DUAL CAVITY TESTING STABILITY RECORD

MIXED ELEMENT INJECTOR-ACOUSTIC CAVITY PROGRAM-N2O4/HMH TESTS

A-AREA TEST SERIES 6KH5-4- 16 IN. HEAT SINK CHAMBER

VARIOUS DUAL RADIAL, AXIAL-RADIAL, AND AXIAL-AXIAL CAVITY CONFIGURATIONS

TEST	MR	PC	TO	TF	FIRST BOMB LOC	TIM	SIZE	DAMP 10%	DAMP TOTAL	FREQ	AMP	CPIA TIME	SECOND BOMB LOC	TIM	SIZE	DAMP 10%	DAMP TOTAL	FREQ	AMP	CPIA TIME	SPONTANEOUS EFFECTS DURATION	FREQ	AMP	WHEN	WHAT	STATUS
DR1 CONFIGURATION																										
101	1.61	124.	84.	70.		.0	.0	0.	0.	0.	0.	0.		.0	.0	0.	0.	0.	0.	0.	0.	0.	0.			STAB
102	1.67	125.	88.	71.	B1	.0	6.5	4.	6.	0.	0.	0.		.0	.0	0.	0.	0.	0.	0.	0.	0.	0.			STAB
103	1.66	124.	97.	219.	B1	1.3	6.5	5.	*******	2600.	5.	25.		.0	.0	0.	0.	0.	0.	0.	0.	0.	0.			STAB
104	1.71	127.	98.	242.	B1	2.4	6.5	5.	10.	5200.	0.	17.		.0	.0	0.	0.	0.	0.	0.	550.	5200.	(10)	PREBUM	2T	U.S.
105	1.64	125.	86.	234.	B1	.0	6.5	4.	6.	0.	0.	0.		.0	.0	0.	0.	0.	0.	0.	0.	0.	0.			STAB
106	1.68	96.	86.	222.	B1	2.1	6.5	6.	22.	5200.	0.	17.		.0	.0	0.	0.	0.	0.	0.	580.	1270.	(40)	PREBUM	1L	U.S.
107A	1.90	150.	95.	245.		.0	.0	0.	0.	0.	0.	0.		.0	.0	0.	0.	0.	0.	0.	0.	0.	0.			STAB
107B	1.39	149.	91.	246.	B1	.0	6.5	4.	6.	0.	0.	0.		.0	.0	0.	0.	0.	0.	0.	0.	0.	0.			STAB
108	1.47	101.	91.	238.	B1	2.1	6.5	5.	12.	5200.	0.	17.		.0	.0	0.	0.	0.	0.	0.	20.	1580.	30.	PREBUM	1L	STAB
109	1.98	151.	94.	242.		.0	.0	0.	0.	0.	0.	0.		.0	.0	0.	0.	0.	0.	0.	0.	0.	0.			STAB
DR2 CONFIGURATION																										
110	1.67	124.	74.	218.	B1	.0	6.5	4.	6.	0.	0.	0.		.0	.0	0.	0.	0.	0.	0.	1500.	5200.	(80)	PREBUM	2I	U.S.
111	2.06	105.	74.	244.	B1	.0	6.5	4.	6.	0.	0.	0.	B2	.0	6.5	4.	6.	0.	0.	0.	20.	2500.	10.	PREBUM	1T	STAB
112	1.67	108.	73.	250.		.0	.0	0.	0.	0.	0.	0.		.0	.0	0.	0.	0.	0.	0.	0.	0.	0.			STAB
113	1.96	101.	70.	248.	H1	2.1	6.5	7.	7.	1270.	0.	35.		.0	.0	0.	0.	0.	0.	0.	400.	1300.	(60)	PREBUM	1L	U.S.
114	1.52	100.	69.	258.	B1	.0	6.5	4.	6.	0.	0.	0.		.0	.0	0.	0.	0.	0.	0.	30.	1370.	30.	PREBUM	1L	STAB
115	1.41	148.	72.	262.	B1	.0	6.5	4.	6.	0.	0.	0.	B2	.0	6.5	4.	6.	0.	0.	0.	0.	0.	0.			STAB
AR1 CONFIGURATION																										
116	1.63	125.	74.	169.	B1	.0	6.5	4.	6.	0.	0.	0.	B2	.0	6.5	4.	6.	0.	0.	0.	1300.	2300.	2.	PREBUM	1T	STAB
117	1.89	146.	74.	189.	B1	.0	6.5	4.	6.	0.	0.	0.	B2	.0	6.5	4.	6.	0.	0.	0.	0.	0.	0.			STAB
118	1.42	147.	73.	196.	B1	.0	6.5	4.	6.	0.	0.	0.	B2	.0	6.5	4.	6.	0.	0.	0.	0.	0.	0.			STAB
119	2.03	96.	69.	120.	B1	.0	6.5	4.	6.	0.	0.	0.	B2	.0	6.5	4.	6.	0.	0.	0.	410.	1300.	(90)	PREBUM	1L	U.S.
120	1.50	96.	68.	129.	B1	.0	6.5	4.	6.	0.	0.	0.	B2	.0	6.5	4.	6.	0.	0.	0.	430.	1300.	(85)	PREBUM	1L	U.S.
DR1(NP) CONFIGURATION																										
121	1.60	124.	78.	205.	H1	.0	6.5	4.	6.	0.	0.	0.	B2	.0	6.5	4.	6.	0.	0.	0.	0.	0.	0.			STAB
122	1.42	101.	82.	212.	B1	.0	6.5	4.	6.	0.	0.	0.	B2	.0	6.5	4.	6.	0.	0.	0.	250.	1340.	(30)	PREBUM	1L	U.S.
BITUNE CONFIGURATION																										
123	1.63	125.	79.	167.		.0	.0	0.	0.	0.	0.	0.		.0	.0	0.	0.	0.	0.	0.	300.	5200.	(10)	PREBUM	2I	U.S.
124	1.39	150.	80.	189.	B1	.0	6.5	4.	6.	0.	0.	0.	B2	.0	6.5	4.	6.	0.	0.	0.	440.	5200.	(10)	PREAFT	2T	STAB
AA1 CONFIGURATION																										
125	1.62	126.	92.	213.	B1	.0	6.5	4.	6.	0.	0.	0.	B2	.0	6.5	4.	6.	0.	0.	0.	180.	5200.	(25)	PREBUM	2T	U.S.
126	1.58	101.	95.	206.	B1	.0	6.5	4.	6.	0.	0.	0.	B2	.0	6.5	4.	6.	0.	0.	0.	400.	1340.	(35)	PREBUM	1L	U.S.
DR1A CONFIGURATION																										
127	1.52	125.	86.	132.	B1	.8	6.5	*********		6450.	(80)	10.	B2	.0	6.5	4.	6.	0.	0.	0.	0.	0.	0.	PREBUM	1R	U.S.
128	1.37	148.	87.	183.		.0	.0	0.	0.	0.	0.	0.		.0	.0	0.	0.	0.	0.	0.	0.	0.	0.			HALF
129	1.53	147.	89.	187.	H1	.0	6.5	4.	6.	0.	0.	0.	B2	.0	6.5	4.	6.	0.	0.	0.	0.	0.	0.			STAB
DR1B CONFIGURATION																										
130	1.54	125.	78.	177.	H1	.0	6.5	4.	6.	0.	0.	0.	B2	.0	6.5	4.	6.	0.	0.	0.	0.	0.	0.			STAB
131	1.53	102.	81.	177.	B1	.0	6.5	4.	6.	0.	0.	0.	B2	.0	6.5	4.	6.	0.	0.	0.	290.	1300.	(25)	PREAFT	1L	U.S.
DR1C CONFIGURATION																										
132	1.56	123.	89.	152.	B1	.0	6.5	4.	6.	0.	0.	0.	B2	.0	6.5	4.	6.	0.	0.	0.	0.	0.	0.			STAB
133	1.45	99.	89.	171.	B1	.8	6.5	***	150.	1300.	20.	35.	B2	.0	6.5	4.	6.	0.	0.	0.	230.	1300.	(30)	PREBUM	1L	U.S.
134	1.40	145.	93.	198.	H1	.0	6.5	4.	6.	0.	0.	0.	B2	.0	6.5	4.	6.	0.	0.	0.	0.	0.	0.			STAB
DR1D CONFIGURATION																										
135	1.51	125.	93.	171.	B1	.8	6.5	4.	6.	0.	0.	0.	B2	.0	6.5	4.	6.	0.	0.	0.	0.	0.	0.			STAB
136	1.49	101.	94.	187.	B1	.8	6.5	5.	50.	1380.	12.	30.	B2	.0	6.5	4.	6.	0.	0.	0.	150.	1380.	(45)	PREBUM	1L	U.S.
DR1E CONFIGURATION																										
137	1.62	123.	99.	196.	B1	.8	6.5	1.	22.	5200.	0.	17.	B2	1.6	6.5	2.	5.	6400.	0.	10.	0.	0.	0.			STAB
138	1.42	97.	102.	200.	B1	.8	6.5	***	200.	1323.	(15)	34.	B2	1.6	6.5	*********		6450.	(65)	10.	240.	1320.	(25)	PREBUM	1R,1L	U.S.
139	1.60	109.	100.	173.	B1	.0	6.5	*********		6300.	(65)	10.	B2	.0	6.5	4.	6.	0.	0.	0.	100.	1320.	(20)	PREAFT	1R,1L	U.S.
140	1.52	81.	101.	175.		.0	.0	0.	0.	0.	0.	0.		.0	.0	0.	0.	0.	0.	0.	440.	1300.	(35)	HUM	1L	U.S.

IX, C, Test Summary (cont.)

On two tests, moderate 1L activity (1300 Hz) was experienced during the start transient -- that is, prior to the fuel injection temperature reaching steady-state conditions -- and on one test some self-damped 2T (5200 Hz) was indicated. Postbomb ringdown frequencies showed the presence of both 1T (2600 Hz) and 2T modes, but in no case did the bomb cause unstable combustion.

DR2 Testing. In order to reduce the sensitivity to the 2T mode, both cavity legs were shortened for the DR2 testing. Six tests were conducted, with seven bombs being fired. Start transient 1L mode was again experienced on two tests, as was some very long duration high amplitude 2T. All firings were bomb-stable.

AR1 Testing. The axial-radial cavity configuration was evaluate next, in five double bomb tests. No postbomb instabilities were evidenced, although the 1L mode did occur at high amplitude during the start transients of two firings.

DR1(NP) Testing. In recognition that it might be impossible to cool the partition between cavities of the dual radial device, the stability of an unpartitioned device was briefly explored. In two double bomb tests, the DR1(NP) configuration was bomb-stable, although 1L was again experienced in the start transient of the low chamber pressure test.

Bitune Testing. To verify that the ME 1B injector was as unstable as the ME 1A, two tests were conducted with a bitune cavity installation similar to that tested previously on NAS 9-13133. This entailed four short axial cavities tuned to the 2T mode and eight longer ones tuned to the 1T mode. The system was spontaneously unstable in 2T and corroborated the basic instability of the pattern.

IX, C, Test Summary (cont.)

AA1 Testing. The dual axial configuration was intended to reproduce the satisfactory damping of the AR1 design while improving the packaging and cooling aspects of it. The unit was spontaneous unstable in 2T in one test and in 1L during the other.

DR1 Area Reduction Testing. This testing, of cavity configurations designed DR1A, B, C, D, and E, was performed to evaluate the effect of variations in cavity cross-sectional area. The cross-sectional area of the two legs, expressed as a percentage of the injector face area, was as follows:

Configuration	Area of Short Leg	Area of Long Leg
DR1	27	27
DR1A	27*	20
DR1B	20	27
DR1C	13.5	27
DR1D	13.5	20
DR1E	13.5	13.5

* Entrance area reduced to 20%

The 1L mode was registered during the start period with most of these, and with both the DR1A and the DR1E units the 1R (6400 Hz) mode was activated by the bomb.

D. TEST RESULTS

Results of these 41 tests can be interpreted in several ways, none of which is entirely satisfactory because the limited number of tests for any condition precludes statistical significance. First, it is probably most pertinent to consider as a group the combustion responses to the bomb perturbations. This is because the bombs were initiated at steady-state conditions, and thus the system was operating at design cavity gas and propellant injection temperatures. Within this category, it is necessary to break

out the nominal operating point results from all the rest. Statistically there seems to be little basis for grouping tests of different mixture ratio and chamber pressure; nonetheless this can be done. Next, the spontaneous responses arising during the start transient can be considered as a group, since the system would in actual application have to operate stably through the transient. Again the nominal operating point responses can be categorized as a separate group and, perhaps more important, those tests in which the 1L mode was experienced can be segregated. The 1L mode occurred only at low chamber pressure but its occurrence likely precluded initiation of other modes.

Table IX is a summary of instabilities along these lines of categorization. It shows that at the nominal operating point, all bomb responses were stable except one -- the 1R mode occurring with the DR1A. Considering all operating points, 1R instabilities occurred also on the DR1E configuration, and 1L mode was evidenced with the DR1C, D, and E units. Since the cavities were not tuned to damp the 1L mode, its occurrence is not indicative of cavity effectiveness. Apart from the 1L responses, all spontaneous instabilities were in the 2T mode. These all occurred at the nominal operating point. Susceptible configurations were the DR1, DR2, Bitune, and AA1. Spontaneous 1L instabilities were experienced by all configurations except the Bitune and DR1A, which were not tested at low chamber pressure.

There were no instabilities, bomb-induced or during the start transient, in the high chamber pressure tests.

E. ANALYTICAL RESULTS

The purpose of the analytical effort was to correlate the hot fire stability results and in so doing evaluate the acoustic bench test and subscale hot fire test results described earlier. The key point in the analysis was the

TABLE IX

SUMMARY OF INSTABILITIES

	Nominal Operating Point			All Operating Points		
	Number*	Number Unstable	Mode	Number*	Number Unstable	Mode
Bomb Response Only						
DR1	3	0	-	7	0	-
DR2	1	0	-	7	0	-
AR1	2	0	-	10	0	-
DR1(NP)	2	0	-	4	0	-
Bitune	0	0	-	2	0	-
AA1	2	0	-	4	0	-
DR1A	2	1	1R	4	1	1R
DR1B	2	0	-	4	0	-
DR1C	2	0	-	6	1	1L
DR1D	2	0	-	4	1	1L
DR1E	2	0	-	6	3	1R, 1R, 1L
Spontaneous Response Only -- Excludes 1L Mode						
DR1	3	1	2T	8	1	2T
DR2	1	1	2T	4	1	2T
AR1	1	0	-	3	0	-
DR1(NP)	1	0	-	1	0	-
Bitune	1	1	2T	2	1	2T
AA1	1	1	2T	1	1	2T
DR1A	1	0	-	3	0	-
DR1B	1	0	-	1	0	-
DR1C	1	0	-	2	0	-
DR1D	1	0	-	1	0	-
DR1E	1	0	-	1	0	-
Spontaneous Response Only -- Excludes 2T Mode						
DR1	2	0	-	9	1	1L
DR2	0	0	-	5	1	1L
AR1	1	0	-	5	2	1L
DR1(NP)	1	0	-	2	1	1L
Bitune	0	0	-	1	0	-
AA1	0	0	-	1	1	1L
DR1A	1	0	-	3	0	-
DR1B	1	0	-	2	1	1L
DR1C	1	0	-	3	1	1L
DR1D	1	0	-	2	1	1L
DR1E	1	0	-	4	3	1L

* Number of applicable responses.

correct definition of acoustic lengths of the legs of the dual cavity configurations, and this understanding resulted directly from the acoustic bench testing discussed in Section VI. Good correlation of the stability trends of the DR1 cavity configuration and several of its variations was obtained.

These variations include the DR1E which had the minimum cross-section in the area reduction test series and was unstable in the 1R mode, the DR1(NP) in which there was no partition between the two legs, and the SR7 which had a single radial cavity identical to the longer leg of the DR1 design. The SR7 was one of several single and dual cavity configurations tested by NASA during 1976 at the NASA White Sands Test Facility (WSTF). The SR7 was not tested at Aerojet but at WSTF exhibited instabilities in the 2T mode. It is included in this analysis because it represents a limiting case, namely the elimination of one of the two cavity legs.

1. Model

The IFAR program has as a subroutine the Cavity Acoustics Program (CAP) which calculates cavity admittance based on geometry, sound speed, and damping and inlet resistance parameters. For the full scale analysis these parameters and the sound speed were assumed to have the same values as derived in the subscale analysis by correlating cavity pressure amplitude ratios, as presented in Section VIII.

Proper treatment of the dual cavity legs was not initially apparent and several alternatives were evaluated by comparing predicted stability with experimental results. Good correlation was obtained only by accounting for the admittance of both legs when the resonant frequencies of

both were less than or near the driving frequency; otherwise, the admittance of the (much) higher frequency leg was neglected. This insight originated with the acoustic bench tests and the cork dust patterns observed in the cavities. Figure 67 reproduces a photograph of the cork dust pattern in an axial-radial configuration in which the higher frequency axial leg is quiescent while the radial leg shows much activity because the driver in the chamber is near the radial leg resonant frequency.

Figure 68 clarifies the assumed leg lengths for the various configurations and outlines the selection of corresponding admittance values. For a generalized dual cavity configuration in which the main leg has a resonant frequency f_B, if both f_M and f_B are less than the driving -- i.e., chamber -- frequency f_D, then the overall admittance is assumed to be approximately equal to the sum of the admittances of the two legs. If the branch leg has a much higher frequency than the driving frequency then the overall admittance is assumed to be that of the main leg only.

Six insets on Figure 68 show the leg lengths chosen to represent the several DR1 variations. Inset A is for the basic DR1 cavity or the DR1E reduced area configuration and applies only to the 1T mode. The acoustic path is defined by the longer cavity leg, and the total admittance is that of the longer leg; the shorter leg acts as a quiescent branch. Inset B shows the representation for higher modes (2T, 3T, 1R) in the same cavities. Here the shorter leg is the main path and, because that occurs, the longer leg becomes a branch of approximately the same length. In this case the admittances of the two legs combine.

Insets C and D identify the leg lengths for the DR1(NP) case. Again the longer leg is activated by the 1T mode, and the shorter leg by higher modes. The wave path into the shorter cavity is delineated by the

$$f_{CHAMBER} \lesssim f_{MAIN}$$

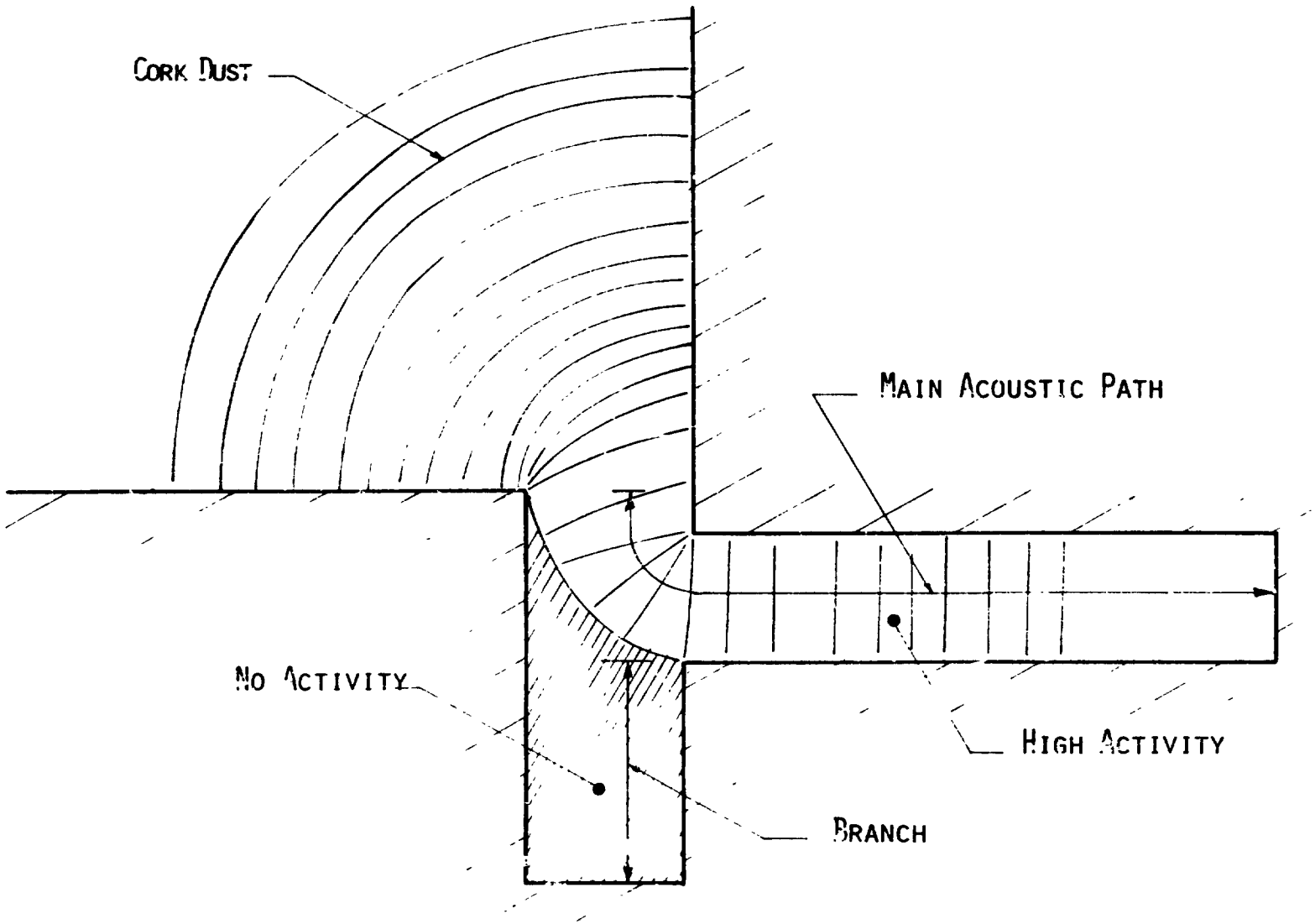

Figure 67. Observed Effect of Chamber Resonant Frequency on Acoustic Cavity Activities

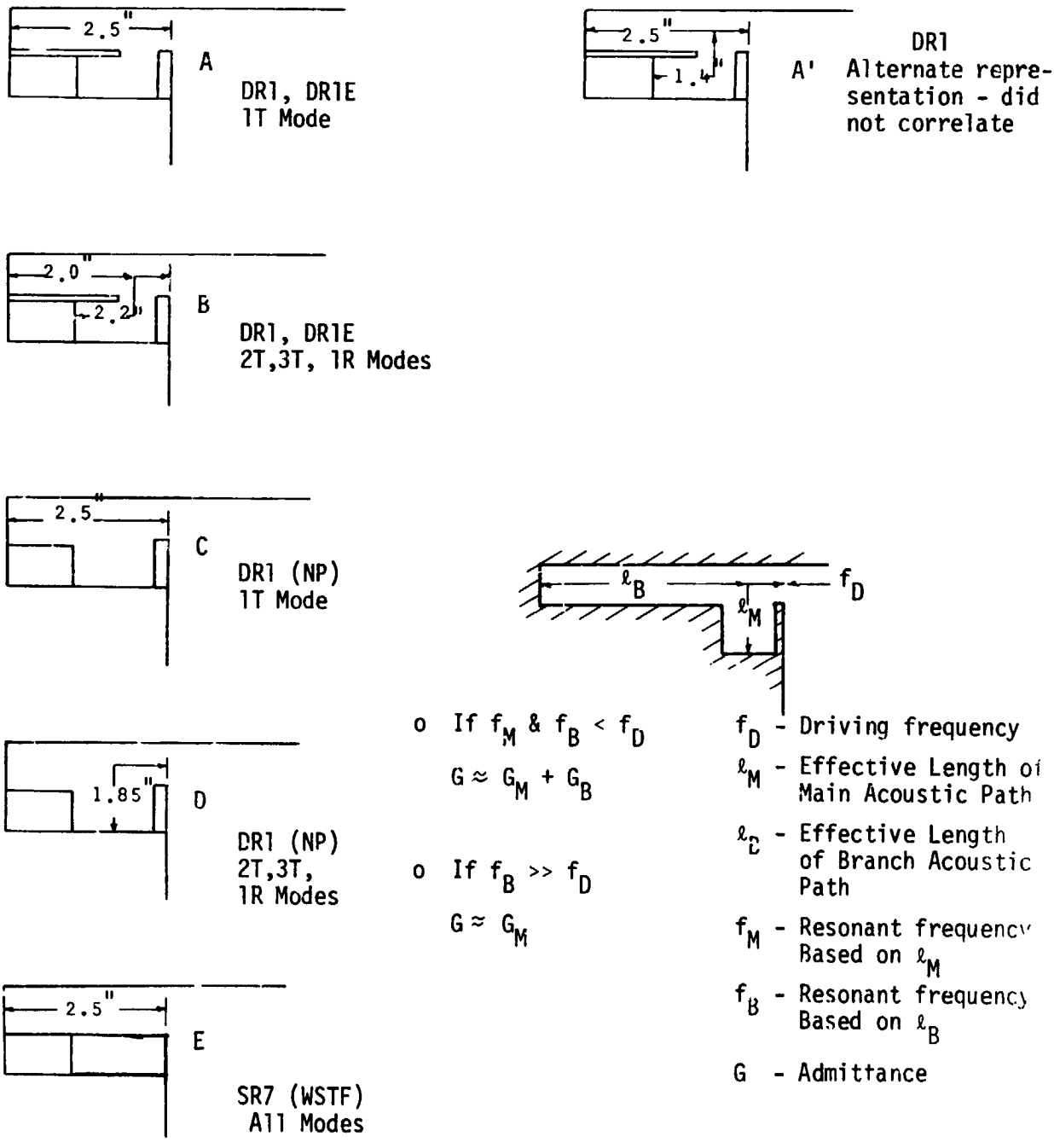

Figure 68. Acoustic Path and Admittance Definition

arrow; the branch formed by the remainder of the longer cavity leg has a much higher resonant frequency and thus the admittance is determined solely by the shorter leg. Inset E relates to the SR7 design, in which the single leg must be applied to all modes. Finally, Inset A' shows one alternative representation of the basic DR1 unit which failed to correlate. In this representation the longer leg is considered to be 2.5 in. long and the shorter leg a 1.4 in. long branch.

The chamber geometry and gas properties used in the analysis are summarized in Figure 69. The X* parameter specifies the distance from the injector face to the plane of combustion, which is assumed to have zero thickness; because of the close burning promoted by the splash plate injector element X* is taken to be zero. Since the chamber and nozzle admittances are the same for all cavity configurations, variations in predicted stability boundaries are a consequence of changes in cavity admittance only.

The n-τ "box" usually plotted on the n-τ plane to represent the injection characteristics has, in the plots discussed below, been reduced to two lines defining the maximum values of n and τ. The reason for this is that that the minimum value of n is never of any importance in the interpretation of analytical results, and for the present system neither is the minimum value of τ. The maximum value of both parameters is based on the figures in Section VII.

2. Correlation of Test Results

The predicted stability of the basic DR1 configuration is shown in Figure 70. As noted, the representations of Insets A and B on Figure 68 define the acoustic lengths of the two cavity legs. The configuration is predicted to be stable, as was experimentally demonstrated. An additional analysis was made to simulate cavity conditions during the start transient by assuming the

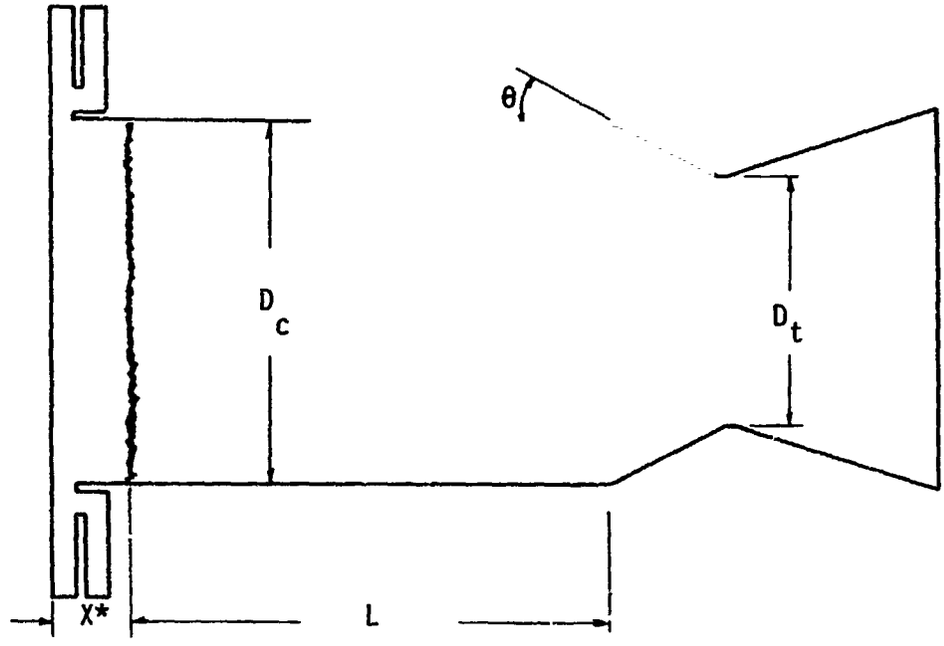

C = 3800 ft/sec

γ = 1.22

D_c = 8.12"

D_t = 5.81"

θ = 30°

L = 13.32"

X* = 0

Figure 69. Chamber/Nozzle Geometry and Gas Properties

Stability		Wave Path Definition
Observed	Calculated	
Stable	Stable	1T - A
Unstable @ f = 5200 Hz (transient)	Unstable @ 2T Mode (Low Sound Speed)	2T - B 1R - B 3T - B

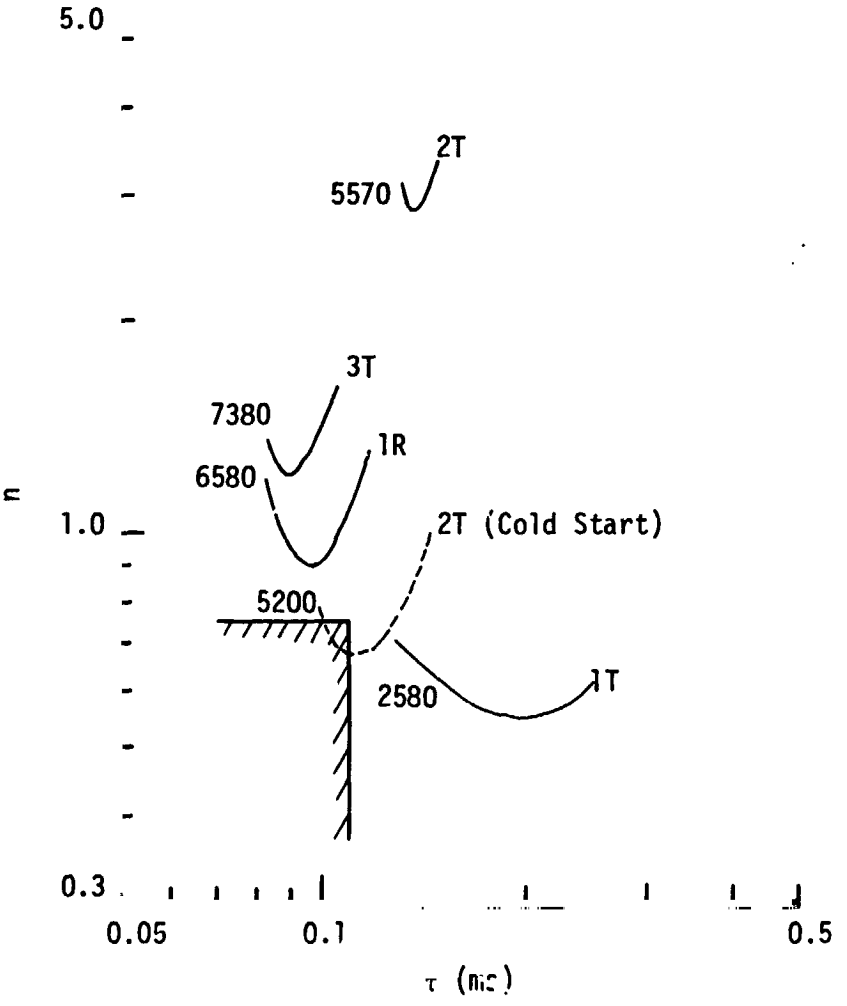

Figure 70. DR1 Calculated Stability

cavity gas sound speed is only 1900 ft/sec, as compared to 3000 ft/sec at steady-state; under this circumstance a 2T mode instability is predicted, as was indeed experienced.

Figure 71 compares the stability prediction for the DR1 as formulated above with the representation of Inset A' on Figure 68. The latter results in a 1R mode instability prediction while the former results in the prediction of stable operation.

The DR1E stability prediction is shown on Figure 72. Insets A and B were again used to represent the leg lengths, which are the same as in the basic DR1 configuration; the change in cross-sectional area is accounted for however. The prediction is for 1R mode instability and this was evidenced experimentally.

The unpartitioned cavity design, DR1(NP), was predicted to be stable, as shown in Figure 73, and it was. Variations of this design were evaluated in the NASA-WSTF testing: the shallow cavity was successively shortened from 1.3 in. to 0.5 in. without a change in stability. The explanation for this is that the higher modes travel across the width of the cavity -- that is, follow the arrow on Inset D -- and shortening it simply reduces the cross-sectional area. Only when the path of these higher modes is eliminated, as in the SR7 cavity pictured in Inset E, does the stability change. That prediction is for 1R or 3T instabilities; the 2T mode was actually experienced, indicating most likely an incorrect choice of cavity gas sound speed. Figure 74 shows the stability prediction for SR7.

In summary, the stability predictions show a remarkably good correlation with test results. The start transient instabilities can be rationalized with the assumption of reduced sound speed in the cavity. The behavior of the unpartitioned dual cavity can be readily explained. The multimode damping capability of dual cavities can be analytically correlated by the

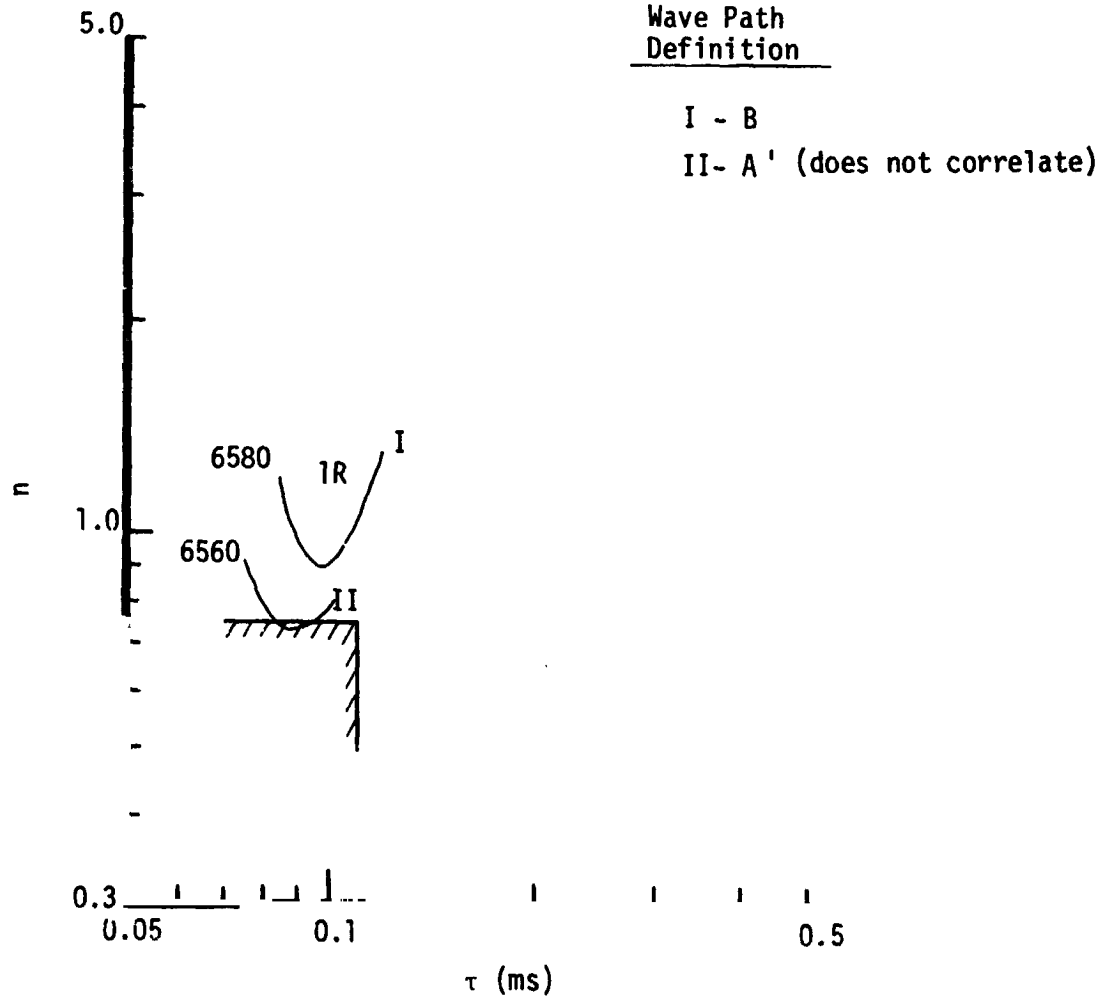

Figure 71. Comparison of Correlation with Alternative Wave Path Definition

Stability		Wave Path Definition
Observed	Calculated	
Unstable @ f = 6450 Hz	Unstable @ 1R Mode	1T - A 2T - B 1R - B 3T - B

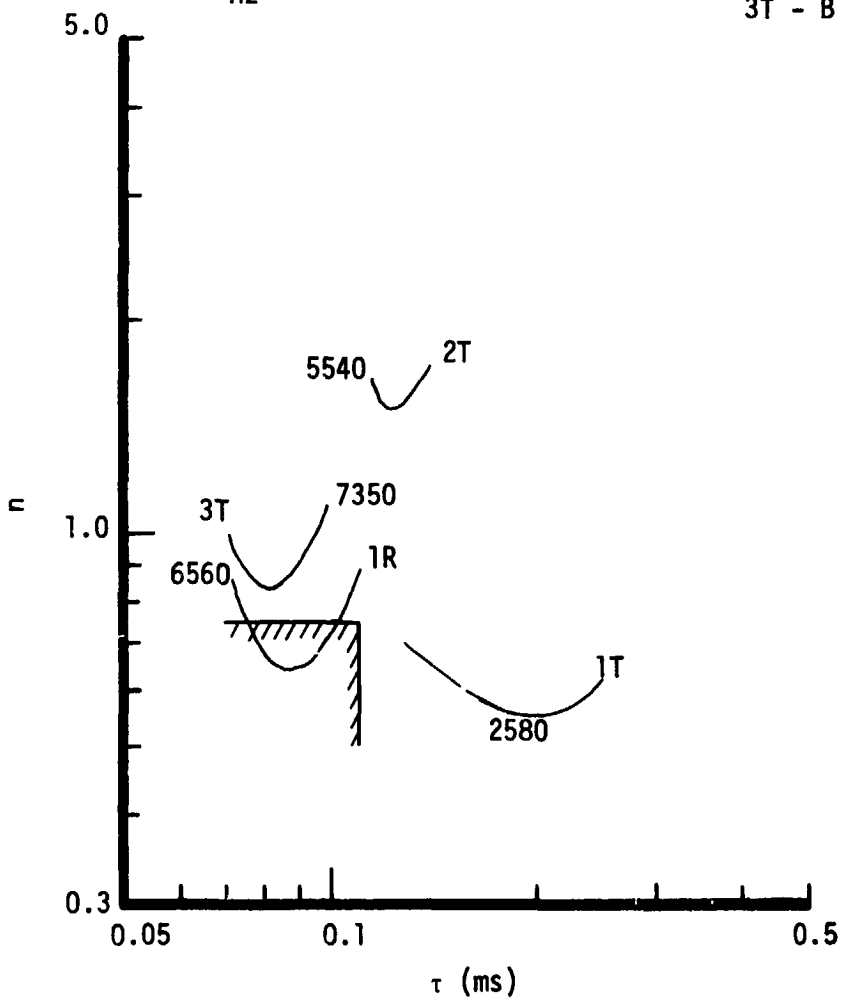

Figure 72. DRIE Calculated Stability

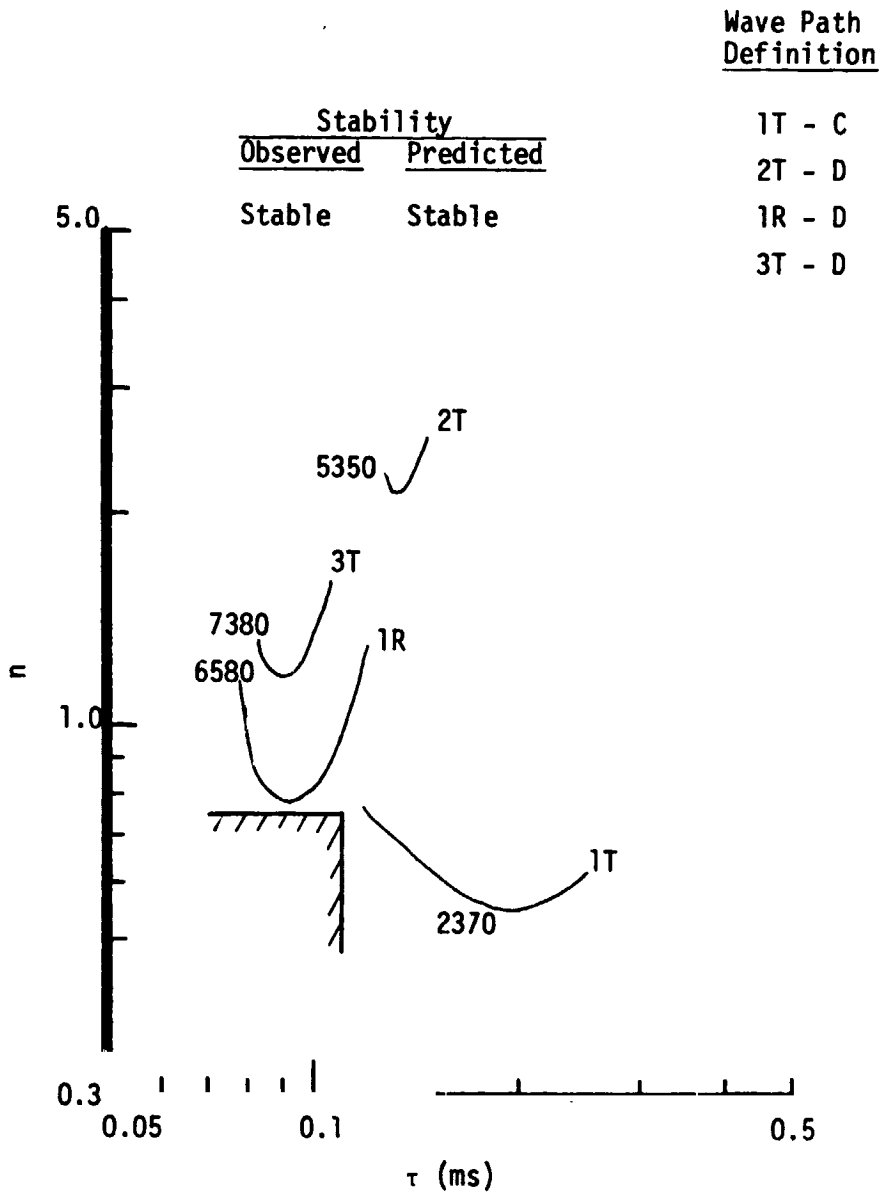

Figure 73. DR1(NP) Calculated Stability

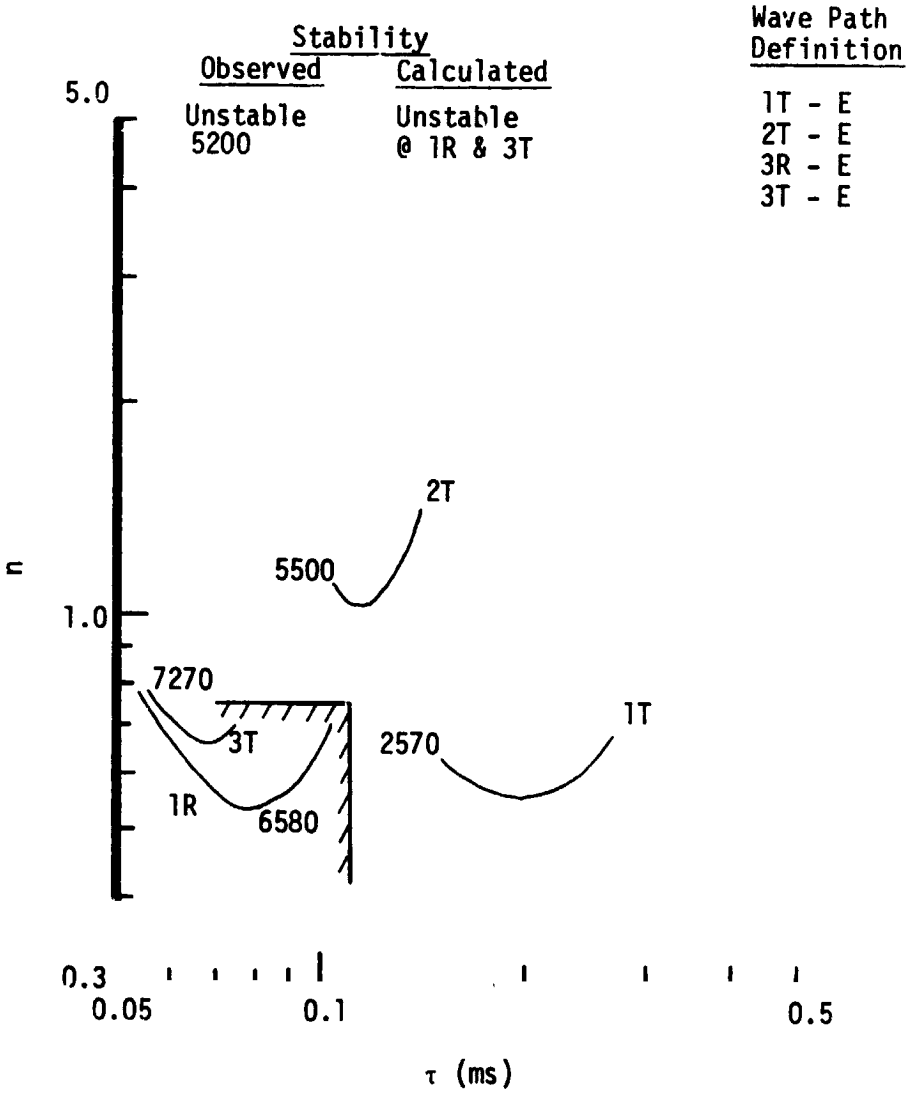

Figure 74. SR7 Calculated Stability

IFAR model. The key to it all is understanding the wave patterns in the cavities and formulating the acoustic lengths and admittances accordingly.

F. CONCLUSIONS

The multimode damping capability of dual cavities having a common entrance was demonstrated for a high performance injector requiring damping in three acoustic modes. However, the small number of data points limits the statistical significance of the test results for several of the cavity configurations.

All of the basic configurations were bomb-stable if the 1L occurrences are overlooked. At the same time, all of the basic configurations except AR1 allowed spontaneous 2T instabilities during the start transient. None of the variations of the basic DR1 arrangement had spontaneous instabilities; two did show bomb-induced 1R instabilities, however.

Analytical calculations by the IFAR model correlated well with test experience for the DR1 and several of its variations. Key to the correlation was the proper formulation of the acoustic wave path and the cavity admittance.

BIBLIOGRAPHY

Monthly Progress Reports:

14232-DRL-1-1, covering July 1974: Initial analysis of configurations to be used in acoustic bench tests, preliminary design of cavity housing for full scale testing, program schedule.

14232-DRL-1-2, covering August 1974: Selection of configurations for bench tests, air-to-hot air scaling factors, vaporization and time lag analysis of full scale x-doublet and aplash plate injectors, fabrication of bench test hardware.

14232-DRL-1-3, covering September 1974: Acoustic analysis of bench test models, formulation of governing equations, preliminary bench test results.

14232-DRL-1-4, covering October 1974: Design of full scale hardware.

14232-DRL-1-5, covering November 1974: Objectives and methods for bench testing, bench test results and conclusions, photographs of mode orientation delineated by cork dust.

14232-DRL-1-6, covering December 1974: Program hold due to loan of hardware to OMS program.

14232-DRL-1-7, covering January 1975: Program hold, preliminary design of 2-D subscale hardware allowing photography of cavity region in hot fire testing.

14232-DRL-1-8, covering February 1975: Program hold.

14232-DRL-1-9, covering March 1975: Analytical and mechanical design of 2-D hardware predictions and recommendations for 2-D tests.

14232-DRL-1-10, covering April 1975: Fabrication of 2-D hardware

14232-DRL-1-11, covering May 1975: Dual cavity testing of dual radial configuration, tests 101-104, photographs of dual cavity hardware.

14232-DRL-1-12, covering June 1975: Dual cavity testing of dual radial configurations #1 and #2, axial-radial #1, tests 105-120, development of high speed photography/oscillography techniques, performance of mixed element injector, stability of configurations tested.

14232-DRL-1-13, covering July 1975: Dual cavity testing of no partition dual radial, OMS baseline, axial-axial, and reduced area configurations, tests 121-140, preliminary conclusions.

14232-DRL-1-14, covering August 1975: Fabrication of 2-D combustor.

14232-DRL-1-15, covering September 1975: Initial testing with 2-D combustor, tests 101-104, interpropellant leaks.

14232-DRL-1-16, covering October 1975: Results of dual cavity testing, photographs and test plan for 2-D hardware.

14232-DRL-1-17, covering November 1975: Fabrication of replacement injectors for 2-D testing.

14232-DRL-1-18, covering December 1975: Fabrication of 2-D injectors.

14232-DRL-1-19, covering January 1976: Evaluation of shock tube system for perturbing combustion field, preparation of apparatus for stroboscopic shadowgraph photography.

14232-DRL-1-20, covering February 1976: Conclusions drawn from shock tube evaluation, further evaluation of stroboscope/shadowgraph techniques.

14232-DRL-1-21, covering March 1976: Interpropellant leaks on replacement injectors.

14232-DRL-1-22, covering April 1976: Repair and leak check of 2-D injector

14232-DRL-1-23, covering May 1976: 2-D testing of 0.5 in. cavity, tests 101-114, analysis of preliminary data, high speed movies of cavity, difficulties with stroboscopic light source.

14232-DRL-1-24, covering June 1976: 2-D testing with 0.5, 1.0, 1.5 in. cavities, rounded inlet, 0.25 in. overlap and zero cavity configuration, tests 115-145, analysis of high speed movies, analysis of temperature and high freq. pressure data, correlation of models.

14232-DRL-1-25, covering July 1976: Analysis of movies from tests 141-145, summary of findings of movies.

Final Report: NAS 9-14232-2-1
Summary Report: NAS 9-14232-3-1

Test Plans:

14232-DRL-5, November 1974: Dual cavity testing: objective, approach, hardware, test procedures, test matrix, schedule.

14232-DRL-5-1, October 1975: 2-D chamber testing: objective, hardware, test matrix, schedule.

Presentations to NASA-JSC

30 July 1974: Program plan and schedule, analysis of acoustic bench test configurations, analysis and design of dual cavity configurations.

14 November 1974: Bench test results, dual cavity configurations.

29 October 1975: Dual cavity test results, 2-D combustor configurations

5 October 1976: Final presentation and program review.